UNIVERSITY OF PRETORIA
DEPARTMENT OF MATERIALS SCIENCE AND METALLURGICAL ENGINEERING

INVESTIGATION INTO THE INFLUENCE OF MAGNESIA CONTENT, ALUMINA CONTENT, BASICITY AND IGNITION TEMPERATURE ON THE MINERALOGY AND PROPERTIES OF IRON SINTER

Submitted in the fulfillment of the requirements for the degree

MSc (Metallurgy)

In the Department of Materials Science and Metallurgical Engineering, Faculty of Engineering, Built Environment and Information Technology,
University of Pretoria

July 2007

By Michel Kalenga wa Kalenga
Supervisor: Prof. A.M. Garbers-Craig

To my wife Georgette and our children Gaudencia and Michel Junior for their patience and understanding while I was working on this project. To God be the glory.

Acknowledgements

First and foremost, my gratitude goes to my supervisor, Professor A.M. Garbers-Craig for the unfailing and unconditional guidance throughout this dissertation. Also, I would like to express my gratefulness to Professor Chris Pistorius for his pertinent remarks and suggestions. I am thankful to Kumba Iron Ore/ Raw Material Technology Management team and technical personnel for their technical support.

ABSTRACT

The sinter quality is dependent on sinter mineralogy, which in turn depends on the chemical compositions of the sinter mix. Although many research works have been conducted, further investigation on the effect of chemical compositions (MgO, Al_2O_3, Basicity) on the sinter quality is still required for further improvement of the sinter and more alternative additives are still being tested. In this project, a sinter pot has been used to manufacture sinters, which were characterized using point-counting to quantify the different phases and X-Ray diffraction to identify the polymorphic forms of Ca_2SiO_4 of the silicate phases. The produced sinters were evaluated with respect to reducibility index (RI), reduction degradation index (RDI), physical breakdown (TI and AI), and production properties (yield, coke breeze rate and production rate). The influence of ignition temperature, magnesium oxide, alumina addition and basicity on the mineralogy as well as physical and chemical properties of iron ore sinters were investigated.

Results were obtained as follows:

1) For the Base case with a basicity of 2, 2.8 mass% MgO content, 1.7 mass % Al_2O_3 and 10 mass% CaO, the effect of ignition temperature, which ranged between 864^oC and 1100^oC, on the sinter quality was investigated. Results showed that the ignition temperature had an effect on the sinter properties: reducibility (RI), physical strength (TI and AI), production properties (yield, coke breeze rate and production rate). The temperature 1053^oC was the best ignition temperature for an economically acceptable sinter. A further increase in ignition temperature was found to form melt on the surface of the sinter produced, leading to a sinter of low quality. Also, X-rays diffraction pattern showed that the allotropic transformation of the Ca_2SiO_4 did not take place.
2) The Low SiO_2 – Low Al_2O_3 sinter had the highest reducibility index and had the highest Abrasion index and the lowest coke breeze rate at 2.8 mass% MgO content compared to all the sinters produced in this project.
3) For the High SiO_2 – Low Al_2O_3 sinter MgO was added through dolomite and fused magnesia. A comparative study on the effect of dolomite and fused magnesia was conducted. The sinter to which fused magnesia was added had lower reducibility,

higher reduction degradation, higher tumble index, lower abrasion index and lower coke breeze rate than the sinter to which dolomite was added.

4) High SiO_2 – High Al_2O_3 sinter had the lowest reducibility index, the lowest reduction degradation, the lowest tumbler index and the highest coke breeze rate.
5) The increase in MgO content in all the sinters produced increased the coke breeze rate.

TABLE OF CONTENTS

Chapter I LITERATURE REVIEW

I.1 INTRODUCTION

The main objective of the Blast furnace is to produce molten iron which has a constant composition at a considerably high rate. Nowadays, the entire iron-making process is well understood. However, the quality of the feed materials for the blast furnace remains an important aspect and much attention needs to be paid to it for a better performance of the blast furnace. Sinter is prone to break down due to degradation during reduction and generation of fines due to handling and abrasion when transported and while it descends in the stack of the blast furnace. This subsequently affects the gas flow in the blast furnace therefore the production of iron becomes inefficient. In order to produce iron at minimum costs, a burden of optimum physical and chemical properties is required. The most significant properties of sinter to be improved include physical strength (tumble index and abrasion index), its resistance to degradation on reduction at relatively low temperatures (reduction degradation index), the rate at which it can be reduced (reducibility) and its performance at high temperatures (softening and dripping temperatures).

Investigations into sinter mineralogy and sinter quality have for long been conducted. It has been reported that the chemistry of iron ore and the variation in process parameters decide the sinter structure which, in turn, governs the sinter quality [1, 2, 3, 4]. Studies on tablets samples as well as in a pot sinter whereby the influence of parameters such as Al_2O_3/SiO_2, basicity and TiO_2 contents on the sinter structure were examined, has shown that there is a relationship between the sinter structural composition of the sinter and its size degradation under low temperature and reducing conditions [5]. Further, a study on the optimization of chemical composition and microstructure of iron ore sinter for low-temperature drip of molten iron with high permeability established that the basicity had a dominant influence on the dripping temperature while low alumina content and high MgO leads to low dripping temperature [6].
The effect of raw material composition on sintering properties has shown that the presence of high alumina and TiO_2 led to the stabilization of calcium ferrite and hematite respectively while sinters with higher addition of alumina and TiO_2 showed a relatively high intensity of disintegration as well as high degradation reduction [3].

Nowadays alternative materials are being tested to replace part of the ores or fluxes with the aim of producing a high quality sinter for optimum performance of sintering mix in the process and a sinter that has a good performance in the Blast Furnace. It was reported that in spite of alternative materials, the evaluation of microstructural properties are still very important in the evaluation of sinter quality [7].

The sintering process is complicated by the fact that not all the starting materials in a sinter mix react during the process, but portions of ores and some fluxes remain in their calcined and unassimilated forms. Main phases include hematite, magnetite, ferrites, glass and silicate phases. The degree of solid solution varies throughout the sinter. It is reported that in order to improve the homogeneity of the composition of the sinter, suitable measures must be taken in preparing the sintermix [2].

Although every precaution is taken to mix the raw materials thoroughly, it is impossible to prevent local inhomogeneities on a microscopic scale. Local differences in basicity, different concentrations of coke and materials such as lime and water, are observed on the microscopic scale [8]. On the other hand, the macroscopic structure of sinter is non-uniform, with large pores and a high permeability. The macroscopic pores yield a highly permeable burden in the blast furnace while on a microscopic scale it is a complex aggregate of phases. The combination of the macroscopic and microscopic structure determines the sinter properties.

The cold strength is reported to be determined by pores, the amount of relict hematite, basicity and composition, as well as slag volume, and domains which have reacted [9].

The disintegration of the sinter is generally attributed to the volume change associated with the reduction of hematite to magnetite. Stresses may develop during the reduction of hematite to magnetite and are absorbed by a porous structure of calcium ferrite [9].

The reducibility is reported to improve with high accessibility of the gas as well as diffusion rates [10]. The variations in compositions of the raw materials also play a big role in the heterogeneity of the phase composition and therefore influence sinter properties. The addition of MgO or increasing MgO/CaO ratio increases the porosity of sinters [11]. The same authors reported that the increase in open porosity improves the reducibility of the sinter and

demonstrated that SFCA stabilizes fine porosity. Therefore, a sinter with good reducibility may be one with a large amount of acicular SFCA and amount of columnar and blocky SFCA. This structure has no cracks and no large pores, which improves the cold strength. But, the decrease in reduction degradation is related to the concentration of skeletal hematite [9,12]. In turn, high basicity, SiO_2 content, Al_2O_2/SiO_2 ratio as well as temperature, oxygen potential and the composition of the raw materials influence the SFCA phase [9,12]. The quality of sinter is therefore determined by the properties of the individual phases and the interaction between them [13,14].

This study includes the following sections:

1. The literature review, which reports different theoretical approaches on sinter mineralogy and morphology as well as properties.

2. The experimental work.

3. The results and discussion

4. Summary and conclusions

5. Recommendations

I.2 AIM OF THIS INVESTIGATION

The correlation between the properties and mineralogy of iron sinters that were constituted from different types of raw materials and with different chemical compositions has been widely published in the literature, but results differ. This project identify the optimum ignition temperature and to investigate the influence of the variation of MgO, SiO_2 and Al_2O_3 contents as well as the basicity on the mineralogy of the iron sinter and draw correlations between certain of its physical and chemical properties and the mineralogy of the iron sinter.

I.3 BRIEF OVERVIEW ON THE BLAST FURNACE AND THE REDUCTION PROCESS

I.3.1 Introduction

The principles behind the operation and design of the blast furnace are well known. The Blast furnace is a chemical as well as a counter-current heat exchanger. The principal objective of the blast furnace is to produce molten iron of constant composition at a high rate. The burden and coke are charged from the top and they descend due to gravity because of the continuous creation of voids by combustion of coke at the tuyeres and removal of iron and slag to the bottom. The hot ascending gases heat up the descending charge materials. This is accompanied by physical changes and chemical reactions [15].

The raw materials require 6 to 8 hours to descend to the bottom of the furnace where they become the final products of liquid slag and liquid iron.

I.3.2 Description of the blast furnace

The Blast Furnace is divided in three different reduction zones according to the temperature of the charge and the composition of the gas: the lower, middle (so-called isothermal or thermal reserve zone) and upper zone. The ascending gases supply the total heat required in the lower and upper zone while in the middle zone the temperature is almost constant [12].

I.3.2.1 The lower (so-called processing or melting) zone

This is the hottest part of the blast furnace where the highly endothermic reactions occur. This zone extends from the tuyeres to 3-5 meters above [15]. The gas cools down to 800^0C –1000^oC by heating the materials, which reach 1400-1500^oC. Generally, the depth of the combustion zone is about 1-2 meters. The more important chemical reactions taking place in this zone include endothermic as well as some exothermic reactions.

A) Endothermic reactions

1. $CaCO_3 = CaO + CO_2$

2. $FeO + C = Fe + CO$
3. $SiO_2 + 2\,C = Si + 2\,CO$
4. $MnO + C = Mn + CO$
5. $P_2O_5 + 5C = 2\,P + 5\,CO$
6. $FeS + CaO + C = CaS + Fe + CO$
7. $CO_2 + C = 2\,CO$ (> 1000C)
8. $C + H_2O = CO + H_2$ (> 1000C)

B. Exothermic reaction:

1. $C + O_2$ (air) $= CO_2 + N_2$

I.3.2.2 The middle or thermal reserve zone

In this part, the temperatures of the solids and that of the gas are similar. There is very little heat exchange and the gas composition is near the equilibrium composition for the reduction of wustite, at the thermal reserve temperature [16]. Most of the indirect reduction, especially of wustite takes place in this zone. The volume of the middle zone is about 50-60 % of the blast furnace volume. Due to the fact that wustite should be given enough time to get reduced indirectly, the extension of this zone is of importance.

I.3.2.3 The upper zone

In this part, so called preparation zone, there is a sharp heat exchange. The ascending gas from the middle zone decreases in temperature from about 1000^0C to 250^0C while the solids temperature rises from the ambient temperature to about 800^0C [15]. The gas temperature is greater than that of the solid materials. In addition, as described in Figure 1a and b, the indirect reduction of hematite and magnetite into their lower oxides can occur. The reduction of the hematite to magnetite is accompanied by the change of crystal structure. This leads to a volume change and porous texture, which favours further reduction, but weakens the physical sinter properties, especially the reduction degradation [15]. The main reactions taking place in this zone include decomposition of carbonates other than that of calcium, vaporization of

moisture and hydrated water of the burden, carbon deposition according to 2 CO = CO_2 + C and partial or complete reduction of hematite as well as magnetite into their lower oxides.

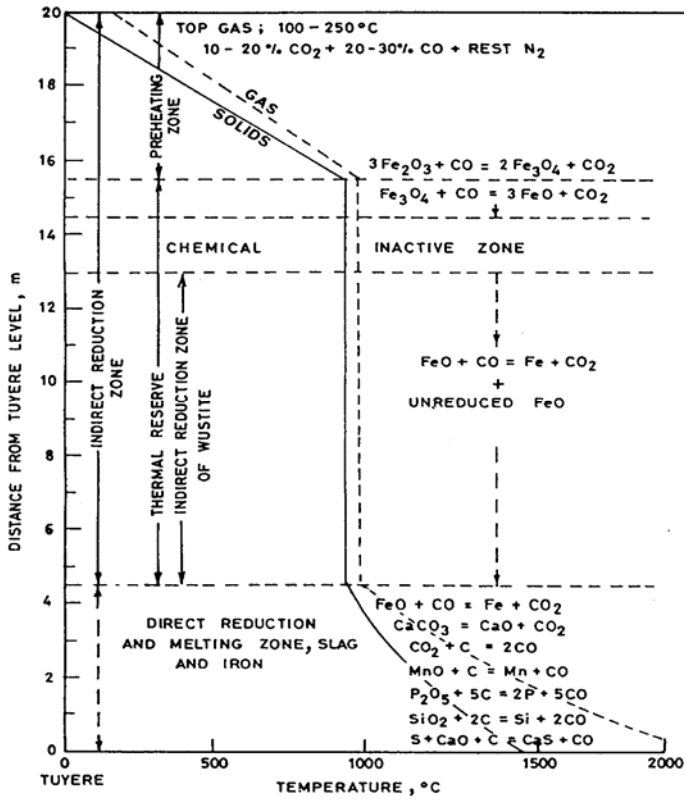

Figure 1.a Schematic diagram of temperature distribution of gas and solids along the height of the blast furnace as well as the chemical reactions in the three main temperature zones [15].

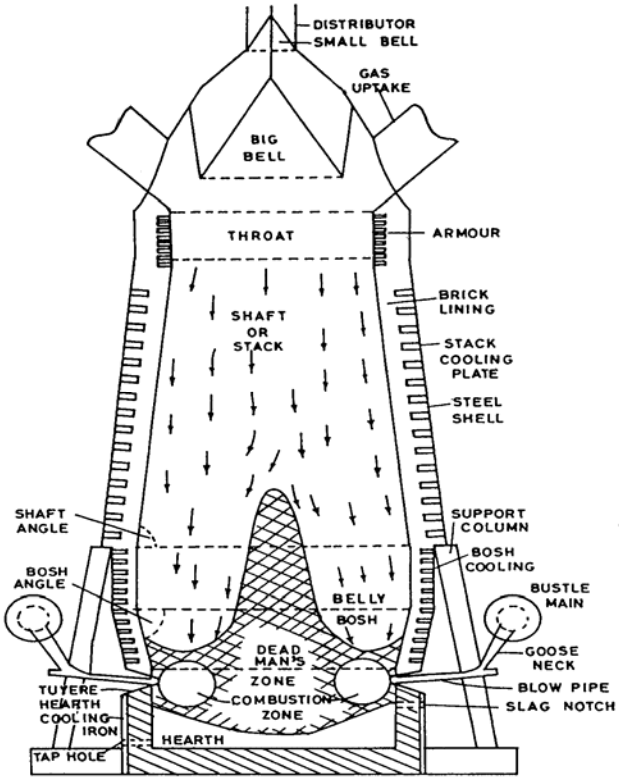

Figure 1.b A section of the blast furnace showing important features including material flow, combustion, dead man, hearth, etc [15].

From a kinetic point of view, the reduction of iron ore by CO is such a varied and complex process since it involves many variables both chemical and physical. The reduction sequence of hematite is given by the following equations:

$$3\ Fe_2O_3 + CO = 2\ Fe_3O_4 + CO_2 \qquad (1)$$

$$Fe_3O_4 + CO = 3\ FeO + CO_2 \qquad (2)$$

$$FeO + CO = Fe + CO_2 \qquad (3)$$

As indicated in Figure 1.a, FeO can remain in the thermal reserve zone. At temperatures higher than 1000^{o}C, the CO_2 reacts with carbon and produces CO according to the reaction (4).

$$CO_2 + C = 2\ CO \qquad (4)$$

The remaining FeO is directly reduced in the melting zone by carbon according to:

$$FeO + C = Fe + CO \qquad (5)$$

The reduction rate depends on the formation of a porous product. This will provide gas access and therefore increase the reduction rate of iron oxides since gas diffusion is of great importance [15].

I.4 THE SINTER PROCESS

I.4.1 Introduction

The first goal of agglomeration is to improve burden permeability and gas-solid contact, and thereby reducing blast furnace coke rates and increasing the rate of reduction. The second consideration is the lessening of the amount of fine material blown out of the blast furnace into the gas recovery system. Fine particles have a detrimental effect on the blast furnace operation because they influence the permeability of the feed materials and the gas distribution within the furnace [16]. It is an imperative that a good gas-solid contact is provided for efficient blast furnace operation. Also, the kinetics of reduction of iron oxide are very low, the residence times in the furnace differ widely: gas time in the order of only few seconds, whereas iron (oxide) remains 5 to 8 hours in the furnace. Therefore, the gas flow distribution within the blast furnace is of great importance and has to be optimized by pelletizing or sintering of the raw materials [16].

Sintering has been referred to as the art of burning a fuel mixed with ore under controlled conditions [16]. The continuous sintering process is carried out on a traveling grate that conveys a bed of fines or some other finely divided iron bearing material intimately mixed with finely divided fuel such as coke. Near the head or feed end of the grate, the bed is ignited on the surface by gas burners, and as the mixture moves along on the traveling grate, air is sucked through the mixture to burn the fuel by downdraft combustion. As the pallets move continuously over the wind-boxes toward the discharge end of the strand, the combustion front in the bed moves progressively downward. Sufficient heat is created and temperature raises up to sinter the fine ore particles together into porous clinkers [17]. The resulting sinter consists of an aggregate of bonding phases, which result from the melt on crystallization, unmelted (relict ore) and flux particles, as well as pores. For the sinter process, different iron ores are blended with revert material, return sinter, fluxes (e.g.: limestone, dolomite) and coke (coal). Fluxes are necessary in the blast furnace process for slag formation, which has to provide desirable metallurgical properties. The addition of fluxes to the sinter, as opposed to separate addition to the blast furnace, has two main advantages:

- Since the fluxes are homogeneously distributed in the iron-bearing blast furnace burden, the formation of slag phases is enhanced [16].

- The endothermic dissociation reaction of lime now does not take place in the blast furnace, but in the sinter process**.** This removes the necessity for additional heat generation by combustion of expensive coarse coke, limits the level of CO_2 in the reducing gas, resulting in higher caloric values of the top gas, and reduces the loss of fines in the top gas [16].

I.4.2 Reaction zones during the sinter process

After a given time, if a cross-section of the sintering bed is considered in more details, four main parts can be identified. As illustrated in the Figure 2, from the bottom to the top, four different zones can be distinguished:

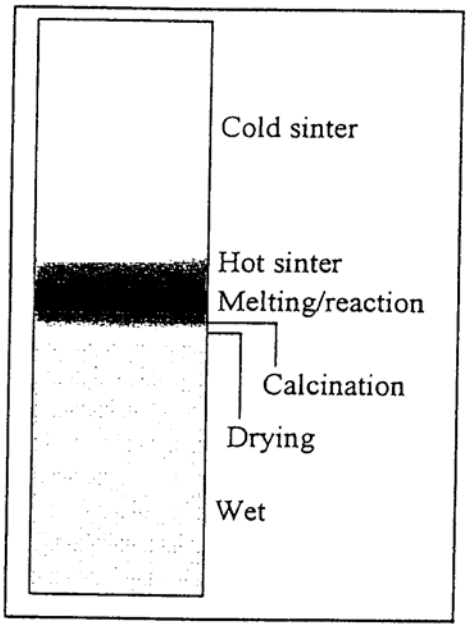

Figure 2 Cross-section of the sintering bed [18].

I.4.2.1 The wet zone

In this zone, the mixture is still cold. The flame front is far away and the air that reaches this zone is cold. This zone is the nearest to the grille.

I.4.2.2 The dry zone

The second zone is that where the mixture is rapidly heated. The water evaporates, and as the temperature increases before the flame front, hydrated lime and limestone dissociate.

I.4.2.3 The combustion / reduction zone

This zone is the flame front itself. In this part, the breeze is ignited and the temperature is the highest. This is called the combustion zone where partial reduction of oxides and partial melt occur with formation of new structures.

I.4.2.4 The cold sinter

The fourth zone is essentially the cooling zone with recrystillization and reoxidation of the porous sinter.

From the thermal point of view, the portion considered above could be assimilated to a system of two heat-exchanges:

The upper heat-exchange and the lower heat-exchange separated by the combustion zone [19].

In the upper heat-exchange, the cooled air is preheated. If the ignition temperature of the combustible is reached (about 700 to 800^{o}C), the combustion reaction increases the temperature of the mixture up to ~1350^{o}C.

In the lower heat-exchange, the hot gas (products of combustion and air excess) preheats the mixture and therefore provides the heats needed for dehydration and decomposition of carbonates. Logically, the combustible content should decrease with increasing in depth in the mixture due to the dehydration and decomposition of carbonates which decrease the amount of heat required by the process. But, because of the presence of the same amount of combustible throughout the sinter, the best sinter is obtained nearby the grate layer due to sufficient heat provided [19].

The high quantity of heat generated through the combustion of the coke breeze causes the fines to react with each other and melt, while larger particles of ore and fluxes partially dissolve into the melt. However, after passage of the flame front, the sinter is cooled by cold air coming in from the top, the melt solidifies and new phases and crystal structures develop, this will be described in more detail later. But, the sinter has heterogeneous structure. Different phases are present in the sinter cake. Because not all the starting materials in the sinter mix react during the process, but portions of the ores and some fluxes remain in their calcined and unassimilated forms, the sintering process seems complicated.

I.5 MICROSTRUCTURE OF FLUXED SINTER

I.5.1 Reactions during the sinter process

Many reactions may take place during the sinter process. These lead to a variety of minerals present in the final product. The reactions that are taking place may occur simultaneously or in a successive order.

The reactions start just when the lime gets in contact with acidic oxides compounds contained in the mixture [19]. Therefore, the calcium silicates, which contain some iron oxides and alumina, form. The new phase is liquid (melting point 1200^0C) and seeps through the big grains of the mixture, which are dissolved progressively [19]. The same author stated that the dissolution rate increases until the flame front passes at the considered point. At this stage, the dissolution of grains is massive or total. This may be favored by the thermal dissociation of hematite in magnetite, which appears at high temperature. The melt-cooling period starts when all the carbon is totally consumed. The gas sucked, at this stage, is only oxidizing the bonded layer. At the same time, holes are made through which reoxidation and solidification occur. The distribution of the temperature inside the material is not regular. Some cracks can appear along the magnetite phase. These cracks and the porosity influence the physical properties of the final product. The melt is saturated in Fe^{3+} and Fe^{2+} ions of hematite and magnetite respectively. These two iron oxides precipitate in the liquid mass or on the oxide grains, which are not entirely assimilated. The nature of the oxide, which precipitates, depends on the Fe^{3+}/Fe^{2+} ratio in solution. Further, the cooling rate plays an important role. In fact, the silicates tend to form either a glass or crystals such as gehlenite, dicalcium silicate while conversely basic oxide such as lime obstructs this phenomenon. Depending on the CaO

content, calcium ferrites can form. The quantities of different phases depend upon the basicity of the mixture and the cooling rate. In addition, at the late stage of cooling, the sinter cake is solid and hot. It oxidizes partially in contact with air. Hence, some of the magnetite transforms into hematite. This is called secondary hematite.

Thermodynamics predict that certain of the reactions in the sinter process are will occur, especially when particles with small sizes are directly in contact with each other (iron oxide and silica in the minerals for instance) [19]. But, since diffusion rates in solid phases are slow and the holding times during the sinter process at high temperatures are short, it can be assumed that diffusion reactions will be very limited.

Some useful ternary diagrams must be considered to justify the order of precipitation during cooling. The main and important diagrams are represented in Figures 3a-c.

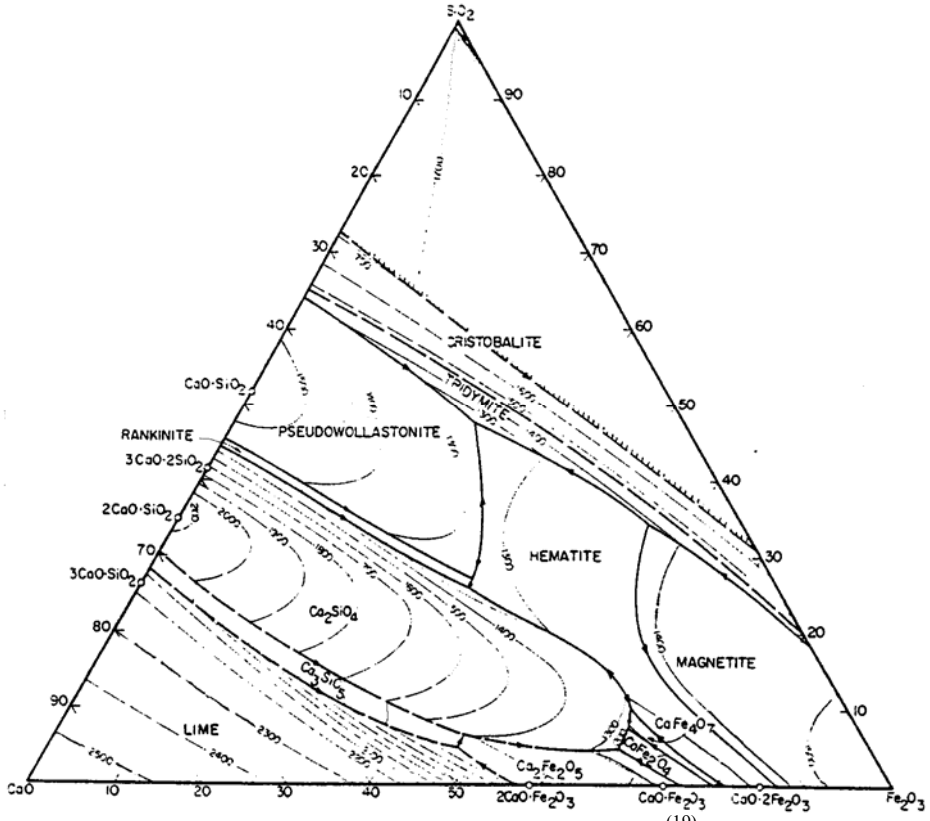

Figure 3a. Ternary diagram CaO- Fe_2O_3-SiO_2[19]

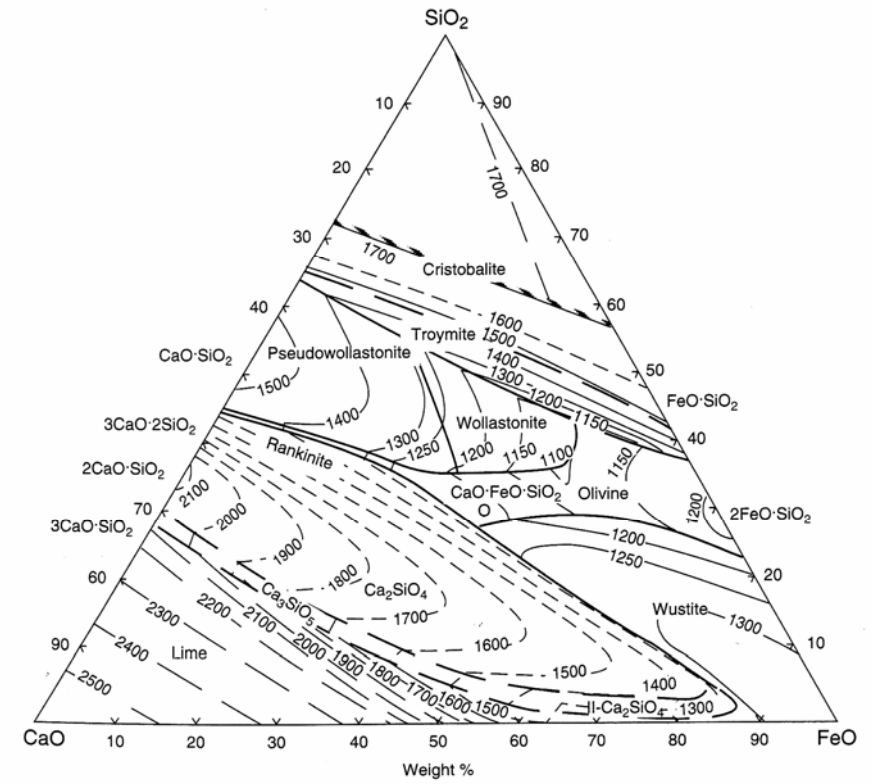

Figure 3b Ternary diagram CaO –FeO- SiO_2[19]

From Figures 3a, b and c, it can be concluded that:

- The initial liquid phase appears at 1200°C and can contain a large amount of Fe^{2+} [19]. This phase can be identified in the system CaO- FeO – SiO_2 (actually a quaternary system CaO- FeO – SiO_2 –Al_2O_3).
- The Fe^{3+}/Fe^{2+} ratio in the liquid phase increases with the CaO content [19]. In fact, CaO decreases the temperature and the viscosity of the liquid. But it favours the oxidation, which is exothermic, of Fe^{2+} to Fe^{3+} (according to $2\ Fe^{2+}_{liq} + ½\ O_{2(g)} = 2Fe^{3+} + O^{2-}_{liq}$). The next is the stabilization of Fe_2O_3 by CaO and whereby the ferrites form [19].
- The ferrite phase, which appears in the sinter of high basicity, is metastable. In fact, according to the binary diagram Figure 3c, it can be seen that CF_2 is not stable below 1155^0C.

  The amount of magnetite increases and the formation of calcium ferrites is retarded with a decrease in oxygen partial pressure [20].

The inability to reach equilibrium due to the flame front that rapidly passes through the sinter bed, the heterogeneity of the mixture and the presence of other oxides such as alumina

(Al_2O_3) and magnesia (MgO) mean that often some other complex other phases can form in the sinter-cake.

Non-equilibrium phases (that are not expected from thermodynamic considerations) can also be found. One such phase is fayalite, which can coexist with a calcium ferrite, although it is thermodynamically expected that these two compounds should react with each other to form calcium silicate and iron oxide as follows [19]:

$$½ \{O_2\} + (Fe_2SiO_4) + 2\ (CaFe_2O_4) = (Ca_2SiO_4) + 3\ <Fe_2O_3>$$

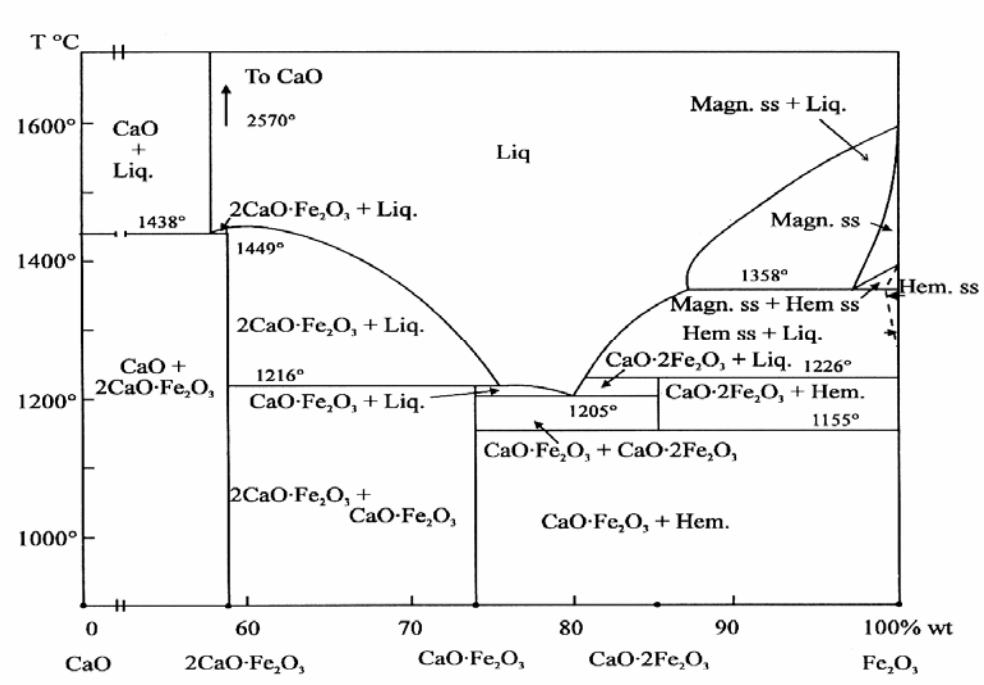

Figure 3c Binary diagram CaO – Fe_2O_3. [19]

I.5.2 Some other useful systems for the theoretical approach to the Sinter process

The formation of melt is of great importance in the production of fluxed sinter. Phase diagrams may be helpful to explain the behaviour of the material during sintering [16]. The main constituents in the fluxed sinters are Fe_2O_3, CaO, SiO_2 and Al_2O_3.

I.5.2.1 The $CaO - Fe_2O_3 - SiO_2$ system.

As abovementioned, local composition or passivity may have an influence on the first melt to form. Generally, the material which can easily melt first is the one with low melting temperature.

From the ternary diagram in Figure 4, two domains with melting temperature below 1300^0C (α and β) can be identified [16]. But, at a specific basicity of 1.5 and below, the first melt formation may result in crystallization of calcium silicates and hematite on cooling. At high basicity with high iron content, the first melt formation may result in crystallization of calcium ferrite on cooling.

There are different possibilities to obtain a melt of type α and β. It is possible to obtain a melt of type β after a solid state reaction between Fe_2O_3 and CaO, whereby a melt which contains high concentrations of iron oxide can form [16]. The same author stated that the abovementioned reaction is known to be faster than the diffusion between CaO and SiO_2 or between CaO and Al_2O_3 and is said to occur at temperatures as low as 600^0C. The diffusion of Ca^{2+}, in the calcium ferrite at 900^0C, is said to be ten times higher if compared with that of Fe^{2+}. Therefore, it can be said that CaO is the first to react with Fe_2O_3 leading to the formation of calcium ferrite at 1205^0C.

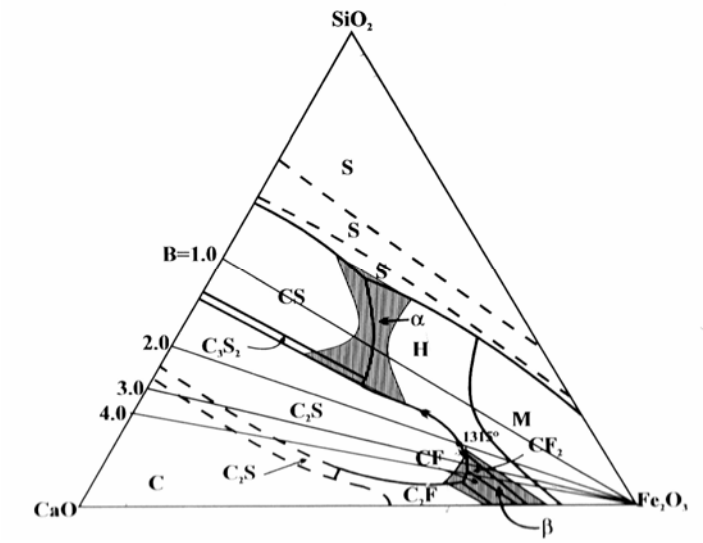

Figure 4 Ternary phase diagram $CaO - SiO_2 - Fe_2O_3$ in air, with melt regions α and β below 1300^0C % wt [21].

For the melt of type α to form, the presence of SiO_2 (in addition to CaO and Fe_2O_3) is said to be necessary from the reaction between hematite and quartz at relatively low rate to form calcium silicates. Thus, the probability to develop such a melt is very low [16].

I.5.2.2 The CaO - Fe_2O_3 - SiO_2 – Al_2O_3 system

Al_2O_3 is very important to stabilize the SFCA phase [3]. From Figure 5.a, it can be seen that the formation of the γ domain is an extension of the β domain [16]. The τ field is contained in the γ domain. From Figure 5.b, it can also be seen that out of the τ field, the solid solution phase $C(A,F)_3$ can crystallize. The entire primary range τ of the ternary solid solution in air, may have an incongruent point and is said to be stable only in contact with melts containing some SiO_2 [16].

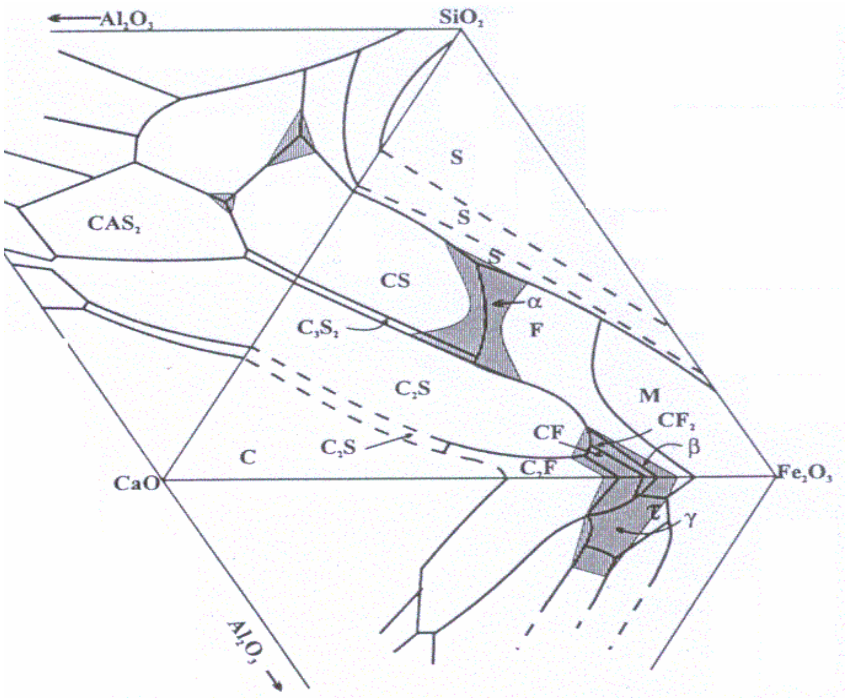

Figure 5.a. The Al_2O_3- SiO_2 – CaO – Fe_2O_3 system [16].

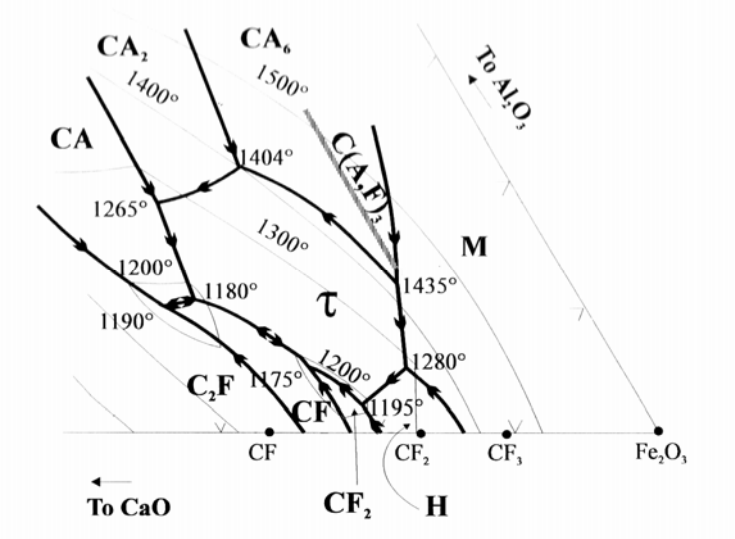

Figure 5.b. Portion of CaO – Al_2O_3 – Fe_2O_3 diagram.[22]

I.5.3 Sinter mineralogy and evolution of the mineralogy in Iron ore sinters

The sinter composition varies from place to place depending on the nature of the individual particles such as ore, fluxes and the extent of reactions between them [20]. The final sinter contains a wide variety of phases. This depends upon the chemical composition of the ore and flux as well as the fuel rate. For the primary requirement of a good sinter, especially a good reducibility and high strength, the types of minerals produced are of great importance. Also, beyond the reducibility and sinter strength, the softening and melting properties are of importance. It has been found that the mineralogical composition has a significant influence on the softening-melting temperature. In the case of iron ore mainly the gangue content determines the softening behaviour, while in the case of sinter not only the gangue content but also the mineral composition influences the softening as well as melting behaviour [2].

Three main types of domains can be identified: relict, matrix and partly reacted. The minerals in iron ore sinters are Hematite (Fe_2O_3), Magnetite (Fe_3O_4), magnesioferrite $(Mg,Fe)_3O_4$, Silicoferrite of calcium and alumina (SFCA) [$M_{14+6n}O_{20+8n}$] and $M_{25}O_{36}$ (with n=0,1 and M= Ca, Fe, Al, Si), anorthite ($CaAl_2Si_2O_8$), Calcium diferrite ($CaFe_4O_7$), Dicalcium ferrite [$Ca_2(Fe,Al)_2O_5$], Dicalcium silicate (Ca_2SiO_4), SiO_2-rich glass, free lime, periclase (MgO) and Olivine $(Mg,Fe)_2SiO_4$ [20]. Their relative proportions depend on the extent of melting and assimilation. Apart from the mineralogy, the porosity is also one of the important parameters,

which influences the sinter properties. The porosity results from the condensation of species, originally present in the raw mix and from combustion, calcinations and melting [23].
Depending on different parameters, such as temperature, composition, oxygen partial pressure, time and atmosphere; different phases form and morphologies develop in sinters [20].

Hematite

The classification is based on the mode of formation of each type of hematite. The most common hematite is relict (unassimilated). Depending on the atmosphere during cooling stage, two secondary types of hematite can form: rhombic hematite and skeletal hematite [20].

a) Relict hematite.

This type is residual from the original ore. It is usually pure with only limited cationic substitution depending on its geological origin [20].

b) Rhombic hematite.

The rhombic type is recrystallized under persistent oxidizing conditions. Different types formed during the cooling include intergrown eutectic forms and dendrites. Smaller crystals may be rounded [20].

c) Skeletal hematite

The skeletal type is formed in the presence of melt with increasing oxygen potential**.** Often this type contains small amounts of Al and Ti in solid solution and occurs as large crystals full of inclusions [20].

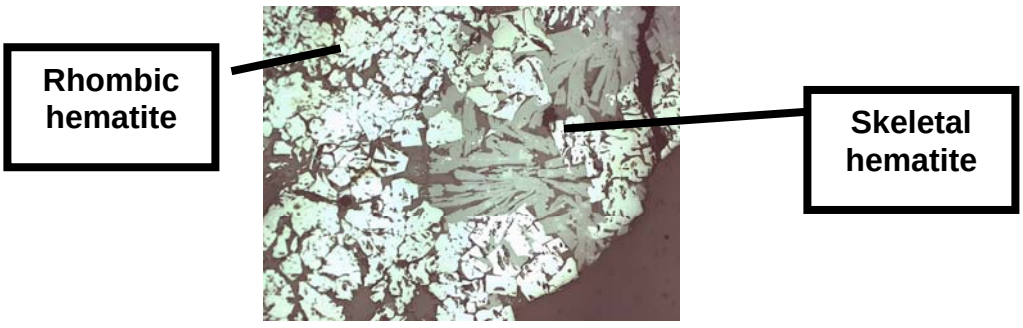

d) Finely granular hematite

Finely granular hematite is referred to as pseudo-relict hematite, which is mainly formed from goethite with clay gangue. This gives rise to readily forme siliceous, viscous melts. The melt (mainly

consisting of Fe_2O_3 and CaO) is generated at about 1200^0C and the iron oxides and sub-materials assimilate with it. If at this time the melt penetrates into the boundaries between the hematite grains in the coarse ores, interfacial break occurs and granular hematite is generated [9].

e) Hematite late stage.

The hematite late is generated from the solid state oxidation on cooling [20].

Calcium ferrite

The main bonding phases and phases that influence sinter properties the most are calcium ferrites [20]. The calcium ferrites can constitute up to 50% v/v of the mineral composition of fluxed sinter [16, 24]. Calcium ferrite, as a mineral produced in the sintering process, usually contains some silica and aluminium as well as small amounts of FeO, MnO and MgO. This is referred to as silicoferrite of calcium and aluminium (SFCA). The formula reported is $5CaO.2SiO_2.9(Fe,Al)_2O_3$ [10]. It was established that the addition of SiO_2 was more effective than the addition of Al_2O_3 for increasing the melting rate and reducing the melt formation temperature in calcium ferrite system while the addition of Al_2O_3 was more effective than the addition of SiO_2 for increasing the dissolution rate of solid hematite into the generated molten ternary calcium ferrite [25].

From the $CaO\text{-}Fe_2O_3$ binary diagram in Figure 3c, it can be seen that the main reaction products are calcium ferrite (CF) and dicalcium ferrite (C_2F) at 1100 ^{o}C. At 1150 ^{o}C, SFCA can be determined, C_2F is still present and calcium diferrite has disappeared. The calcium ferrite referred to as calcium diferrite (CF_2) is stable only between 1155^0C and 1226^0C.

a) Silicoferrite of Calcium and Aluminum (SFCA).

The SFCA plays an important role in the sinter properties. The SFCA is said to promote the high-temperature reduction properties of iron ore sinters by retaining a high concentration of high fine porosity [26]. From the formula above, it can be seen that there is neither FeO nor Fe_3O_4 in the SFCA phase, but Fe_2O_3. Thus, the lower the FeO content the more the SFCA.

Studies conducted in-situ X-ray diffraction (XRD) on the formation of the SFCA suggested the following mechanism [24]:

From the starting materials including hematite, calcite, gibbsite and quartz, different steps were observed and are said to proceed as follows:

1.Starting materials: hematite, calcite, gibbsite and quartz

2.From ~200^{o}C, Gibbsite decomposition.

$$Al(OH)_3 = Al_2O_3 \text{ (amorphous)} + 3H_2O$$

3.From ~600^{o}C, Calcite decomposition:

$$CaCO_3 = CaO + CO_2$$

4.From ~ 750^{o}C, formation of C_2F (dicalcium ferrite) according to the reaction:

$$2CaO + Fe_2O_3 = Ca_2Fe_2O_4$$

5.From ~950^{o}C, formation of CF (calcium ferrite):

$$Ca_2Fe_2O_5 + Fe_2O_3 = 2CaFe_2O_4$$

6. From ~1000^{0}C, formation of SFCA-I and SFCA:

$$CaFe_2O_4 + Fe_2O_3 + SiO_2 + Al_2O_3 = \text{SFCA-I} + \text{SFCA}$$

7. From ~1200^{o}C, the SFCA-I is consumed in the production of SFCA as follows:

$$\text{SFCA-I} + Fe_2O_3 + SiO_2 + Al_2O_3 = \text{SFCA}$$

The correlation between the amount of different phases and temperature is shown in Figure 7.

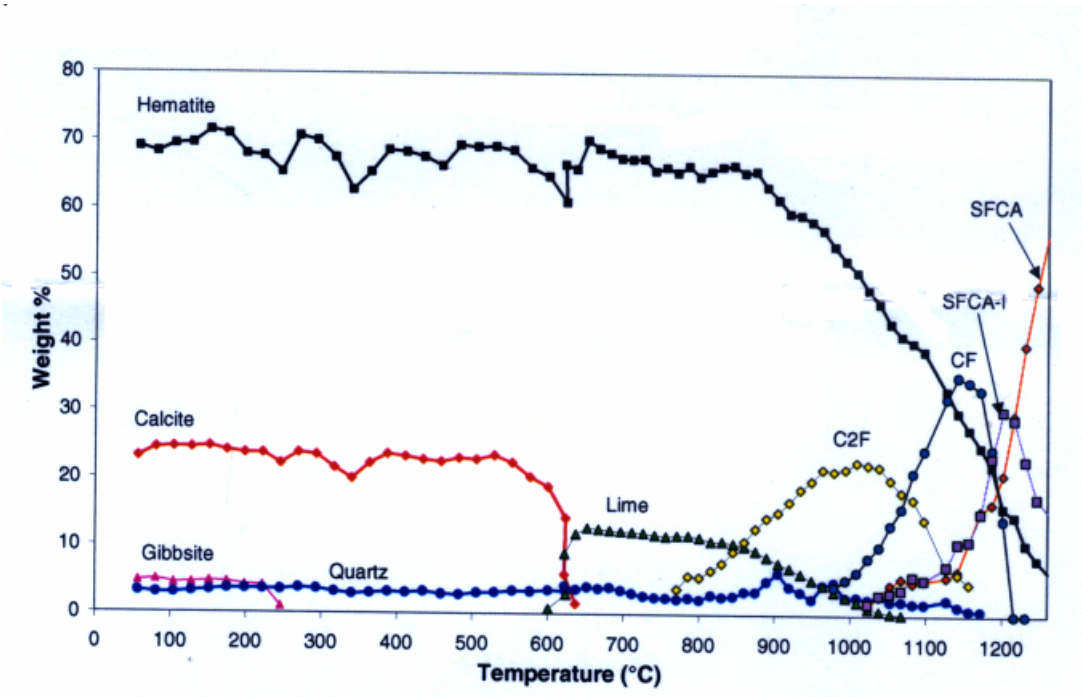

Figure 7 Quantitative phase analysis of sinter as function of temperature [24]

The SFCA-I phase is the most desirable bonding phase in iron ore sinter since microstructures composed of SFCA-I show higher physical strength and higher reducibility than microstructures composed predominantly of SFCA [7]. The same authors stated that lower Fe grade (< 62% Fe) ores and concentrates typically form SFCA as part of the final assemblage while medium grade (62 – 65% Fe) ores forms a mixture of SFCA and SFCA-I and high grade (65-68% Fe) ores forms largely SFCA-I. Different structures of SFCA include SFCA ($M_{14}O_{20}$; Hamilton et al., 1989), SFCA-I ($M_{20}O_{28}$; Mumme et al.; 1998) and SFCA-II ($M_{34}O_{48}$; Mumme, 2003) have been reported [24].

I.5.3.1 Morphology

The morphology essentially reflects the mode of formation and is related to a particular chemical composition, heating and cooling rate.

At lower temperatures the SFCA forms more slowly and is retained longer while at high temperatures it forms and disappears rapidly [1]. The same authors stated that, the holding sintering time plays an important role in producing more SFCA. From Figure 8, it can be seen that more SFCA can be obtained at lower temperatures if there is enough time for sintering to take place than at high temperatures.

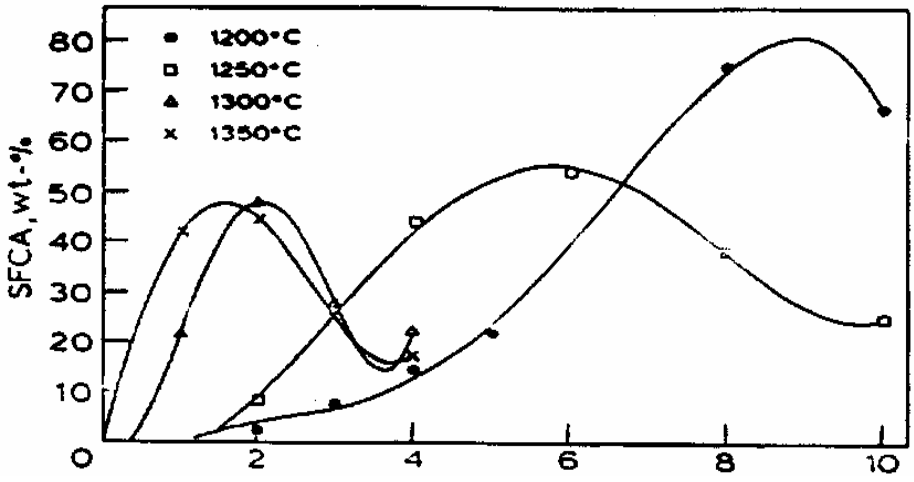

Figure 8 Variation of percent SFCA with time (min) for different temperatures [1].

Three types of morphologies are generally defined:

- Acicular: needle-like.
- Columnar: large crystals.
- Dendritic: very small, tree-like.

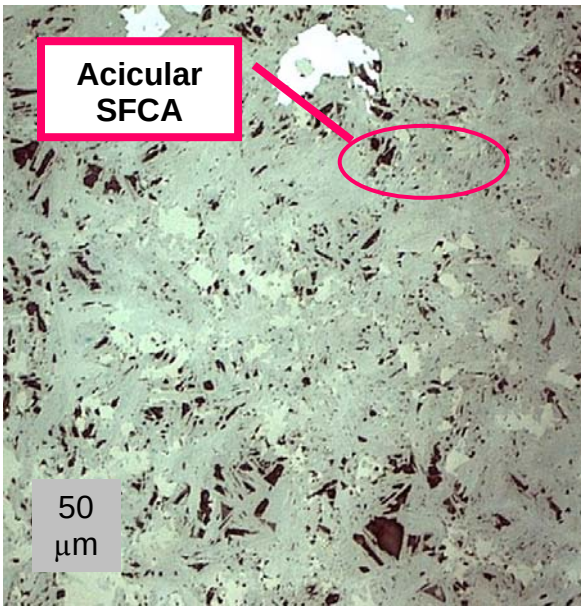

Figure 9a. Acicular SFCA

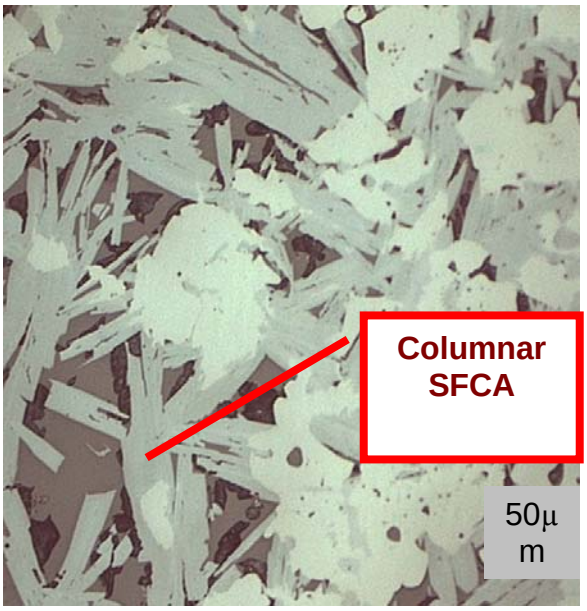

Figure 9b. Columnar SFCA

The mechanism of formation of the acicular SFCA was studied. The formation was measured during the experiment using SEM. It was reported that lime reacted first with hematite [27]. The same authors explained that the resultant monocalcium ferrite melt formed above about 1200°C. The acicular calcium ferrite forms as a solid solution phase from the reaction between hematite in the ore and the Fe_2O_3 – CaO melt that contains small amounts of SiO_2 and Al_2O_3.

Another property, which cannot be neglected, is the viscosity. A low viscosity melt is very fluid and the solidification rate of such a melt is very high. Consequently, this allows very little time for SFCA to precipitate out [1].

The acicular calcium ferrite has been reported to form during heating as well as cooling stages depending on the oxygen potential [8]. Using a specimen containing hematite or magnetite and heating it up to 1180C, the acicular calcium ferrite was formed in a gas mixture of CO= 1%, CO_2=24%, N_2= 75% (with $pO_2 = 2.10^{-8}$atm calculated from gas composition and temperature) and at a higher oxygen partial pressure of 5.10^{-3}atm [13]. But no acicular calcium ferrite formed in a gas mixture of CO= 8% and CO_2= 92% (pO_2=5.10^{-9}atm). However, with magnetite ore, the acicular calcium ferrite was not formed in pure CO_2 gas (pO_2= 2.10^{-4}atm),

but formed at a higher oxygen partial pressure of 5.10^{-3}atm (on the surface of the specimen). Also, the amount of the acicular calcium ferrite increased with the oxygen potential. Therefore, it might be concluded that a higher oxygen potential favours the formation of acicular calcium ferrite in the heating stage; the acicular calcium ferrite is produced from a hematite ore mixture at lower oxygen potential.

It was also reported that other research revealed at increasing temperatures (>1250^{0}C), the calcium ferrite may transform to hematite at high pO_2, or magnetite at low pO_2, both in a calcium silicate melt [16]. The same author added that the pO_2 may be governed by the combustion of the coke breeze. As consequence, in oxidizing cooling stage, magnetite reacts with the calcium silicate melt and oxygen to produce a large amount of calcium ferrite and tertiary hematite [16].

b). Calcium diferrites and dicalcium ferrites.

It has been reported that the type of ferrite depends on the oxygen partial pressure. The dicalcium ferrite forms in neutral and reducing atmospheres while the calcium diferrite forms in oxidizing atmospheres [1].

I.5.3.1.1 Magnetite

During the sintering process, in the melting zone the temperature increases and the conditions are reducing. Therefore, the hematite from the ore is being reduced to magnetite. The presence of magnetite in the sinter greatly influences the sinter properties. This is discussed later. Magnetite is difficult to distinguish from magnesiospinel at the microscope, reason why magnesiospinel, with its general chemical formula [(Mg, Fe)O.Fe_2O_3)], is then quantified. This phase is said to be more stable than magnetite due to the solid state diffusion of Mg^{2+} which replaces some of the Fe^{2+} from the magnetite lattice [28].
There are two genetic types, unassimilated magnetite and crystallized magnetite from the melt. The unassimilated type is found in a number of ways depending on the nature of the original ore. Much magnetite is anhedral, often with resorbed margins to calcium ferrites as a

result of their incongruent crystallization. Usually, ionic substitution by Al, Mg, Mn, Ca, etc. is limited, although a wide range is possible [20].

During the cooling stage, the magnetite tends to react with the silicate melt and oxygen to generate calcium ferrite at a medium oxygen partial pressure of about 10^{-2}atm [12].
In contrast, hematite can be formed from magnetite at high oxygen potential of about 5.10^{-2} atm [12]. However, acicular calcium ferrite may also be generated from magnetite ore at higher oxygen potential during the heating stage of sintering [12].

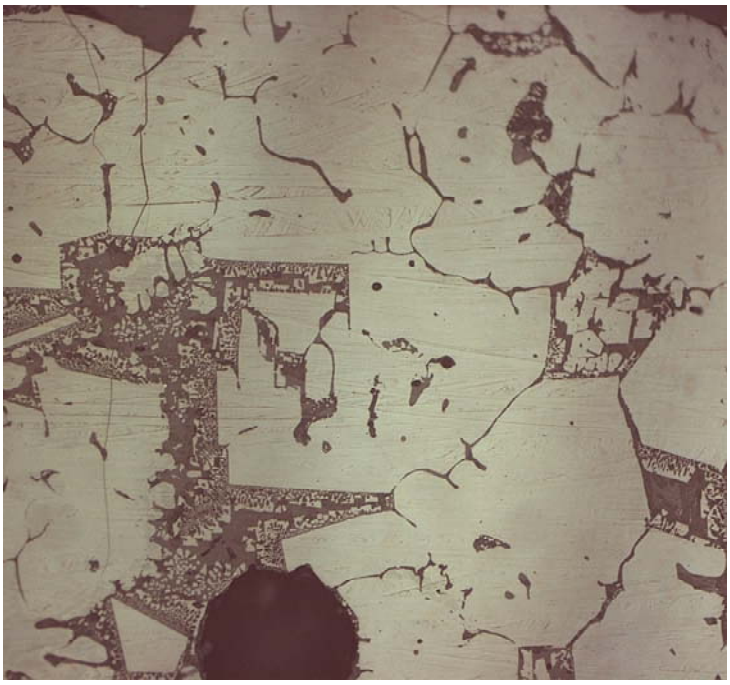

Figure 10 Crystallized magnetite from the melt.

This means that even from magnetite as iron ore, it is also possible to generate desirable sinter phases. But, many parameters such as oxygen potential, temperature must be taken in account which will make the process very difficult to control.

I.5.3.1.2 Glass and Calcium silicates

Calcium silicates have been reported to form a matrix to the main Fe-bearing phases, dicalcium silicate being the most common. Some other silicates may also occur. Among them are Kirschsteinite ($CaFeSiO_4$), melilite $\{(Ca,Na)_2(Mg,Al,Fe)[(Al,Si,)_2O_7]\}$, merwinite ($Ca_3MgSi_2O8$), anorthite ($CaAl_2Si_2O_8$) and some other silicates [20].

I.5.3.1.3 Relict particles

The relict particles consist of large iron ore particles, fluxes (olivine) and any raw material that was added. It is said that sometimes no reaction between particles takes place partially due to the particle size, sintering temperature or chemical composition [16].

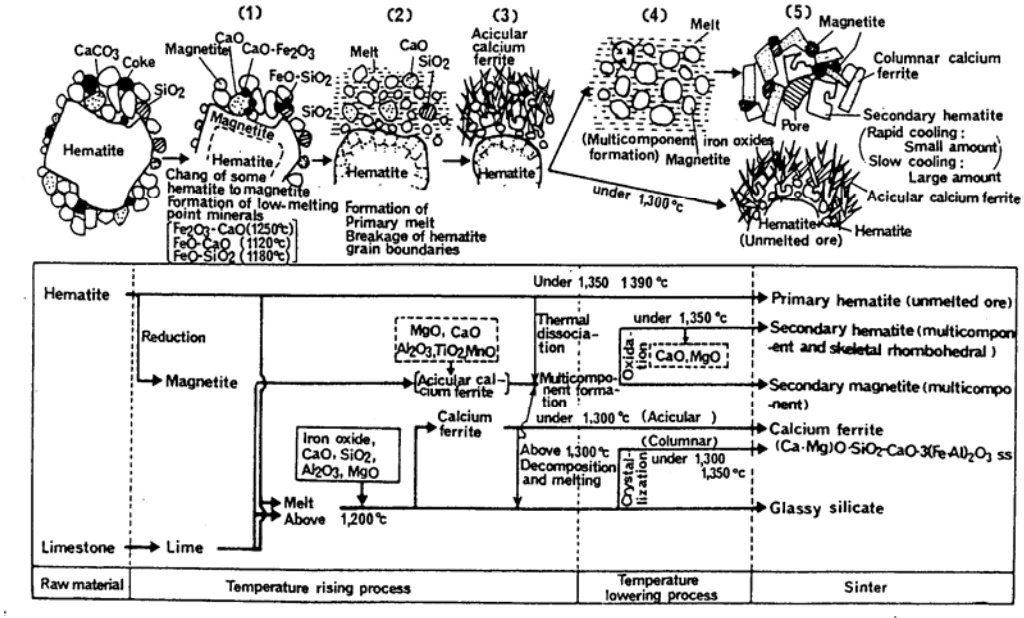

Figure 11 Schematic diagram of sintering reaction process [9].

According to Figure 11, it can be seen that four periods can be distinguished in the sintering process. They include fresh raw material, rising temperature period, lowering temperature period and sinter product. During the temperature rising period, limestone is decomposed in lime and carbon dioxide while some hematite changes to magnetite and low-melting minerals form. This mainly includes Fe_2O_3 - CaO, FeO – CaO, FeO-SiO_2 which form at temperature about 1250^0C, 1120^0C and 1180^0C respectively. During the second period, particles are fused partially and the primary melt forms with a breakage of hematite grain boundaries leading to the formation of calcium ferrite, acicular at a temperature below 1300 ^{0}C and columnar above 1300^0C. During the lowering temperature period, depending on the cooling rate and the atmosphere, different phases can be obtained. Under 1300^0C, the formation of acicular calcium ferrite is favorable. But depending on the cooling rate, large amounts of acicular

calcium ferrite can form with slow cooling rates, while small amounts are formed on rapid cooling. In contrast, above 1300^0C columnar calcium ferrite is formed [13].

I.6 SINTER PROPERTIES

Generally, the sinter quality is defined as a combination of the following properties:

- The cold strength
- The Reduction Degradation (RDI) at low temperatures.
- The high temperature properties: Softening and melting
- The reducibility of the sinter.

I.6.1 Cold strength

The strength of sinter particles has been reported to be closely related to the production yield and therefore productivity of the sintering process [29]. During the transportation and charging into blast furnace, degradation of the sinter must be minimized; thus high cold strength is required. The sinter is a porous, brittle body with many internal cracks. Sinters with many cracks and large pores of about 100 microns or more show a high disintegration degree in tumbler strength tests [9].

It has also been established that metallurgical and physical sinter properties are strongly related to the mineralogy, microscopic and macroscopic structure [30]. Also, sinter in which the melt bridges the relict particles generally has a high cold strength [16].

I.6.1.1 Influence of the Mineralogy on the cold strength

It has been established that the cold strength of the sinter is related to the pore microstrength in it, reacted and relict domain, composition and matrix basicity as well as slag volume [20]. Further, it was reported that if the sinter does not have many cracks and large pores, its strength is governed by the state of dispersion of hematite, magnetite and calcium ferrite in the glassy silicate phase, which is the continuous matrix in the sinter [9].

Furthermore, it has been found that MgO influences the cold strength. It has been stated that in acidic sinter with up to 4% MgO the tumbler strength increases [28]. This has been attributed to the fact that pyroxene and olivine precipitate in the glass phase with high degree of recrystallisation. In addition, it was stated that the high concentration of stress shown by the vitreous matrix and the formation of melt of low concentration during the sinter process result from the addition of MgO [28]. Such sinter is said to have high porosity which results in a sinter with low strength [28].

But, in superfluxed and self-fluxing sinters, the tumbler strength is reported to decrease with the addition of MgO [31, 28]. Also, it was reported that MgO addition is of great influence on the sinter mineralogy because it suppresses the formation of calcium ferrites while it increases the formation of the vitreous glass matrix in certain slag pools [28]. Due to the thermal expansion and contraction between the glass phase and the crystalline phase it encloses, the vitreous glass exhibits a high degree of stress. These structures have been found to be harmful to the sinter strength, and hence resulted in a remarkable drop in sinter tumbler index [28]. The same authors have found that at about 697^{o}C, the dicalcium silicate undergoes an allotropic transformation from β-$2CaO.SiO_2$ to ϒ-$2CaO.SiO_2$. This allotropic transformation is accompanied by a large volume change, which causes stress to develop leading to dusting under load. But, this can be avoided if extra coke is added [28].

Further, it was reported that a decrease in silica content from 4.6 to 4.3 mass% to increase the basicity from 1.85 to 1.98 and a decrease in MgO from 1.2 to 0.9 mass%, the tumbler index has been improved [3]. The same author established that the dense low alumina iron ores form sinters of higher tumbler strengths.

I.6.1.2 Test procedure

According to ISO 3271 (1995 E), a test portion of 15 Kg tumbled is used in a circular drum with the following characteristics [32]:

- Internal diameter: 1000 mm
- Internal length: 500 mm

- 25 r/ min ± 1 r/min
- Total of revolutions: 200

Sieving with test sieves, this test includes square apertures of 6.30 mm and 0.5 mm.

Each size fraction is weighed out, thus the tumble index (TI) as well as the abrasion index (AI) can be calculated as follows:

$$TI = (m_1 / m_0) * 100$$

$$AI = [\{m_0 - (m_1 + m_2)\}/ m_0] \text{ X } 100$$

Where:

m_0 = mass of the test portion, in kg, weighed and placed in the tumble drum

m_1 = mass of + 6.30mm fraction test portion of the tumbled, in kg

m_2= mass of – 6.30 mm + 0.5 mm fraction of the tumbled test portion, in kg

I.6.2 Reduction disintegration

In the upper part of the blast furnace shaft, the permeability of the burden may be influenced by the breakdown of sinter upon reduction. This is referred as Reduction degradation [15, 33]. Also, the degradation of sinter during reduction in the upper part of the blast furnace may depend on the reduction degradation index and the temperature profile, especially heating rate at about 600^{o}C [34]. The reduction disintegration Index is defined as a quantitative measure of the disintegration of the sinter that could occur in the upper part of the blast furnace after some reduction [35]. Sinter with low reduction disintegration generates fines in the top of the furnace; this affects the flow distribution within the blast furnace.

I.6.2.1 Influence of the sinter Mineralogy on the reduction degradation

The degradation of the sinter during reduction has been reported to be caused by an expansion of the iron oxide phase resulting from the reduction of hematite to magnetite, which is

accompanied by a volume increase [33, 18]. The same authors stated that due to the volume increase, stresses can initiate cracking within the surrounding material. Upon further reduction, these cracks are said to be responsible of the propagation and branch out, which can ultimately lead to fragmentation of the sinter material. However, a porous structure of the ferrite can absorb such stresses, thus preventing crack development. But, major cracks do not appear to be arrested by the ferrite pores once they have developed [14].

Also, the presence of columnar calcium ferrite, glassy silicate and skeletal rhombohedral hematite increase the degradation. The skeletal rhombohedral hematite is suggested to be a major cause for high degradation values. As reported at a low basicity, the addition of MgO decreases the hematite content and leads to the formation of magnesio-spinel phase [33, 18]. However, the same authors stated that even if MgO is not added, in spite of higher hematite; at higher basicity the sinter RDI has been found to be low. This has been attributed to the sinter structure at higher basicity which consists of a continuous ferrite frame which is able to arrest the propagation of cracks initiated at the hematite crystals. Also, it has been reported that the reduction degradation decreases with increasing alumina while it increased with increasing MgO and increased with just a slight increase in basicity [3]. The same author stated that for a more increase in basicity, the reduction degradation decreased. Also, it was reported that sinters with higher additions of alumina and TiO_2 show a relatively high intensity of disintegration [5]. Moreover, the titanium content was reported to deteriorate the sinter in terms of RDI [34].

I.6.2.2 Test procedure

This is a part of ISO 4696-1 (1996E). The principle consists of a test portion of specified size range. This is subjected to static reduction at a temperature of 500^0C using a reducing gas consisting of [37]:

CO: 20 % (V/ V) ± 0.5 %(V/V)

CO_2: 20% (V/V) ± 0.5% (V/V)

H_2: 2.0% (V/V) ± 0.5 % (V/V).

N_2: 58% (V/V) ± 0.5% (V/V).

The test portion is cooled to a temperature below 100^0C and tumbled using a tumbler drum of 130 mm (inner diameter), after 1 hour reduction time. The number of revolutions is fixed to 300 in total. The test portion is then sieved with test sieves, which have square mesh apertures of 6.30 mm, 3.15 mm and 0.5 mm. The reduction disintegration index (RDI) is calculated as follows:

$$RDI\text{-}1_{+6.3} = [m_1/ m_0] X100$$

$$RDI\text{-}1_{-3.15} = [\{m_0 -(m_1 + m_2)/ m_0\}] X100$$

$$RDI\text{-}1_{-0.5} = [\{m_0 (m_1 + m_2 + m_3)\}/ m_0] X100$$

With: m_0 = mass in grams of the test portion after reduction and before tumbling

$m_{1,2,3}$ = mass in grams of the oversized fraction retained on the 6.30, 3.15, 0.5 sieves respectively.

I.6.3 Reducibility

The reducibility depends on the gas accessibility i.e. the pore and surface structure, the intrinsic reducibility of the minerals and their assemblages, and the additional surface area generated during reduction as a result of the inherent volumetric changes that take place.

The variation in reducibility has been reported to be related to the micro-pores and mineralogical structure [38]. The same authors found that the reducibility increased with increasing basicity. The Figure 12 shows the influence of the basicity on the reducibility of a sinter for a small cracked sinter.

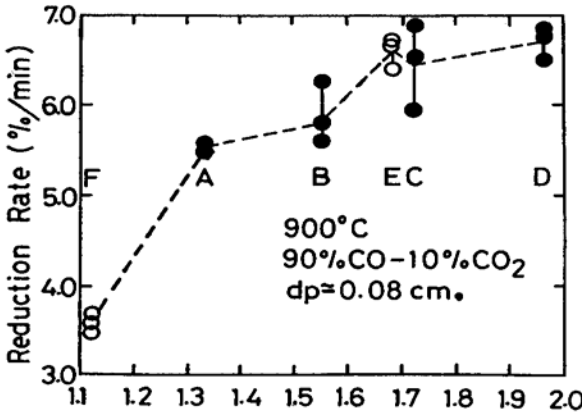

Figure 12 Reducibility rate variation with basicity [38]

I.6.3.1 Influence of the Mineralogy on the sinter reducibility

It has been established that finely granular hematite, relict hematite, acicular ferrite and rhombic hematite matrix assemblages are reducible [23]. Also, it was reported that high FeO sinter blended with high coke breeze addition to high MgO content have low reduction degree while low SiO_2, low CaO and high MgO sinter has high reducibility [33, 17].

The addition of MgO has been reported to accelerate the thermal decomposition of Fe_2O_3 and to favour the formation of less reducible Fe_3O_4 ($FeO.Fe_2O_3$)-Mg phase [28].

Also, the MgO addition restricts melt formation, this is reported to lead the increase in porosity of the sinter, which in turn provides more surface area exposed to the reducing gases, resulting in higher reducibility and reduction degradation index [28]. Further, it has been established that an increase in pisolitic ore could also improve the reducibility of the sinter [3]. This was sustained by the increase in fine porosity of the sinter [28]. Furthermore, it has been established that lowering the amount of silica, while keeping the basicity constant; would cause an increase in reducibility because the amount of silicate slag, which has low reducibility compared to hematite; would decrease [39]. The same authors reported that the solid state or solid-liquid reaction between CaO and Fe_2O_3 leads to the formation more SFCA when dolomite is used than serpentine. This was essentially related to small distance between MgO and CaO in the dolomite. A small distance leads to an active reaction between MgO and SFCA. Thus, more Mg is found in SFCA. They also reported a strong relationship between Mg and Si content in SFCA. The more the Mg content in SFCA phase, the more Si is present in the SFCA phase, which is the main cause of the decrease in the amount of silicate slag. Serpentine has an MgO-silicate structure which is stable at elevated temperatures compared to dolomite which is more reactive after its dissociation.

I.6.3.2 Test procedure

This is done according to the ISO 4695:1995(E). In a fixed bed at 950 ^{0}C, using a reducing gas composition consisting of 40% v/v of CO and 60% v/v of N_2 a test potion is reduced isothermally. The test portion is weighed at specified time intervals and the weight loss is calculated.

I.6.4 High temperature properties

High temperature properties are generally evaluated by softening, melting and dripping temperatures during reduction at temperatures above1150^{0}C. At a certain temperature the bed height starts to decrease, as a result of the deformation of the bed components. This phenomenon is referred to as the onset of softening. It is usually associated with a concurrent decrease in the reduction rate. Further, the onset of melting is usually referred to the temperature at which melt starts to drip from the bed [40].

The softening, melting and dripping temperatures may increase with increasing basicity CaO/SiO_2 up to 1,6 and decrease again at higher basicity. Also, the permeability of the burden is less distributed when a narrower interval exists between the softening and melting temperatures of the material. Also, the addition of MgO up to two percent may lead to increasing softening, melting and dripping temperatures [8]. However, the same author emphasized that a further increase in MgO may lead to decreasing melting temperatures.

I.6.4.1 Influence of the Mineralogy on the high temperature properties

Calcium ferrite such as SFCA plays an important role in determining the high temperature reduction properties of ferrous materials. During reduction, total porosity is said to increase with time. Also, the addition of MgO has been reported to have an influence on the softening –melting characteristics of sinter.

It has been established that with increase of MgO, the softening-melting characteristics of sinter improve [28]. The same authors found that by increasing the sinter MgO content from 2.3 to 3.2%, the softening and the melting start temperatures increased from 1305 to 1391^{o}C and from 1467 to 1525^{o}C respectively. Also, it was found that sinter with basicity ranging between 1.0 and 1.5 have low drip temperatures, which was related to low liquidus temperature, low viscosity and fast smelting-reduction of slag [6]. The same authors added that the dripping temperature decreased with decreasing A_2O_3 content and increasing MgO content in the sinter for the basicity range 1.0 – 1.5. It has also been reported that low SiO_2 and low CaO sinter have good sinter properties while high MgO sinter using dolomite instead of serpentine have better softening properties [39]. The same authors added that sinter containing

high FeO, high MgO and high coke breeze have better softening properties while the effect of Al_2O_3 content on softening properties is negligible.

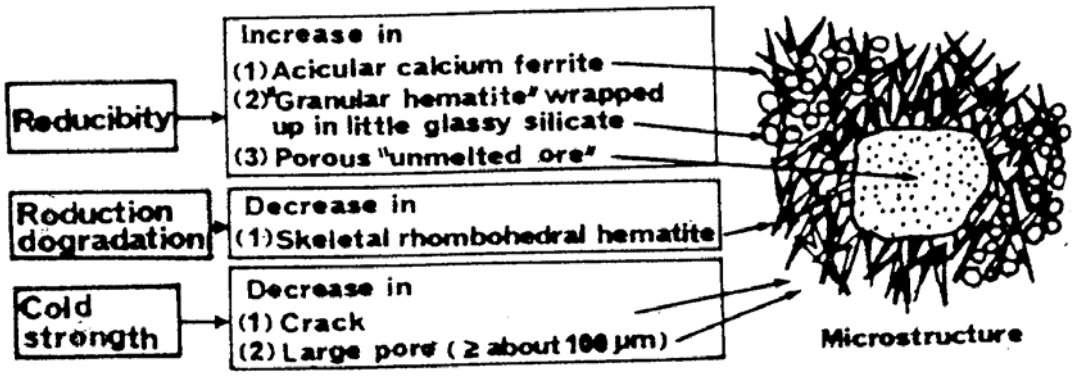

Figure 13 Image of high reducibility sinter with low degradation property [9]

In Figure 13 the desired mineralogy and morphology for the different sinter properties are summarized.

I.7 CONCLUSION

From the literature, the correlation between mineralogy and sinter properties is clearly stated. Investigations into sinter mineralogy and sinter quality have for long been conducted. It has been reported that the chemistry of iron ore and variation in process parameters determine the sinter structure which, in turn, governs the sinter quality [1, 2, 3, 4]. Studies on tablets samples as well as sinter pot samples to evaluate the influence of some parameters such as Al_2O_3/SiO_2 ratio, basicity and TiO_2 contents on the sinter structure have shown that there is a relationship between sinter structural composition and its size degradation under low temperature reducing conditions [5]. Further, a study on optimization of chemical composition and microstructure of iron ore sinter for low-temperature drip of molten iron with high permeability has established that the basicity had a dominant influence on dripping temperature while low alumina content and high MgO led to achieve low dripping temperature [6].

Furthermore, the effect of raw material composition on sintering properties has shown that the presence of high alumina and TiO_2 led to stabilization of calcium ferrite and hematite respectively while sinters with higher addition of alumina and TiO_2 showed a relatively high intensity of disintegration as well as high degradation reduction values [3].

Also, nowadays alternative materials are being tested to replace part of the ores or fluxes seeking to obtain a better performance of sintering mix in the process and a sinter that had a good performance in the Blast Furnace. It was reported that in spite of alternative materials, the determination of microstructural aspect is still very important in the evaluation of the sinter quality [7]. The sintering process being a further complicated process by the fact that not all the starting materials in a sinter mix react during the process, but portions of ores and some fluxes remain in their calcined and unassimilated forms, suitable measures must be taken in preparing the sintermix [2]. Although every precaution is taken to mix the raw materials thoroughly, it is impossible to prevent local inhomogeneities on a microscopic scale. Local differences of different chemical compounds in basicity, different concentrations of coke and absorbing materials such as lime and water cause local variation, which is observed on the microscopic scale [8].

Main phases include hematite, magnetite, ferrites, glass and silicate phases. The degree of solid solution varies throughout the sinter. It is reported that in order to improve the homogeneity of the composition of the sinter measures must be taken to well mix the raw materials. On the other hand, the macroscopic structure of sinter is not uniform, with large pores and a high permeability. The macroscopic pores yield a highly permeable burden in the blast furnace while on a microscopic scale it is a complex aggregate of phases. The combination of the macroscopic and microscopic structure determines the sinter properties.

The cold strength is reported to be determined by pores, relict hematite, basicity and composition, as well as slag volume, and domains which have reacted [9].

The reducibility is reported to improve with high accessibility of the gas as well as high diffusion rates [10]. The variations in compositions of the raw materials also play a big role in the heterogeneity of the phase composition and therefore influence sinter properties. The addition of MgO or increasing MgO/CaO ratio increases the porosity of sinters [11]. The same authors reported that the increase in open porosity improves the reducibility of the sinter and demonstrated that SFCA stabilizes fine porosity. Therefore, a sinter with good reducibility may be one with a large amount of acicular SFCA and minor columnar and blocky SFCA. This structure has no cracks and no large pores, which improves the cold strength. The disintegration of the sinter is generally attributed to the volume change associated with the

reduction of hematite to magnetite [6]. Stress may develop during the reduction of hematite to magnetite and are absorbed by a porous structure of calcium ferrite [6]. But, the decrease in reduction degradation is related to the abundant skeletal hematite. In turn, high basicity, SiO_2 content, Al_2O_2/SiO_2 ratio as well as temperature, oxygen potential and the composition of the raw materials influence the amount of SFCA [9, 12]. The quality of sinter is therefore determined by the properties of the individual phases and the interaction between them [13, 14].

Therefore, although a number of studies on the influence of chemical composition of the raw mix, the basicity, MgO content as well as the addition of alternative materials on the sinter microstructure have been conducted, the evaluation of sinter quality by varying the composition of the raw mix and considering some possible scenarios by combining the basicity, MgO, SiO_2 as well as Al_2O_3 contents still need further investigations.

Chapter II EXPERIMENTAL

Included in this chapter are the experimental procedure and the sinter compositions.

The experimental procedure gives a brief description on the preparation of the sinter mixture (raw materials used and their proportions in the mixture), the set-up used for agglomeration, the production of sinter as well as the sample preparation for the evaluation of sinter properties. The sinter compositions include the preparation of different categories of sinters and the specifications and conditions under which different experiments were performed.

II.1 PROCEDURE

The raw materials consisted of a mixture of iron ore from Sishen and Thabazimbi mines and different raw materials used in the sinter plant namely dolomite, lime, coke and return fines. The composition of the sinter mixture was adjusted in order to obtain a basicity ratio (mass%CaO / mass%SiO_2) of two and a FeO content that range between 7.0- 9.0 %. The dry raw materials were weighed into the required proportions and then mixed dry in a rotary drum mixer. A desired granulation resulted from a further mixing for six minutes after water and $FeCl_3$ have been added. $FeCl_3$ was added to allow alkalis removal on during sintering.

The sinter experiments were performed in a sinter pot at the pilot plant of Kumba Iron Ore (Pretoria West / South Africa). The sinter pot test conditions were simulated to the real plant conditions.

After mixing, the raw materials were fed into the sinter pot via a conveyor onto a grid layer consisting of – 40mm +20mm sinter particles, 50mm in height. This was done in order to avoid fine particles to be removed in the off-gas. After feeding the sinter pot, the bed was ignited using a gas flame, sintered and cooled down. The sintering process ended when the off-gas reached the highest temperature and started to decrease. The sinter produced was then broken and sieved into different size fractions. The sinter pot test equipment is schematically shown in Figure 14.

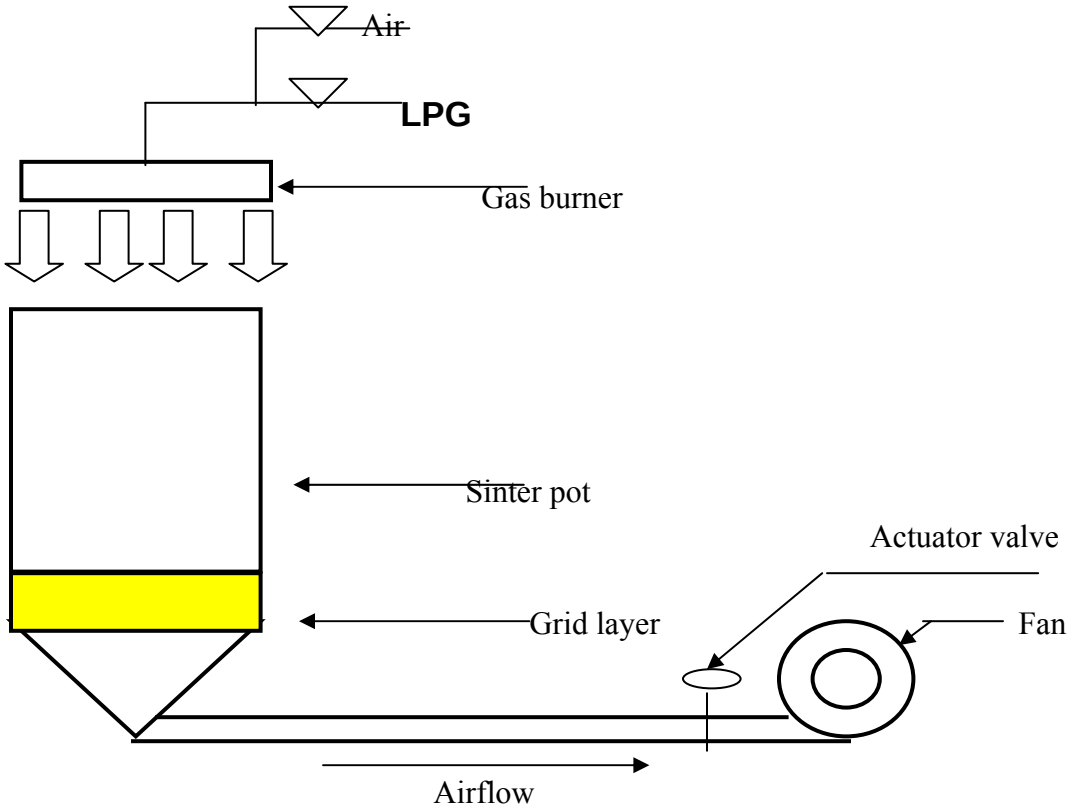

Figure 14 Sinter pot test equipment

Apart from the ignition temperature, other parameters such as ignition time, ignition pressure drop, sintering pressure as well as the cooling pressure drop were kept constant for all the sinter pot tests.

II.1.1 Sampling and analysis

Samples were taken for the evaluation of the cold strength, reduction degradation and reducibility of each sinter as described in Chapter I (paragraphs I.6.1.2, I.6.2.2 and I.6.3.2 respectively). The -12mm +10mm size fraction sinter was further crushed:

1. Micronized for XRD analysis
2. -2mm for SEM analysis (using Energy Dispersive Spectroscopy (EDS))

The XRD analysis was performed, using a Siemens D-501 spectrometer with Cu $K\alpha$ (1.5418 Å) radiation. The -2mm size fraction was mounted in resin and polished. The polished section was then used for EDS analysis and point counting.

II.2 SINTER COMPOSITION

Sinter experiments included the preparation of the following sinters:

II.2.1 Base case sinter

The base case sinter is the standard sinter that is currently produced at Mittal Steel Vanderbijlpark, and was used to examine the influence of ignition temperature on the physical and metallurgical properties of the sinter.

The raw materials mixture is given in Table 1, while the sinter composition and conditions are given in Table 2.

Table 1 Proportions of the raw materials in the Base Case sinter mixture

Raw material	Mass [kg]	Mass [%]
Thabazimbi iron ore	38.37	25.58
Sishen iron ore	38.37	25.58
Return fines	37.50	25.00
Coke	6.60	4.40
Lime	9.24	6.16
Dolomite	10.94	7.29
Silica	0.30	0.2
Water	7.65 (6611ml)	5.10
$FeCl_3$	1.04 (1039ml)	0.69
TOTAL	**150**	**100**

Table 2 Composition and sintering conditions for the base case sinter

Sinter composition (mass %)		***Sinter pot test conditions***	
Basicity (CaO/SiO_2)	2	**Ignition**	
FeO	7.0-9.0	Temperature [^0C]	865 – 1100^{0}C (with 50 ^{0}C shifts)
Fe	53.0	Time [min]	1.5
CaO	10.00	Pressure drop [mmH_2O]	500
SiO_2	5.00	**Sintering**	
Al_2O_3	1.7	Pressure drop [mmH_2O]	1200
MgO	2.8	**Cooling**	
		Pressure drop [mmH_2O]	1500

After starting the ignition with the gas flame, the pressure drop was increased to 1200mm H_2O as soon as the desired ignition temperature was reached. A thermocouple was placed on the surface of the sinter bed in order to read the ignition temperature. But, sometimes difficulties were experienced to reach the exact ignition temperature due to the gas flame, which was not easy to manipulate.

II.2.2 Low Silica- Low alumina sinter

This sinter was produced by keeping the SiO_2 content constant at 5% and adjusting the CaO content through the addition of lime to keep the basicity constant at two. The ignition temperature used was the optimum ignition temperature determined for the Base Case sinter. The MgO content was adjusted through dolomite addition. The composition and sinter conditions are given in Table 3.

Table 3 Composition and sintering conditions for Low Alumina-Low Silica sinter

Sinter composition (mass %)		***Sinter pot test conditions***	
Basicity (CaO/SiO_2)	2	**Ignition**	
FeO	7.0-9.0	Temperature [^0C]	1050^0C
Fe	53.0	Time [min]	1.5
CaO	10.3	Pressure drop [mmH_2O]	500
SiO_2	5.1	**Sintering**	
Al_2O_3	1.6	Pressure drop [mmH_2O]	1200
MgO	1/2/3	**Cooling**	
		Pressure drop [mmH_2O]	1500

II.2.3 High Silica – Low Alumina sinter

This sinter was produced by increasing the SiO_2 content of the sinter up to 5.6% through the addition of silica sand and adjusting the CaO content through the addition of lime to keep the basicity constant at two. The ignition temperature used was the optimum ignition temperature that was determined for the base case sinter while other conditions remained constant. The influence of MgO content on this sinter was evaluated by preparing sinters that contain 1 mass%, 2 mass % and 3 mass% MgO respectively. The MgO was added through fused magnesia addition. The sinter composition is given in Table 4, while the chemical composition of the fused magnesia is given in Table 5.

Table 4 Composition and conditions for the High silica- Low alumina sinter

Sinter composition (mass %)		***Sinter pot test conditions***	
Basicity (CaO/SiO_2)	2	**Ignition**	
FeO	7.0-9.0	Temperature [^0C]	1050^0C
Fe	53.0	Time [min]	1.5
CaO	11.2	Pressure drop [mmH_2O]	500
SiO_2	5.6	**Sintering**	
Al_2O_3	1.7	Pressure drop [mmH_2O]	1200
MgO	1 / 2 / 3	**Cooling**	
		Pressure drop [mmH_2O]	1500

Table 5 Chemical composition of the fused magnesia (mass %)

MgO	**MnO_2**	**CaO**	**Fe_2O_3**	**Al_2O_3**	**SiO_2**	**Cr_2O_3**	**LOI**
96.80%	0.06%	1.42%	0.55%	0.17%	0.33%	0.01%	0.39

II.2.4 High Silica – High Alumina sinter

The silica content of this sinter was kept constant at 5.6% while the alumina content was increased up to 3% through the addition of bauxite, which contains 80% alumina. The chemical composition of the bauxite is given in Table 6. To increase its reactivity, the bauxite was crushed down to -3mm.

Table 6 Chemical composition of the bauxite (mass %)

Al_2O_3	**SiO_2**	**TiO_2**	**CaO+MgO**	**Na_2O+K_2O**	**P_2O_5**	**Fe_2O_3**
80	11	2.2	0.7	0.4	<4.0	<1.5

The basicity was kept constant at two. The sinter composition and conditions are given in Table 7.

Table 7 Composition and conditions for the High silica- High alumina sinter

Sinter composition (mass %)		***Sinter pot test conditions***	
Basicity (CaO/SiO_2)	2	**Ignition**	
FeO	7.0-9.0	Temperature [^{0}C]	1050^0 C
Fe	53.0	Time [min]	1.5
CaO	11.2	Pressure drop [mmH_2O]	500
SiO_2	5.6	**Sintering**	
Al_2O_3	3	Pressure drop [mmH_2O]	1200
MgO	2,8	**Cooling**	
		Pressure drop [mmH_2O]	1500

Chapter III RESULTS AND DISCUSSION

III.1 BASE CASE SINTER

The chemical compositions of the raw material for the Base case sinters, as well as different ignition temperatures are given in Table 8. It can be seen from Table 8 that very slight variation in chemical composition of the raw materials used at different ignition temperatures could be observed. However, the theoretically expected compositions for the different components are slightly different from those obtained. Namely the basicity ratios are slightly lower than the aimed for value of two.

This section describes the influence of the ignition temperature on the sinter properties of the base case sinter. The ignition temperatures chosen ranged from 865 to 1100^{o}C as indicated in Table 2. A maximum ignition temperature of 1100^{o}C was chosen to prevent the non permeability of the sinter bed due to the melt formation on the surface of the bed at higher ignition temperatures. In this category of sinter the influence of ignition temperature on the sinter quality has been investigated. It was difficult, at the pilot plant, to exactly reach the required basicity reason why slight differences in basicity can be seen in Table 8.

Table 8 Chemical compositions of the mixture of raw materials used at different ignition temperatures for the Base case sinter (mass%)

Comp.	***Ignition temperature (^{0}C)***						
	864	***897***	***917***	***963***	***983***	***1053***	***1100***
Fe (total)	56.1	56.5	56.7	56.2	56.1	56.6	56.7
FeO	7.8	7.9	8.1	8.1	7.8	7.6	8.1
Fe_2O_3	71.2	71.8	71.8	70.3	71.4	72.1	71.9
Fe (met)	0.3	0.2	0.2	0.3	0.1	0.3	0.2
CaO	9.8	9.6	9.4	9.8	10.0	9.5	9.5
MgO	2.8	2.9	2.8	2.9	2.9	2.7	2.9

Table 8 Continued							
SiO_2	5.6	5.2	5.3	5.5	5.3	5.3	5.6
Al_2O_3	1.8	1.7	1.7	1.8	1.7	1.7	1.7
K_2O	0.1	0.1	0.0	0.0	0.1	0.1	0.0
Na_2O	0.0	0.0	0.0	0.0	0.0	0.0	0.0
TiO_2	0.1	0.1	0.1	0.1	0.1	0.1	0.2
MnO	0.4	0.4	0.4	0.3	0.3	0.4	0.3
P	0.0	0.1	0.1	0.0	0.1	0.0	0.0
S	0.0	0.0	0.0	0.0	0.0	0.0	0.0
C	0.1	0.1	0.1	0.1	0.1	0.1	0.1
Basicity	1.8	1.8	1.8	1.8	1.9	1.8	1.7

**Comp.= Compound*

III.1.1 Morphological analysis

The point-counting technique was used to determine the percentages of different phases. The technique consists of counting at least hundred points on a polished block. Each point corresponds to one phase observed with an optical microscope connected to the point-counting machine. The percentage of different phases and different morphologies are determined as ratios between the number of times that each phase or morphology is present and the total number of points counted on the sample. The volume percentages of all the phases of different morphologies are given in Table 9. Each sample was counted three times and the average values are reported.

The amount of the spinel phase (magnetite and magnesioferrite) increased moderately up to an ignition temperature of 1053^{o}C then only increased drastically at an ignition temperature of 1100^{o}C. Figure 15 gives the variation of the spinel phase with ignition temperature.

Table 9 Quantification of phases for the Base Case sinter

Point-counting categories	Ignition temperature (^{0}C)						
	864	**897**	**917**	**963**	**983**	**1053**	**1100**
Spinel	28.2 ± 0.01	29.7 ± 0.02	31.0 ± 0.02	31.8 ± 0.03	32.1 ± 0.02	30.2 ± 0.02	40.4 ± 0.01
Hematite relict	18.2 ± 0.01	8.1 ± 0.02	7.9 ± 0.01	7.5 ± 0.01	7.3 ± 0.02	3.5 ± 0.01	0.2 ± 0.01
Hematite rhombic	6.2 ± 0.01	6.5 ± 0.02	5.0 ± 0.01	5.2 ± 0.01	6.9 ± 0.02	4.1 ± 0.01	0.4 ± 0.02
Hematite Finely granular	2.0 ± 0.02	4.7 ± 0.01	2.5 ± 0.02	2.6 ± 0.01	4.0 ±0.01	1.9 ± 0.02	1.2 ± 0.01
Hematite skeletal	2.9 ± 0.01	4.7 ± 0.01	5.6 ± 0.02	5.9 ± 0.01	6.2 ±0.01	5.5 ± 0.01	6.6 ± 0.02
Total Hematite	29.3 ± 0.02	24 ± 0.01	21 ± 0.01	21.2 ± 0.02	24.4 ± 0.01	15 ± 0.01	8.4 ± 0.01
SFCA acicular	11.5 ± 0.01	13.0 ± 0.01	11.4 ± 0.01	10.3 ± 0.01	14.2 ± 0.01	16.7 ± 0.01	9.5 ± 0.01
SFCA columnar & Blocky	14.2 ± 0.2	15.1 ± 0.02	13.9 ± 0.02	12.9 ± 0.01	17.0 ± 0.02	18.5 ± 0.02	22.4 ± 0.02
SFCA dendritic & Eutectic	6.9 ± 0.02	6.0 ± 0.02	5.8 ± 0.01	4.1 ± 0.01	4.1 ± 0.01	6.5 ± 0.01	3.0 ± 0.01
Total SFCA	32.6 ± 0.02	34.1 ± 0.01	31.1 ± 0.02	27.3 ± 0.02	35.3 ± 0.01	41.1 ± 0.01	34.9 ± 0.01
MO/ (Fe,Mg)O Magnesiowustite	0.7 ± 0.02	0.9 ± 0.02	1.9 ± 0.01	1.3 ± 0.01	1.2 ± 0.02	3.5 ± 0.02	2.2 ± 0.02
Crystalline silicate	4.7 ± 0.01	5.9 ± 0.02	5.3 ± 0.02	5.9 ± 0.01	6.4 ± 0.01	7.4 ± 0.01	6.5 ± 0.01
Glass	4.5 ± 0.02	5.1 ± 0.01	5.4 ± 0.02	5.9 ± 0.02	5.3 ± 0.02	5.5 ±0.02	7.7 ± 0.02
SFCA acicular/columnar. ratio	0.80 ± 0.02	0.86 ± 0.02	0.82 ± 0.02	0.80 ± 0.01	0.83 ± 0.01	0.90 ± 0.01	0.41 ± 0.02

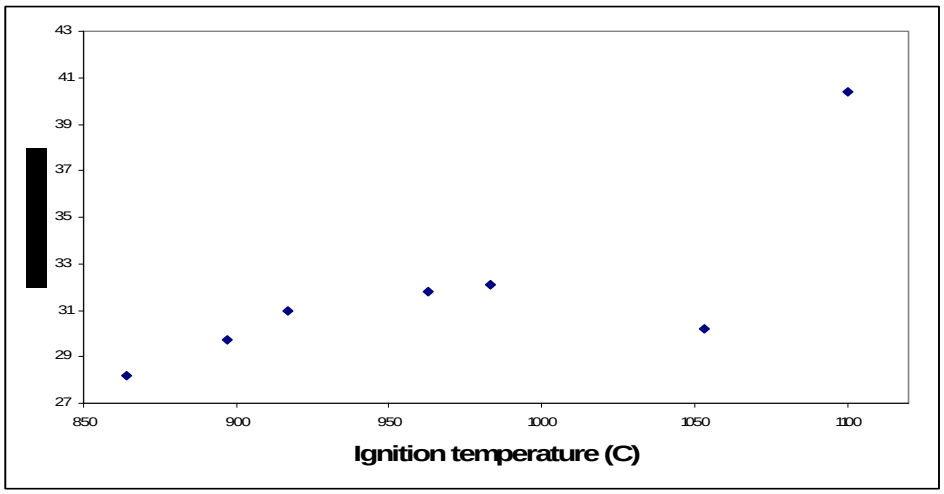

Figure 15 Variation of the volume % of the spinel phase with ignition temperature

The sharp increase in the amount of the spinel phase at the ignition temperature of 1100 ^{o}C is presumably be due to more liquid that probably formed on the surface of the sinter therefore increasing the sintering time which in turn allowed the heat to be kept for longer inside the sinter, thus more spinel phase formed.

The hematite relict, hematite rhombic and hematite finely granular decreased with increasing ignition temperature while skeletal hematite increased with increasing ignition temperature. The total hematite decreased with increasing ignition temperature.

The ratio SFCA acicular to columnar remained almost constant and only decreased considerably at 1100^{o}C ignition temperature.

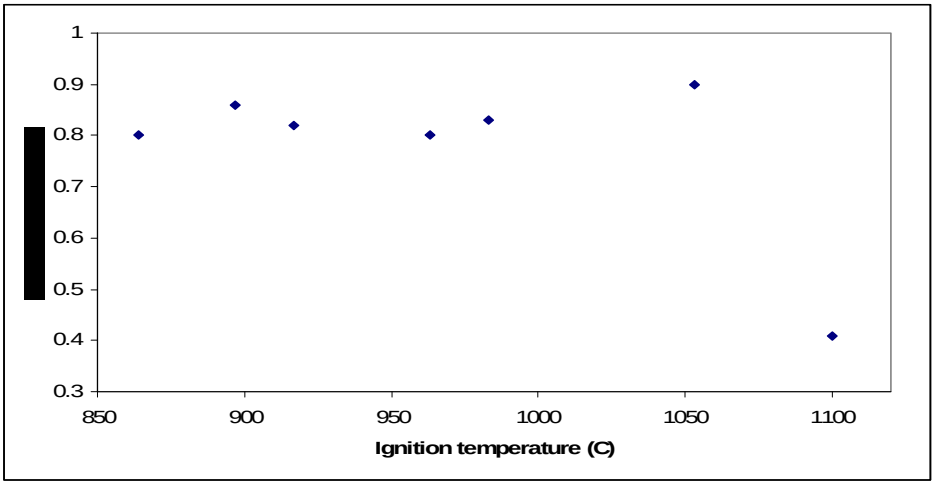

Figure16. Variation of the ratio SFCA acicular/columnar

The constancy in SFCA acicular over SFCA columnar ratio is associated with:

1) A slight increase first then a slight decrease in the spinel phase
2) The decrease in hematite
3) An increase in glassy phase

It was presumed that a further increase in ignition temperature may have led to the formation of an additional amount of melt in the top layer of the sinter. Consequently, larger SFCA crystals may have grown, and the ratio of the volume % acicular SFCA to volume % columnar SFCA would therefore decrease.

The amount of crystalline silicates reached a maximum at 1053^{o} C and then decreased again at 1100^{o} C, while the amount of glassy phase reached its maximum at 1100^{o}C.

III.1.2 Sinter properties

III.1.2.1 Reducibility

The influence of the ignition temperature on the reducibility index is given in Table 10 and shown in Figure 17. It can be seen that the reducibility index remained almost constant with increasing ignition temperature. The constancy may be explained by:

1) Constancy of SFCA acicular columnar ratio.
2) Negligible change in amount of the spinel phase.

Table 10 Variation of the reducibility with ignition temperature

Ignition temperature (^{0}C)	Reducibility Index (RI)(% / min)	
864	0.98	1.05
897	1.06	0.99
917	1.06	1.04
963	1.02	0.99
987	1.03	1.02
1053	1.00	0.93
1100	1.02	0.97

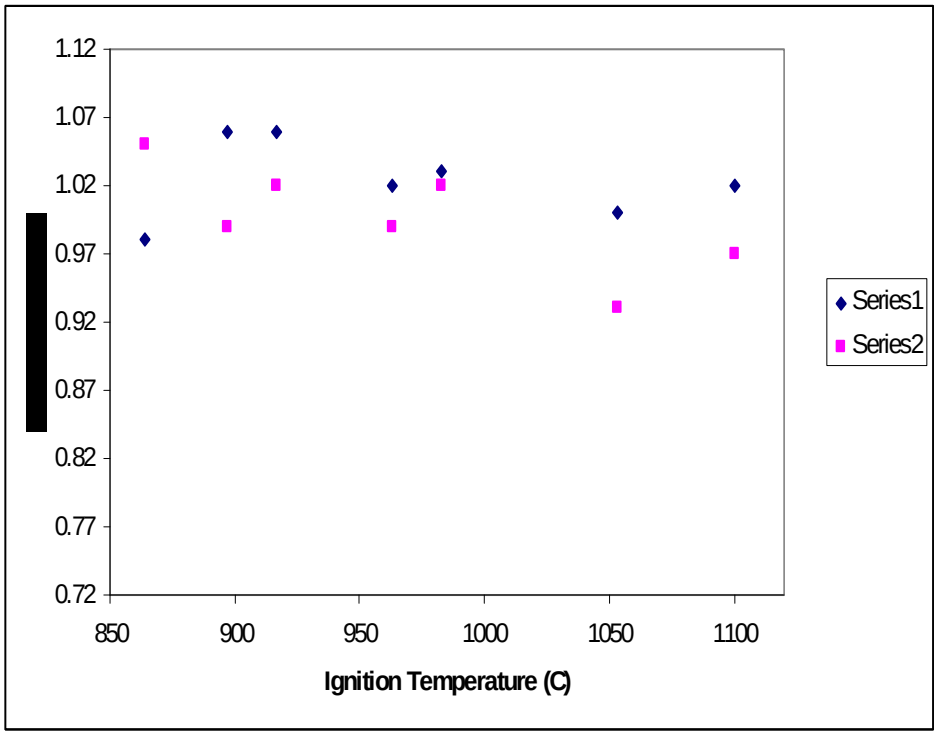

Figure 17 Variation of the RI with ignition temperature

III.1.2.2 Reduction Degradation Index (RDI)

The RDI decreased slightly with increasing ignition temperature (Table 11, Figure 18). The decrease in RDI is associated with:

1) A slight increase in the amount of the skeletal hematite with increasing ignition temperature.

2) The amount of the glassy silicate. Although the variation of the glassy silicates phase shows some discrepancies, the trend shows an increase. The presence of glassy silicates is one of the major causes in the decrease of the reduction degradation index due to their property to break easily.

Table 11 Reduction degradation index

Ignition Temperature (^oC)	*RDI (%)*					
	+6.3mm	*+6.3mm*	*+3.15mm*	*+3.15mm*	*-0.50mm*	*-0.50mm*
864	75.3	75.3	90	91	2	1.2
897	66.5	62.4	96.9	84.6	2.3	2.7
917	82.2	80	92.6	92	1.4	2.0
963	74.8	69.5	89.3	87.9	2.0	2.3
987	70.1	70.6	87.6	87.6	2.3	2.3
1053	76.6	71.0	94.8	84.2	2.0	2.3
1100	67.2	68.6	86.1	87.8	2.9	2.3

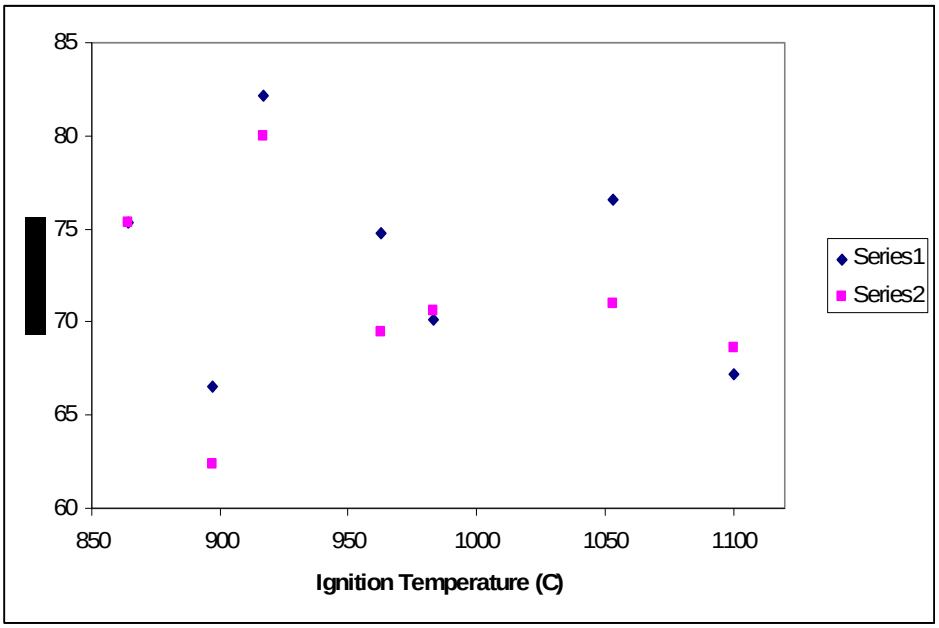

Figure 18 a Variation of the RDI with ignition temperature

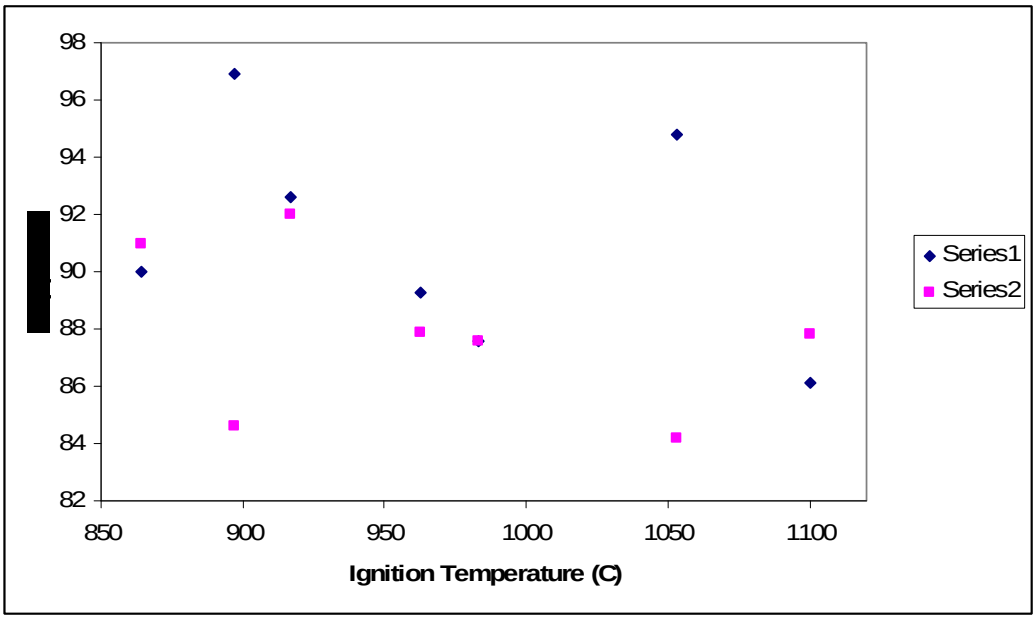

Figure 18 (b) Variation of the RDI with ignition temperature

III.1.2.3 Tumble Index and Abrasion Index

The variations of the Tumble Index (TI) and Abrasion Index (AI) with ignition temperature are given in Table 12 and in Figure 19.

It can be seen that the tumble index increased and the abrasion index increased slightly with increasing ignition temperature. The increase in abrasion index means that the resistance of the sinter product to abrasion decreases with increasing ignition temperature.

Table 12 Variations of TI and AI (%)

Ignition temperature (^{0}C)	*864*	*897*	*917*	*963*	*987*	*1053*	*1100*
Tumble Index (TI)	73.6	71.6	72.8	72.9	74.2	74.2	74.9
Abrasion Index (AI)	5.1	5.4	5.8	4.8	5.1	5.5	5.7

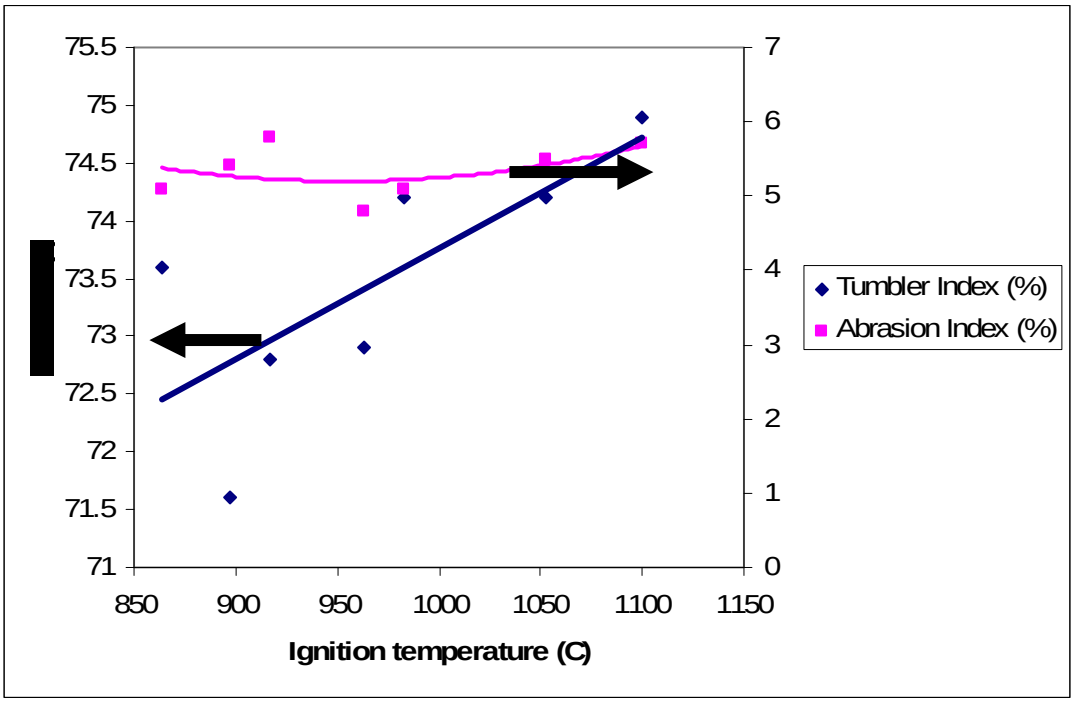

Figure 19 Variation of the TI and AI with ignition temperature

Point-counting showed that the crystalline silicate phase increased with increasing ignition temperature. But, this phase is harmful to the strength of the sinter if it undergoes the allotropic transformation from β- Ca_2SiO_4, which is monoclinic, to γ- Ca_2SiO_4, which is orthorhombic, during the cooling stage. The allotropic transformation is accompanied by an increase in volume leading to stress development. The increase in crystalline silicates should have led to a decrease in tumbler index if this allotropic transformation occured. But, the results showed the contrary. An investigation onto whether or not the allotropic transformation took place, now follows.

III.1.2.3.1 XRD analysis

The XRD analyses of the base case sinter samples are given in the Appendix. Figure 20 shows the XRD results of the base case sinter at 1100^{o}C as ignition temperature. The XRD lines for the monoclinic crystalline silicates are indicated with arrows in Figure 20. The Table 13 gives the respective amounts of β- Ca_2SiO_4 and γ- Ca_2SiO_4.

Table 13 concentration of β- Ca_2SiO_4 and γ- Ca_2SiO_4, using quantitative XRD

Sample	% β- Ca_2SiO_4	% γ- Ca_2SiO_4
Base Case 864	0.53	0
Base Case 897	0.37	0
Base Case 917	10.48	0
Base Case 963	7.3	0
Base Case 987	7.17	0
Base Case 1053	3	0
Base Case 1100	5.68	0

It can clearly be seen that the expected allotropic transformation from β- Ca_2SiO_4 to γ- Ca_2SiO_4 did not take place.

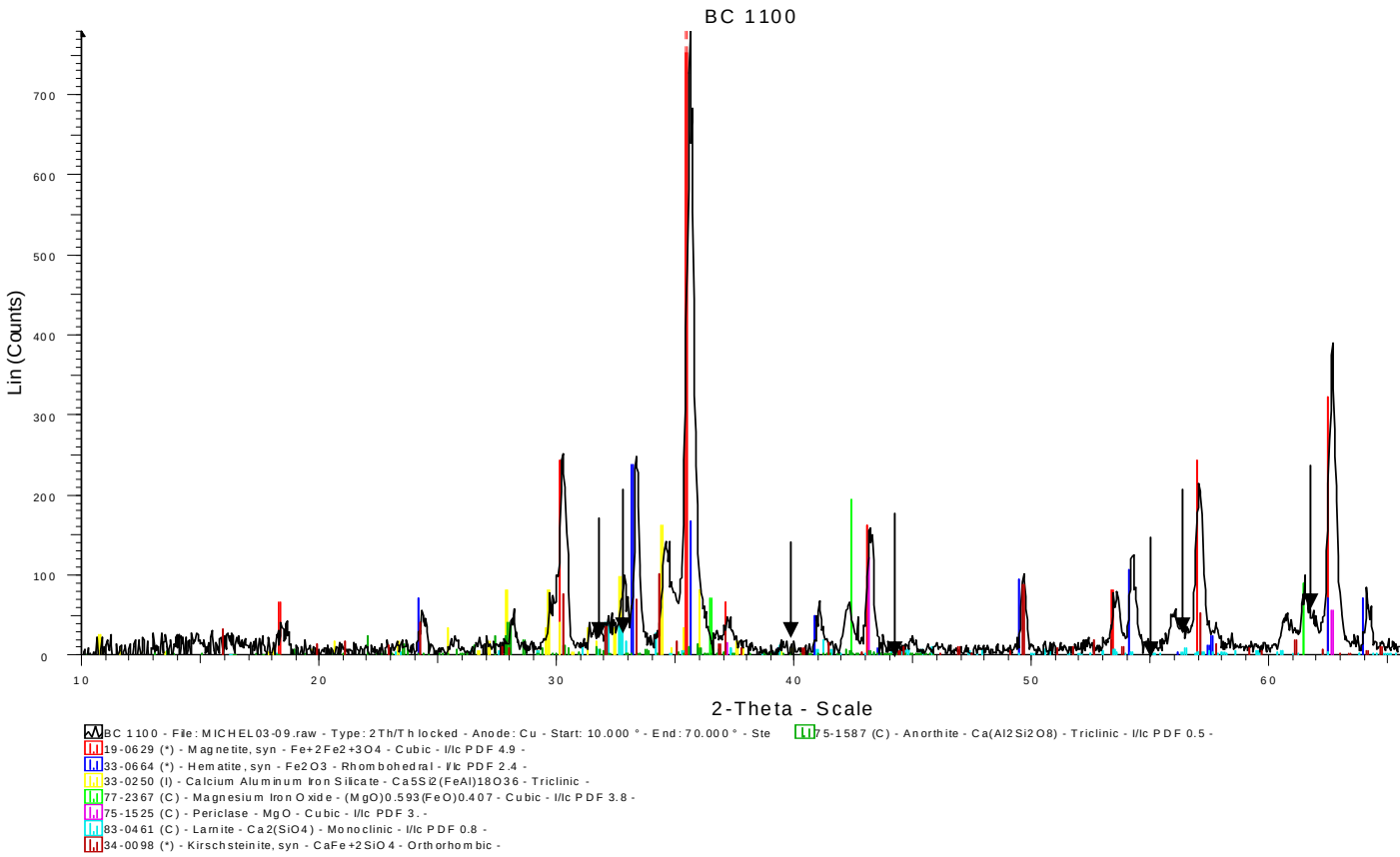

Figure 20 XRD analysis of the Base Case sinter at an ignition temperature of 1100°C.

III.1.2.3.2 EDS analysis

A sample of the –12mm +10mm size fraction was crushed and mounted on a polish block in order to conduct the EDS analyses.

EDS analyses of the crystalline silicate phase in the sinter samples are given in Table 14.

Table 14 EDS analyses of the crystalline silicate phase

Component Temperature	*P2O5*	*Al2O3*	*Fe2O3*	*CaO*	*SiO2*
963 °C	1.0	1.0	1.6	64.5	31.9
983 °C	1.2	0	2.1	64.3	32.4
1053 °C	1.3	0	1.5	63.2	33.9
1100 °C	1.2	0	1.1	65.7	31.9

It can be seen, from Table 14; that within the crystalline silicate crystal structure, some other metal oxides were dissolved. Amongst these metal oxides are phosphorus oxide and iron oxide.

It has been reported that the high temperature forms of Ca_2SiO_4 could be stabilized if even a small amount of P_2O_5, Cr_2O_5 or B_2O_3 is present in the structure [41]. These oxides are said to be effective in inhibiting the allotropic inversion to the γ- Ca_2SiO_4. The same authors emphasized that the inhibiting effect probably occurs because of the substitution of P^{5+}; Cr^{5+} or B^{3+} ions for Si^{4+} ions in the β- Ca_2SiO_4 to a greater extend than in γ- Ca_2SiO_4. This can explain why the allotropic transformation to γ- Ca_2SiO_4 did not take place in the examined sinter samples.

III.1.2.4 Yield

The yield is defined as the ratio of the amount of sinter produced to the raw materials fed into the process [42].

Yield = Total mass of sinter produced/ (mass of total mixture + grit layer mass – surplus mixture – grit layer recovery)*100

The variations in the yield versus ignition temperature are given in Table 15 and shown in Figure 21.

Table 15 Variation of the yield

Ignition temperature (^0C)	**864**	**897**	**917**	**963**	**987**	**1053**	**1100**
Yield (%)	79.2	78.2	81.3	81.4	81.9	79.1	82.3
LOI (%)	-0.33	-0.62	-0.51	-0.05	-0.23	-0.28	-0.62

The general trend of the yield showed that the yield increased with increasing ignition temperature. This may mainly be explained by the LOI which shows an increase in mass most probably due to oxidation of some low oxides to higher oxides that may have taken place on heating.

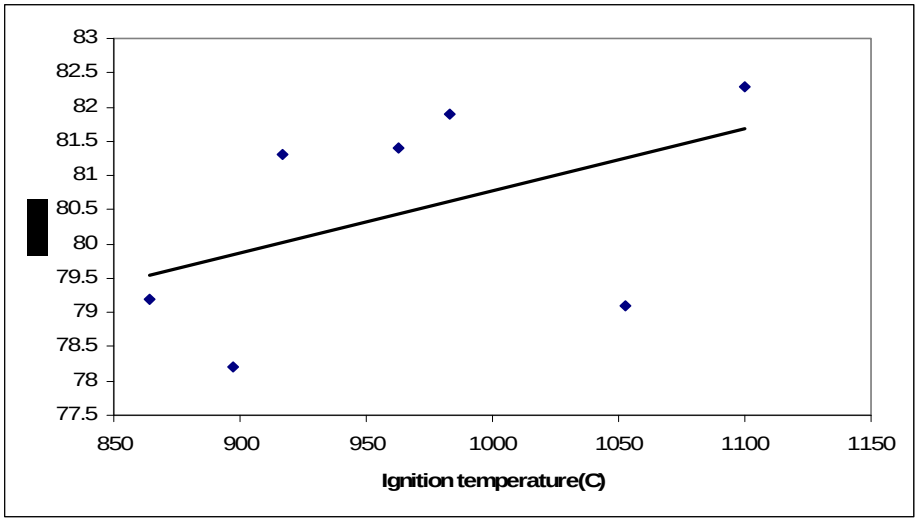

Figure 21 Variation of the yield with ignition temperature

III.1.2.5 Sinter production rate

The production rate of the sinter machine is linked to the sintering time. Table 16 and Figure 22 below give the variation of the sinter production rate and that of the sintering time according to the ignition temperature. Theoretically, the shape of the sinter production rate may presumably be explained by a good permeability obtained at the ignition temperature of 963 ^oC, which shows the highest value of the production rate, thus low sintering time.

Table 16 Sinter production rate and sintering time

Temperature [°C]	**Sintering time** [min]	**Sinter production rate** [t sinter/m2/24h]
864	27	25
897	26	26
917	29	24
963	25	30
987	28	26
1053	29	25
1100	31	23

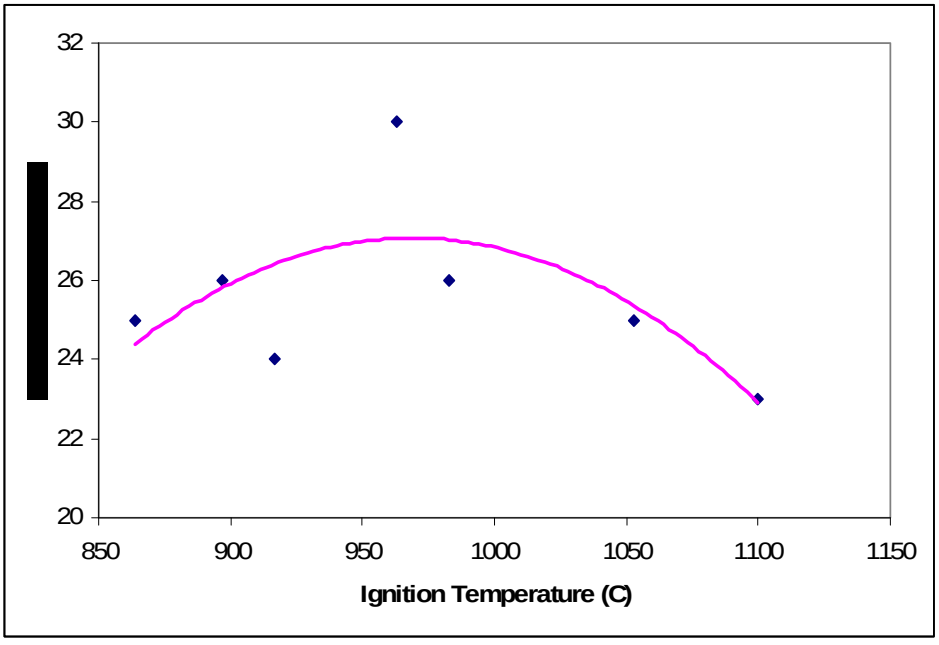

Figure 22 Sinter production rate variation with ignition temperature

It can be seen that the sinter production rate showed an increasing trend at lower ignition temperatures and reached a maximum at 963^{o}C then decreased at higher ignition temperatures then decreased thereafter.

III.1.2.5 Coke consumption

The coke consumption is defined by the following equation [43]:

Coke consumption = [{coke mass in mixture*(mass of total mixture – surplus mixture)/ mass of total mixture}/{(total mass of produced sinter – the minus 5 mm sinter produced) – (grit layer mass in – grit layer recovered)}]

The coke consumption decreased with increasing ignition temperature. The lowest coke consumption was obtained at an ignition temperature of 1053^{o}C. The coke consumption with ignition temperature is given in Table 17 and Figure 23.

Table 17 Coke consumption

Ignition temperature [^{o}C]	**864**	**897**	**917**	**963**	**987**	**1053**	**1100**
Coke consumption [kg/t sinter]	82	84	79	80	77	76	78

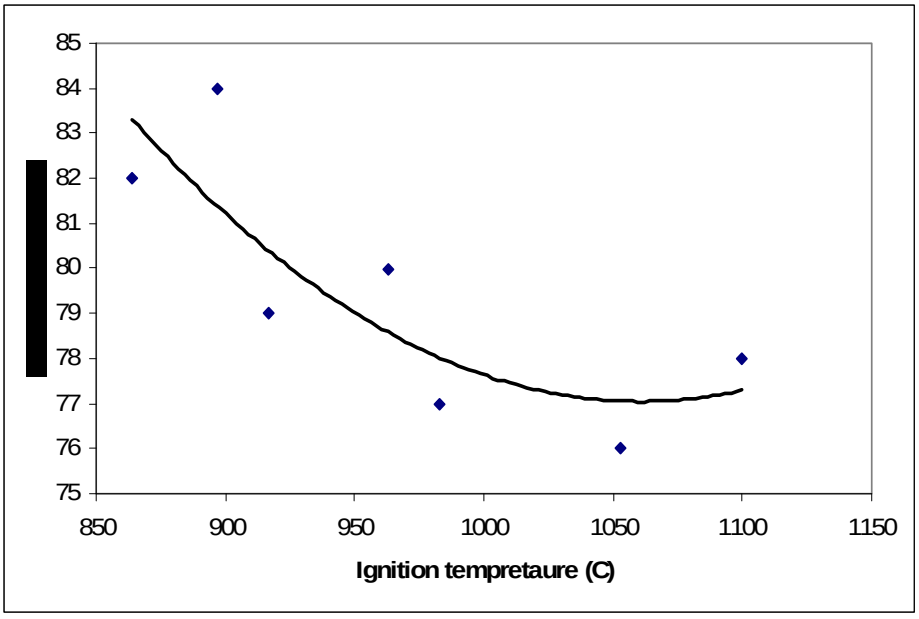

Figure 23 Variation of coke consumption with ignition temperature

III.1.3 Conclusion

With the aim to determine the optimum ignition temperature, a compromise had to be found. Table 18 gives the requirements of Kumba Iron Ore for sinter of acceptable quality.

Table 18 Sinter properties required by Industry [43]

RI (%/min)	**RDI (%)**	**TI (%)**	**AI (%)**
	+6.3mm		
≥ 1	≥ 70	≥ 70	≤ 5

The general trend of the reducibility shows that the reducibility is almost constant, about the value of 1%/min; with increasing ignition temperature.

The reduction degradation index decreased slightly with increasing ignition temperature. The recommended value for RDI is at least 70% for the +6.3mm size fraction.

The sinter of lowest quality, according to the requirements of Kumba Iron Ore, was obtained at an ignition temperature of 897^{o}C, while the highest quality sinter was obtained at an ignition temperature of 917 ^{o}C.

The tumbler index as well as the abrasion index values increased also slightly with increasing ignition temperature. But, the increase in abrasion index indicated that the resistance of the sinter to abrasion decreased with increasing ignition temperature. With regard to the abrasion index recommended by Kumba Iron Ore, only that obtained at 963 ^{o}C was acceptable.

The yield increased with increasing ignition temperature. The highest value was obtained at 1100 ^{o}C.

The lowest sintering time was obtained at 963 ^{o}C while the highest was obtained at 1100 ^{o}C ignition temperature. Thus, the best ignition temperature was 963 ^{o}C.

The highest production rate was obtained at 963° C while the lowest was obtained at 1100° C. Therefore, the best ignition temperature would be 963° C. The lowest coke consumption was obtained at 1053° C while the highest was obtained at 897° C. The best ignition temperature would be 1053° C.

From the above conclusions, using the Kumba Iron Ore set of values as guideline, a compromise had to be found. Table 19 includes all the sinter properties of the Base Case Sinter.

Table 19 Sinter properties of the Base Case Sinter

Sinter properties	**Ignition Temperature (^{0}C)**						
	864	**897**	**917**	**963**	**987**	**1053**	**1100**
RI *[%/min]*	1.02	1.03	1.04	1.00	1.02	0.97	1.0
RDI *[%]*	75.3	64.5	81.1	72.2	70.4	76.6	67.9
TI *[%]*	73.6	71.6	72.8	72.9	74.2	74.2	74.9
AI *[%]*	5.1	5.4	5.8	4.8	5.1	5.5	5.7
Yield *[%]*	79.2	78.2	81.3	81.4	81.9	79.1	82.3
Sintering time *[min]*	27	26	30	25	29	29	31
Production rate *[t/m2/24h]*	25	26	24	29	26	25	23
Coke consumption *[kg/t sinter]*	82	84	79	80	77	76	78

According to the requirements of Kumba Iron Ore of sinter properties; the ignition temperature should be 963^{0}C. But, looking at the economical aspect, it can be noticed that at 963^{0}C ignition temperature, the coke consumption was 80 kg/t sinter while at 1053^{0}C ignition temperature the coke consumption was 76kg/t sinter. Apart from the abrasion index, which was above the required value, the reducibility index, reduction degradation index, tumbler index, yield, sintering time and production rate of the sinter that was ignited at 1053°C met the requirements of Kumba Iron Ore. It was therefore decided to conduct all further experiments at an ignition temperature of 1053^{0}C.

III.2 LOW ALUMINA – LOW SILICA SINTER

The expression of a Low alumina – Low silica sinter varies from one plant to another. In this study, the specific composition in alumina and silica content for a low alumina-low silica sinter is indicated in Table 20.

Table 20 Chemical composition of the Low alumina – Low silica sinter

Compound		*Fe (total)*	*FeO*	*Fe_2O_3*	*Fe(met)*	*CaO*	*MgO*	*SiO_2*	*Al_2O_3*	*K_2O*	*Na_2O*	*TiO_2*
MgO Mass%	**1**	**57.6**	**8.0**	**73.2**	**0.13**	**9.6**	**1.2**	**5.0**	**1.7**	**1.0**	**0.0**	**0.1**
	2	**58.0**	**7.9**	**74**	**0.12**	**9.8**	**2.0**	**5.1**	**1.7**	**0.0**	**0.0**	**0.1**
	3	**56.1**	**8.1**	**71.1**	**0.0**	**10.3**	**2.8**	**5.2**	**1.8**	**0.0**	**0.0**	**0.1**

Keeping the alumina and silica content constant, the influence of varying MgO content on the physical and chemical properties as well as mineralogy of the sinter was studied. The MgO content was changed in percentage from 1, 2 and 2.8 mass% through dolomite addition. The basicity was kept constant at two. The sinter specifications and conditions are given in Table 21.

Table 21 Low alumina-Low silica sinter

Sinter composition (mass %)		***Sinter pot test conditions***	
Basicity (CaO/SiO_2)	2	**Ignition**	
FeO	7.0-9.0	Temperature [^{0}C]	1050^0 C
Fe	53.0	Time [min]	1.5
CaO	10.3	Pressure drop [mmH_2O]	500
SiO_2	5.1	**Sintering**	
Al_2O_3	1.6	Pressure drop [mmH_2O]	1200
MgO	1 /2 / 2.8	**Cooling**	
		Pressure drop [mmH_2O]	1500

III.2.1 RESULTS

III.2.1.1 Quantification of the phases

The point-counting results are given in Table 22.

Table 22 Quantification of phases in the low Al_2O_3-low SiO_2 sinter

Point-counting categories	***MgO added (mass %)***		
	1	**2**	**3**
Spinel	32.5 ± 0.01	37.4 ±0.01	42.5±0.01
Hematite relict	12.5 ± 0.01	9.1 ±0.01	4.6 ± 0.02
Hematite rhombic	7.5 ± 0.01	6.4 ±0.01	4.1 ±0.01
Hematite Finely granular	0.8 ± 0.02	0.5 ±0.01	0.2 ±0.01
Hematite skeletal	4.7 ± 0.01	4.0 ± 0.02	4.7 ± 0.02
Hematite late stage	0.8 ± 0.01	1.4 ± 0.01	2.1 ±0.01
Total Hematite	26.3 ± 0.01	21.4 ± 0.02	15.7 ±0.01
SFCA acicular	13.1 ± 0.01	10.2 ±0.01	8.2 ± 0.01
SFCA columnar & Blocky	15.1 ± 0.01	12.7 ±0.01	10.8 ±0.01
SFCA dendritic & Eutectic	5.9 ± 0.01	8.3 ± 0.01	9.3 ± 0.02
Total SFCA	34.1 ± 0.02	31.2 ±0.01	28.3 ±0.01
SFCA acicular/columnar	0.87	0.80	0.76
MO/(Fe,Mg)O	1.2 ± 0.01	2.1 ±0.01	4.2 ±0.01
crystalline silicates	5.8 ± 0.01	4.7 ±0.01	3.6 ±0.01
Glass	3.9 ± 0.01	4.3 ±0.01	6.8 ±0.01

From the mineralogy, it can be seen that the volume percentage of the spinel increased with increasing MgO content in the sinter mix. EDS analyses also indicated that the MgO content of the magnesiospinel phase increased with increasing MgO content in the sinter. The MgO content of the spinel phase however vary throughout the sinter presumably, due to the fact that equilibrium phase relations were not obtained. The amount of spinel phase obtained in this case with 2.8% MgO content, is more than that obtained in the Base Case with 2.8% MgO content. This may be well explained by the fact that the higher the MgO content, the higher the concentration of the spinel phase.

The primary hematite so-called relict hematite, the secondary hematite, which includes rhombic and skeletal hematite decreased with increasing MgO content in the sinter, while tertiary hematite increased. But, the total amount of hematite decreased. Previous studies supported this variation of different types of hematite and explained that the MgO addition stabilizes the cation vacancies in the spinel structure, which results in a decrease in primary hematite and secondary hematite and which favours the formation of tertiary hematite or reoxidised hematite along certain preferential crystal orientations [28].

The total amount of silicoferrites of calcium and aluminum decreased with an increase in MgO content of the sinter. Most probably, this may be due to the increase in the amount of spinel phase that formed. The amount of total SFCA phase formed in this case with 2.8% MgO is lower than that obtained in the Base Case sinter with 2.8% MgO at 1053^{O}C as ignition temperature. This may be explained by the amount of MgO added.

The amount of magnesio-wustite phase (MO/(Fe,Mg)O) increased with increasing MgO. Compared to the amount of magnesio-wustite formed in the Base Case sinter, it could be seen that more magnesio-wustite formed in the low alumina-low silica sinter with 2.8% MgO added.

The crystalline silicates decreased with increasing MgO content. The amount of crystalline silicates obtained in the (low alumina-low silica sinter with 3% MgO) is less than that obtained in the Base case sinter with 2.8% MgO.
The amount of the glassy phase increases with increasing MgO content of the sinter.

III.2.2.2 Sinter properties

III.2.2.2.1 Reducibility

The reducibility index decreased with an increase in MgO as reported in Table 23 and Figure 24.

Table 23. Variation of RI with MgO content

MgO(mass%)	*RI (%/min)*	
1.0	1.02	1.01
2.0	0.94	0.92
2.8	0.92	0.92

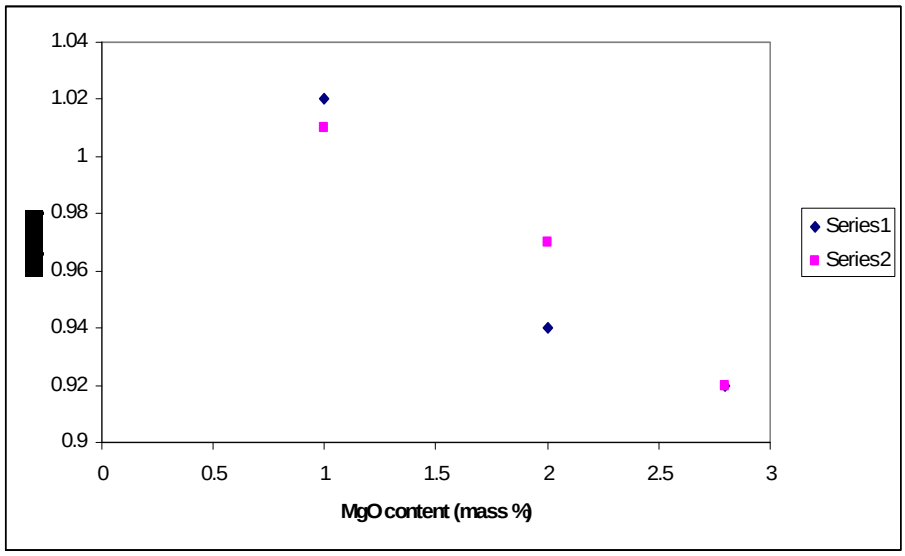

Figure24. Influence of MgO content on the reducibility index

The decrease in reducibility is associated with:

1)The decrease in rhombic hematite (total hematite)

2)The decrease in Silicoferrite of calcium and aluminum (SFCA) in general and in acicular SFCA in particular.

3)The increase in magnesio-spinel phase.

III.2.2.2.2 Reduction Degradation

The variation of the reduction degradation index is given in Table 24 and Figure 25. The reduction degradation index decreased slightly then slightly increased with increasing MgO.

Table 24 Variation of the Reduction Degradation Index with MgO content of the sinter (RDI)

MgO(mass%)	RDI (%)			
	+6.3 mm	*+6.3mm*	*-3.15mm*	*-3.15mm*
1.0	79.9	82.6	1.8	2.0
2.0	79.3	78.8	2.2	1.9
2.8	82.7	82.7	1.6	1.5

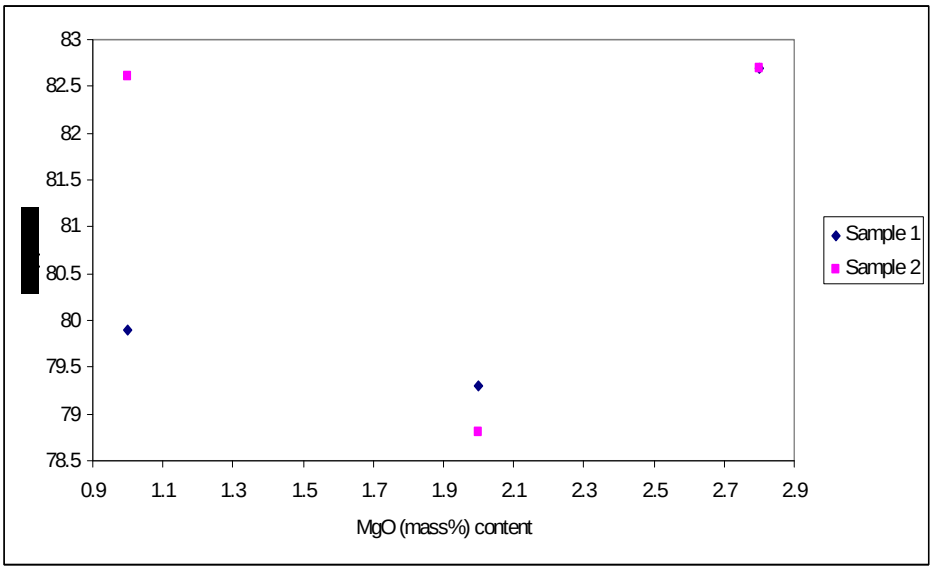

Figure 25 (a) Variation of RDI (+6.3mm) with MgO content

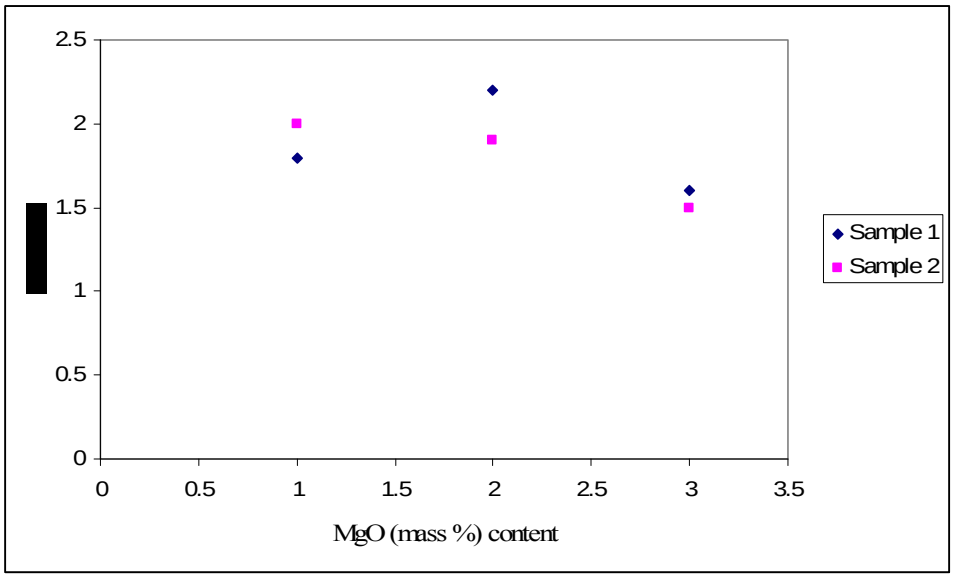

Figure 25 (b) Variation of RDI (-3.15mm) with MgO content

The slight increase in reduction degradation may be explained by the decrease in hematite content and an increase in spinel phase.

III.2.2.2.3 Abrasion Index

The variation of the abrasion index with MgO addition is given in Table 25 and Figure 26. The abrasion index increased with increasing MgO content of the sinter. This may be associated with the increase in amount of glass with increasing MgO.

Table 25 Variation of the abrasion index (AI) with MgO content of the sinter

MgO	*AI (%)*	
1.0	4.88	4.81
2.0	5.06	5.05
2.8	5.12	5.08

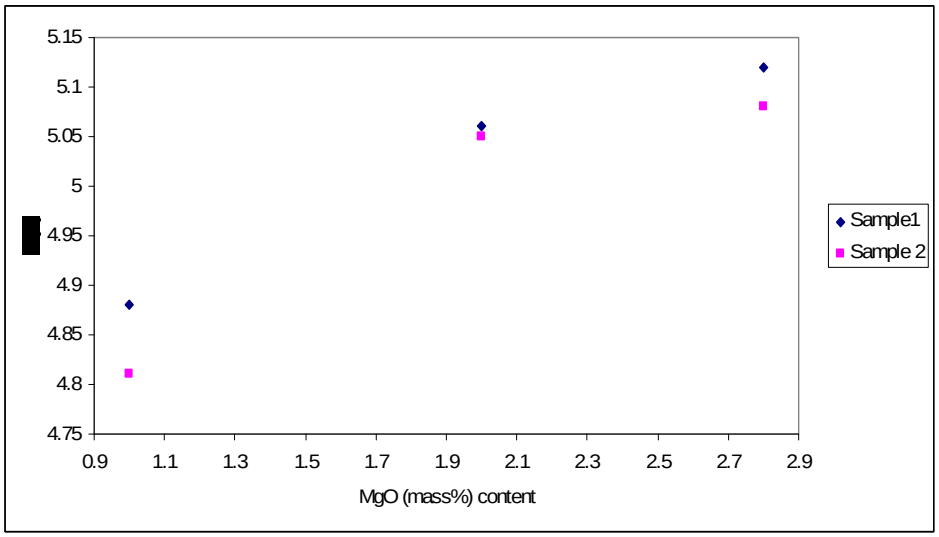

Figure26. Variation of Abrasion Index with MgO content

III.2.2.2.4 Tumbler Index

The variation of the tumbler index with MgO addition is given in Table 26 and its trend in Figure 27. It can be seen that the trend of the tumbler index with increasing MgO content increases when MgO increased from 1% to 2% MgO, but is uncertain at 2.8% MgO although the error falls within the acceptable limits of 1.4 applied by Kumba Iron Ore [37].

Table 26 Variation of the Tumble Index with MgO content of the sinter(TI)

MgO(mass%)	*TI(%)*	
1.0	73.74	73.92
2.0	74.38	74.37
2.8	75.56	73.60

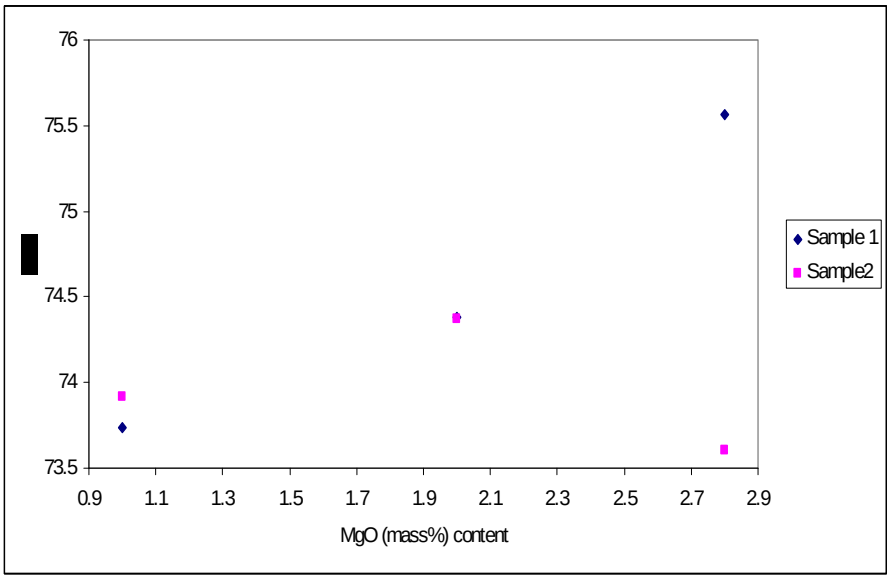

Figure27. Variation of Tumble Index with MgO content

The mineralogical analysis showed that the amount of the glassy silicate phase increased with increasing MgO content, while the crystalline silicates and acicular SFCA decreased with increasing MgO.

III.2.2.2.5 Influence of MgO on coke breeze rate

The results for the influence of MgO addition on the coke breeze rate are given in Table 27 and Figure 28. It can be seen that the coke breeze rate increased with increasing MgO. This may be due to the fact that MgO have been increased through dolomite addition and more energy was required for carbonate decomposition and dehydration of $Mg(OH)_2$ that forms after decomposition.

Table 27 Variation of the coke breeze rate as function of MgO content

MgO(mass%)	*Coke (kg/t sinter)*	
1.0	73.48	73.71
2.0	75.72	75.72
2.8	78.10	77.85

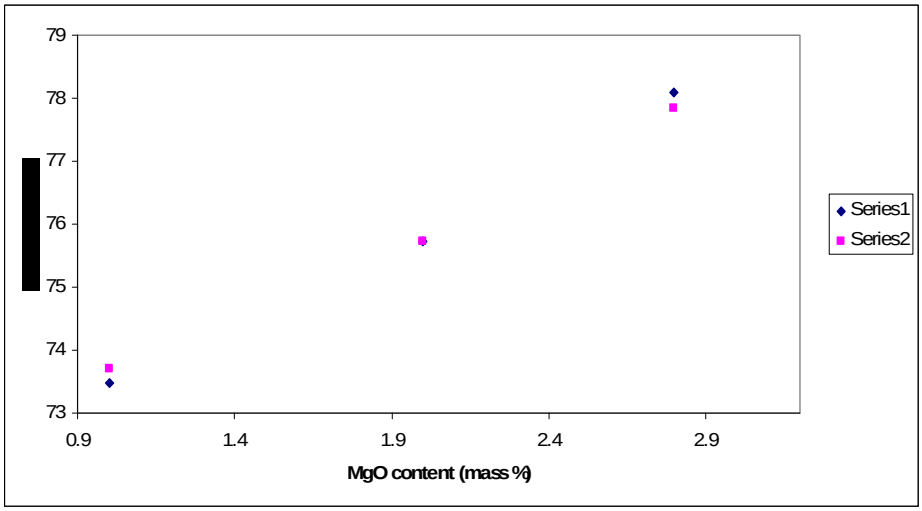

Figure 28 Influence of MgO content of the sinter on coke breeze rate

III.2.3 Conclusions

III.2.3.1 Mineralogy of the Low silica – Low alumina sinter

MgO addition not only changes the mineralogy of the sinter product, but also influences the amount of different morphologies for typical phases present in the sinter product. From the results obtained, it can be concluded that:

The amount of the spinel phase increased with increasing MgO content of the sinter. The ignition temperature being 1053^{o}C, the amount of spinel phase obtained with 5.1% SiO_2 and 2.8 MgO is higher than that obtained at the same ignition temperature in the Base case sinter.

The amounts of primary hematite as well as the secondary hematite decreased with increasing MgO content of the sinter while the amount of tertiary hematite increased slightly. This

however resulted in an overall decrease in the total amount of hematite present in the sinter with increasing MgO content. The amount of total hematite at 2.8% MgO content of the low alumina – low silica is similar to the total amount of hematite in the Base Case sinter at an ignition temperature of 1053^{o}C.

The amount of acicular SFCA decreased with increasing MgO content while the dendritic and eutectic SFCA increased. This led to a decrease in the total amount of SFCA with increasing MgO content. The total amount of SFCA in the low silica – low alumina sinter at 2.8% MgO content is lower than that obtained in the Base Case sinter at ignition temperature of 1053^{o}C.

The amount of magnesio-wustite phase increased with increasing MgO. But, the amount of magnesio-wustite formed at 2.8% MgO content for the low silica – low alumina sinter was higher than the amount of magnesio-wustite that formed in the Base Case sinter at an ignition temperature of 1053^{o}C.

The crystalline silicates decreased with increasing MgO while for the Base Case sinter the crystalline silicates increased with increasing ignition temperature. The amount of crystalline silicates that has formed at 2.8% MgO in the low silica – low alumina sinter was less than that has formed at 1053^{o}C in the Base Case sinter.

The sinter produced in the Base Case sinter at an ignition temperature of 1053^{o}C had higher reducibility index than the sinter produced in low silica – low alumina sinter with 2.8% MgO content.

III.2.3.2 Properties of the low silica – low alumina sinter

The reducibility index decreased with increasing MgO content of the sinter. This is associated with a decrease in the amount of relict, rhombic and total hematite, an increase in the amount of spinel phase and a decrease in acicular, columnar as well as total SFCA phase. The Base Case sinter at ignition temperature of 1053^{o}C had a high reducibility index than the low alumina – low silica sinter with 2.8% MgO content. This is presumably due to its lower spinel and higher total SFCA contents.

The reduction degradation index of the low silica – low alumina sinter increased with increasing MgO. The increase in RDI is associated with a decrease in the total amount of hematite as well as the increase in the amount of the spinel phase. The RDI values obtained for the low silica –low alumina sinter with 2.8% MgO content were higher than those obtained in the Base Case sinter at an ignition temperature of 1053^{o}C.

The tumbler index for the Base Case sinter at an ignition temperature of 1053^{o} was almost similar to the TI obtained for the low silica – low alumina sinter with 2.8% MgO content, and exceeded the minimum acceptable value of 70% for the TI. The mineralogical analysis showed that the amount of the glassy silicate phase increased with increasing MgO while the crystalline silicates and acicular SFCA decreased with increasing MgO content. From the higher concentration of the glassy phase and lower concentration of acicular SFCA would be expected that the TI would decrease with increasing MgO content. This could however not be confirmed due to the uncertainty at 2.8% MgO content.

The abrasion index increased with increasing MgO content of low silica – low alumina sinter. The decrease in abrasion resistance is associated with an increase in the volume percentage of the spinel phase, glassy silicates, dendritic and eutectic SFCA. The Abrasion index values obtained in the Base Case sinter at an ignition temperature of 1053^{o} was almost the same as the one obtained in the low silica – low alumina sinter with 2.8% MgO content. Another parameter, which is said to be in correlation with the abrasion index, is the porosity. This was not investigated in this work. But, previous studies showed that the increase in MgO may lower the abrasion resistance because of its inverse relationship with porosity [46].

The coke breeze rate for the low silica-low alumina sinter with 2.8% MgO content is slightly higher than that of the Base Case sinter at an ignition temperature of 1053^{o}C. The coke breeze rate increased with increasing MgO. This can mainly be attributed to the fact that MgO was added through dolomite addition which required additional heat for the decomposition of the calcium carbonate and magnesium carbonate and the dehydration of $Mg(OH)_2$ that usually forms after decomposition of magnesium carbonate.

Proof by thermodynamics of the amount of coke needed for $CaMg(CO_3)_2$ decomposition and dehydration of $Mg(OH)_2$:

1^o) For dolomite decomposition: $CaMg(CO_3)_2 = CaO.MgO + 2CO_2$ ΔH_{Rx}= 295401 J/mol and ΔS^o_{Rx}=338.69 J/mol K, thus $T_{diss} = \Delta H^o_{Rx}/\Delta S^o_{Rx}$ = 872 K

Mass of total mixture = 150 kg

If we consider 1% mass of MgO = 1.5 kg = 37.22 moles of MgO produced by 37.22 moles of $CaMg(CO_3)_2$

Minimum heat required to decompose 37.22 moles of dolomite:

$Q = n .C. \Delta T$ Thus, Q = 37.22 X 157.8 X(872 – 298) = 3371625 J

Heat provided by coke: $C + O_2 = CO_2$ ΔH^o_{Rx} = -393505 J/mol

Mass of coke require with coke containing 90% Carbon:

$M_{C(1)}$ = (3371625 X12 X 100)/(393505 X 90) = 114.2 g of coke

2^o) For dehydration of $Mg(OH)_2$:

$Mg(OH)_2 = MgO_{(s)} + H_2O_{(g)}$ ΔH^o_{Rx} = 81598 J/mol

Mass of coke required for dehydration of 37.22 moles of $Mg(OH)_2$:

$M_{C(2)}$= (37.22 X 81598 X12 X 100)/(393505 X 90) = 103g of coke required

Mass of coke required for dehydration of 37.22 moles of $Ca(OH)_2$:

$Ca(OH)_2 = CaO_{(s)} + H_2O_{(g)}$ ΔH^o_{Rx} = 108284 J/mol

Q = 37.22 mol X 108284 J/mol = 403033 J

Mass of coke required: $M_{C(3)}$ = (37.22 X 108284 X 12/100)/(39505 X 90) = 136.6 g of coke

Total mass of coke required $M_T = M_{C(1)} + M_{C(2)} + M_{C(3)}$= 142 + 103 + 136= 353.6g of coke

For 1t of sinter, mass of extra coke required = (353.6/150) X 1000

= 2.4 kg of coke required/ t of sinter produced

III.3 HIGH SILICA- LOW ALUMINA SINTER

The composition and conditions of the sinter are given in Table 4. The silica content of this sinter was increased up to 5.6%, while the MgO content was varied from 1, 2 to 3 mass %. Al_2O_3 was kept constant at 1.7 mass % as described in Chapter II Section 2. Two MgO-bearing materials were used to adjust the MgO content of the sinter: Fused magnesia and Dolomite. The chemical compositions of these high silica-low alumina sinters while changing MgO contents are given in Tables 28 and 29.

Table 28 Chemical composition of the High silica – Low alumina Sinter mixture (mass %) With dolomite addition

Comp.	1% MgO			2% MgO			3% MgO		
	SPL 1	SPL2	*Average*	SPL 3	SPL4	*Average*	SPL 5	SPL6	*Average*
$Fe_{(total)}$	58.80	57.10	57.95	56.60	55.90	56.25	55.70	55.20	55.45
FeO	7.70	8.14	7.92	7.98	8.01	8.00	7.12	7.89	7.51
Fe_2O_3	72.50	72.40	72.45	71.64	70.64	71.14	71.72	71.10	70.41
$Fe_{(met)}$	0.10	0.11	0.11	0.29	0.27	0.28	0.01	0.05	0.03
CaO	10.50	10.20	10.35	10.20	10.70	10.45	11.20	11.00	11.10
MgO	1.10	1.14	1.12	1.65	1.94	1.80	2.92	2.71	2.82
SiO_2	5.76	5.69	5.73	5.60	5.77	5.69	5.80	5.57	5.69
Al_2O_3	1.70	1.68	1.69	1.67	1.68	1.68	1.73	1.69	1.71
K_2O	0.06	0.06	0.06	0.05	0.04	0.05	0.04	0.05	0.04
Na_2O	0.01	0.01	0.01	0.01	0.01	0.01	0.01	0.01	0.01
TiO_2	0.10	0.10	0.10	0.10	0.10	0.10	0.11	0.10	0.10
MnO	0.32	0.31	0.31	0.32	0.32	0.32	0.35	0.14	0.35
P	0.05	0.04	0.04	0.04	0.04	0.04	0.04	0.05	0.05
S	0;01	0.01	0.01	0.02	0.01	0.01	0.01	0.01	0.01
C	0.08	0.06	0.07	0.15	0.14	0.16	0.28	0.28	0.28
Basicity	1.82	1.79	1.81	1.82	1.85	1.84	1.93	1.97	1.95

SPL 1,2, 3,4: Sample 1,2,3,4

Table 29 Chemical composition of the High silica – Low alumina Sinter mixture (mass %) : With fused magnesia addition

Comp.	1% MgO			2% MgO			3% MgO		
	SP1	SP2	*Average*	SP3	SP4	*Average*	SP5	SP6	*Average*
$Fe_{(total)}$	56.40	56.70	56.55	56.80	55.70	56.55	55.7	55.40	55.60
FeO	8.21	7.36	7.72	7.45	7.36	7.41	8.00	7.64	7.80
Fe_2O_3	71.60	72.80	72.15	72.70	72.20	72.45	70.5	70.60	70.6
$Fe_{(met)}$	0.05	0.07	0.06	0.17	0.20	0.19	0.21	0.65	0.10
CaO	11.20	11.00	11.10	10.90	10.50	10.70	10.8	11.00	10.9
MgO	1.00	1.00	1.00	1.36	1.75	1.56	2.50	2.80	2.70
SiO_2	5.79	5.54	5.67	5.44	5.54	5.49	5.65	5.47	5.56
Al_2O_3	1.75	1.71	1.73	1.64	1.67	1.66	1.70	1.65	1.70
K_2O	0.07	0.07	0.07	0.06	0.10	0.08	0.07	0.08	0.08
Na_2O	0.01	0.01	0.01	0.01	0.01	0.01	0.01	0.02	0.01
TiO_2	0.10	0.10	0.10	0.09	0.10	0.09	0.11	0.10	0.10
MnO	0.31	0.28	0.29	0.29	0.30	0.30	0.40	0.14	0.35
P	0.08	0.04	0.06	0.04	0.05	0.05	0.04	0.05	0.05
S	0.01	0.02	0.01	0.02	0.01	0.02	0.01	0.01	0.01
C	0.25	0.19	0.22	0.60	0.17	0.12	0.28	0.28	0.28
Basicity	1.82	1.79	1.81	2.00	1.90	1.95	1.93	1.97	1.95

The chemical composition of the mixtures where dolomite and magnesia were used was almost the same except for 2% MgO sinters where the basicity was 1.85 with dolomite addition against 1.95 with magnesia addition. The slight difference noticed was that the CaO content in the mixture with dolomite addition was used to adjust the MgO content of the sinter was slightly higher than in the mixture with fused magnesia addition.

III.3.1 Quantification of phases

Point-counting data in Table 30 gives the variation of the volume percent of different morphologies depending on the MgO content of the sinter.

It can be seen that the volume percentage of the spinel phase increased with increasing MgO content while the total hematite decreased with increasing MgO. This is similar to what was found previously in the low alumina – low silica sinter. The amount of the spinel phase is slightly higher where fused magnesia was added than where dolomite was added. It can also be seen that the total hematite decreased with increasing MgO content of the sinter, similar to what was reported for the low alumina – low silica sinter (section III.2). However, the decrease in total hematite for the sinter to which fused magnesia was added, is more pronounced than for the sinter to which dolomite was added.

The total amount of SFCA decreased in both types of sinters with increasing MgO content. However, more of the SFCA phase was produced with dolomite addition, while the columnar and blocky SFCA content of the sinter to which dolomite was added, was significantly higher than in the sinter to which fused magnesia was added. The SFCA acicular/columnar ratio in the sinter to which dolomite was added decreased with increasing MgO content. The same trends have been found in the low silica – low alumina sinter. The higher amount of SFCA in sinter where MgO was added through dolomite than the sinter where MgO was added through fused magnesia could be probably be due to the fact that more SFCA can be obtained at lower temperatures (with dolomite addition, due to the decomposition of the carbonates) than at higher temperatures (with fused magnesia addition) similar to what was reported by Egundebi and Whiteman [(1)]. The crystalline silicates increased as well as the glassy phase while the MO/(Fe, Mg)O phase increased slightly for both types of sinters products. But more crystalline silicates were formed with dolomite addition.

Table 30 Quantification of phases

Composition	MgO (mass%)					
	1		2		3	
	FM	Dolo	FM	Dolo	FM	Dolo
Spinel	31.2±0.01	31.3±0.01	38.7±0.01	37.0±0.01	43±0.01	41.2±0.01
Hematite relict	12.3±0.02	13.4±0.01	11.2±0.01	14.2±0.01	1.6±0.01	2.0±0.01
Hematite rhombic	4.2±0.01	4.9±0.02	1.4±0.01	1.5±0.01	3.1±0.01	3.3±0.01
Hematite finely granular	1.2±0.01	1.4±0.01	0.1±0.02	1.0±0.01	0.1±0.01	1.8±0.01
Hematite skeletal	8.5±0.02	7.2±0.01	5.40±0.01	4.0±0.02	7.8±0.02	6.7±0.02
Total Hematite	26.2±0.02	26.9±0.01	17.9±0.01	20.7±0.01	12.6±0.02	13.8±0.01
SFCA acicular	7.5±0.01	7.9±0.02	5.2±0.02	8.8±0.02	5.6±0.01	5.8±0.01
SFCA columnar and blocky	14.9±0.01	15.1±0.01	13.6±0.02	20.0±0.02	11±0.01	14.6±0.01
SFCA dendritic and eutectic	12.9±0.01	13.1±0.01	11.8±0.01	5.4±0.01	10±0.01	12.7±0.01
Total SFCA	35.3±0.02	36.1±0.02	30.6±0.01	34.2±0.02	26.6±0.01	33±0.01
MO/(Fe,Mg)O	0.3±0.01	0.2±0.02	0.4±0.02	0.2±0.01	0.7±0.01	0.7±0.02
Crystalline silicates	3.6±0.01	5.4±0.01	4.9±0.01	5.5±0.01	5.6±0.01	6.0±0.01
Glass	3.0±0.01	2.7±0.01	3.2±0.01	3.2±0.01	4.8±0.01	5.8±0.01
***SFCA* acicular/columnar ratio**	0.50	0.52	0.38	0.44	0.51	0.40

FM = Fused Magnesia **Dolo** = Dolomite

III.3.2 Sinter properties

III.3.2.1 Reducibility Index

The reducibility of sinters to which both fused magnesia and dolomite were added, increased with increasing MgO content. The variation of the reducibility index is given in Table 31 and in Figures 29a and 29b.

Table 31 Variation of the reducibility index (%/min) with increasing MgO

MgO mass %	*Reducibility Index*			
	Fused magnesia		*Dolomite*	
1.0	0.81	0.82	0.86	0.89
2.0	0.72	0.76	0.92	0.96
2.8	0.90	0.96	0.92	0.97

The values for the reducibility index obtained for the high silica in this sinter are lower than those obtained for the low SiO_2 sinter although the increase with increasing MgO content while the reducibility decreases with increasing MgO content for the low silica sinter. This is presumably due to the fact that when the SiO_2 content in the sinter is higher, a higher

concentration of iron-containing silicates form which are not as high readily reducible as hematite, SFCA or spinel phases.

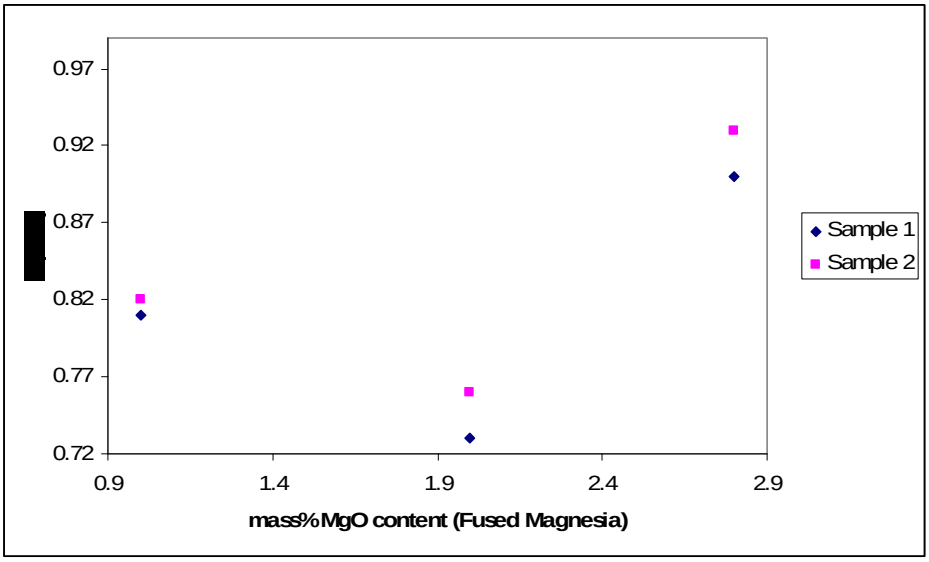

Figure 29.a Variation of Reducibility Index (RI) with MgO (Fused magnesia)

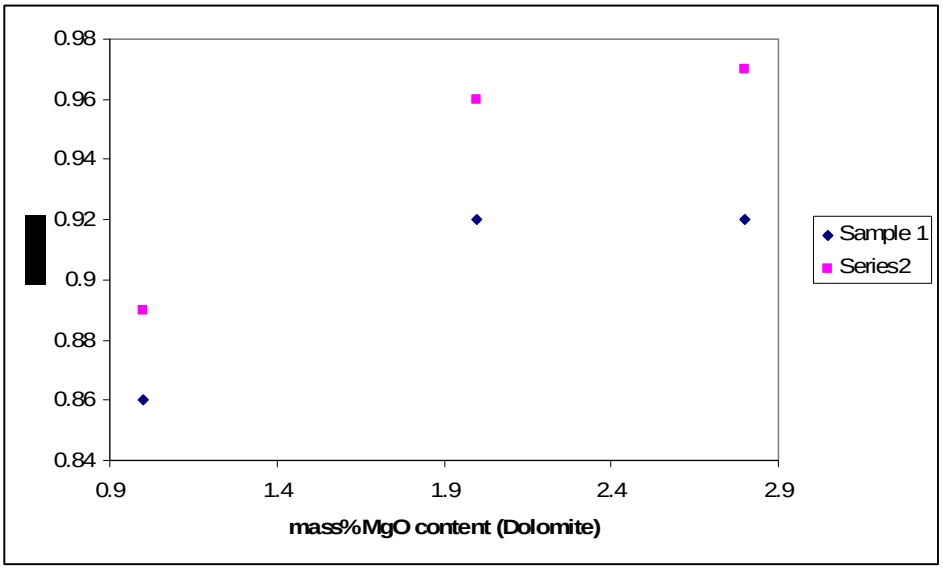

Figure 29.b Variation of Reducibility Index (RI) with MgO (Dolomite)

The values of the reducibility index obtained when MgO was added through dolomite addition were higher than those obtained with fused magnesia. This can be explained from the lower spinel, higher total hematite and higher SFCA content in the sinter where dolomite was added. Also, dolomite being a carbonate, some of the heat provided by the combusted

coke was used to decompose the carbonate. This implies that slight lower temperatures would be reached when MgO is added through dolomite addition, and the oxygen partial pressure would be relatively higher due to CO_2 that is evolved. However, the reducibility increased with increasing MgO content in the sinter. This is opposite to what was found in the low silica-low alumina sinter. The increase in silica content seems to have a pronounced effect on the reducibility.

III.3.2.2 Reduction degradation index (RDI)

The influence of MgO on the reduction degradation index is given in Table 32 and shown in Figures 30 when fused magnesia is added and 31 when dolomite is added.

Table 32 Variation of RDI (%) versus MgO (mass%)

Mass% MgO	**Fused magnesia**				**Dolomite**			
	+6.3mm	***+6.3 mm***	***+3.15 mm***	***+3.15 mm***	***+6.3 mm***	***+6.3 mm***	***+3.15 mm***	***+3.15 mm***
1.0	92.07	91.85	97.0	96.8	91.8	92.90	97.00	96.80
2.0	88.95	91.95	94.05	95.35	87.00	88.10	94.05	95.35
2.8	92.05	93.3	89.0	93.1	77.00	82.00	89.00	93.10

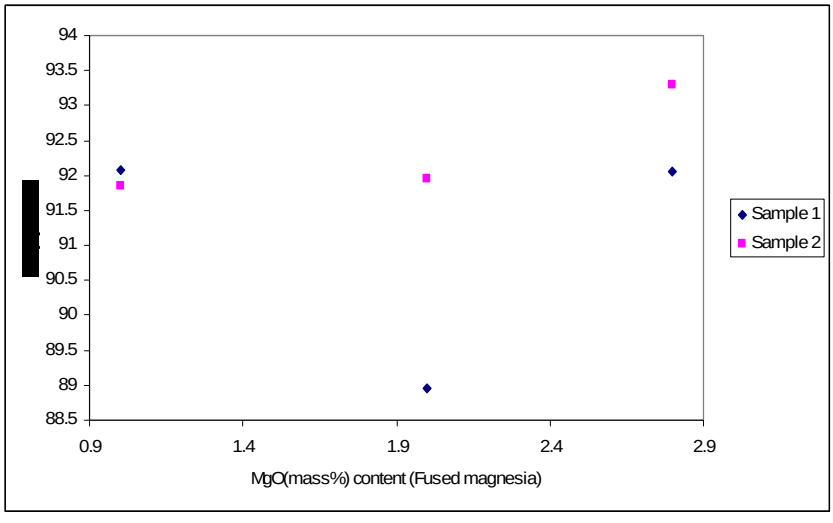

Figure 30(a) Influence of MgO (added as Fused Magnesia) content on the RDI (+6.3mm)

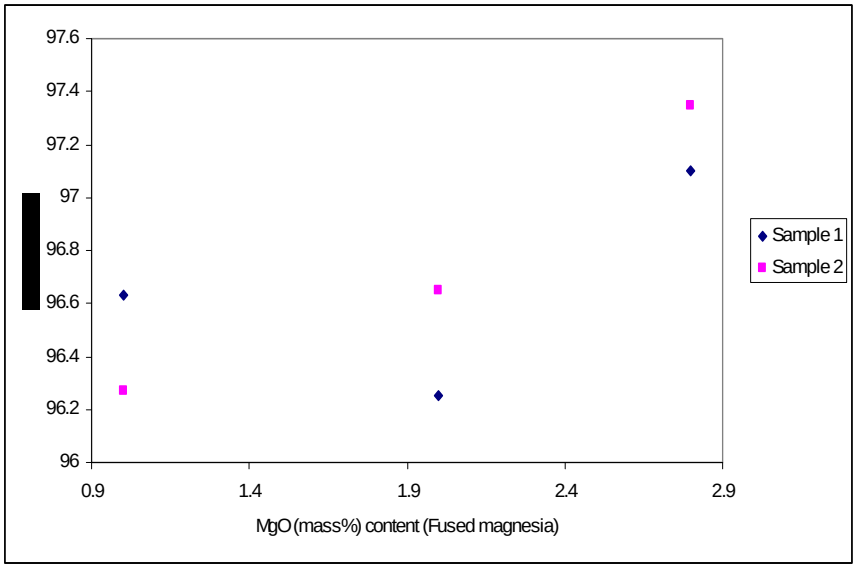

Figure 30(b) Influence of MgO (added as Fused Magnesia) content on the RDI (+3.15mm)

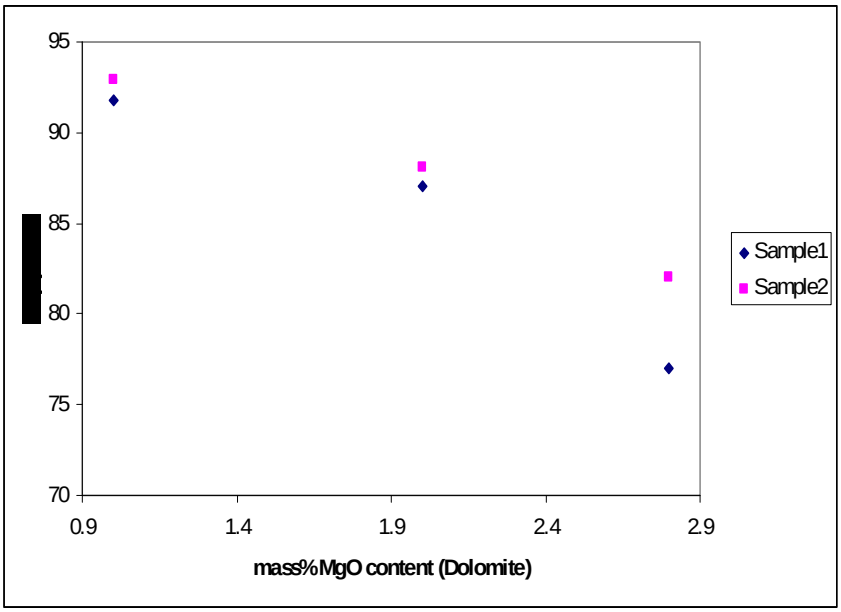

Figure31(a). Influence of MgO (added as dolomite) content on the RDI (+6.3mm)

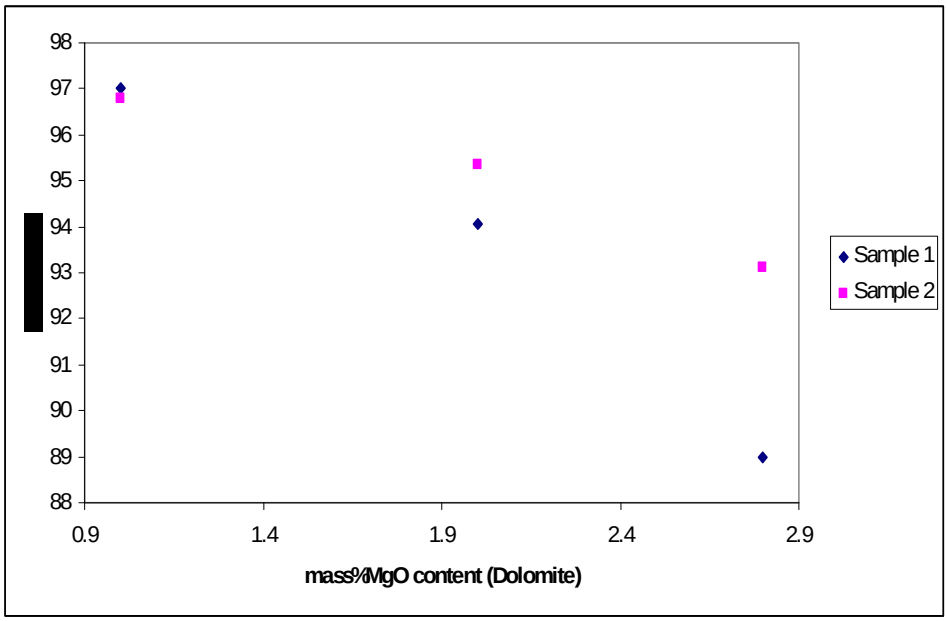

Figure31(b) Influence of MgO (added as dolomite) content on the RDI (+3.15mm)

For the sinter where MgO was added through fused magnesia, the reduction degradation index increased with increasing MgO content (similar to the low silica – low alumina sinter). This could be due to a decrease in hematite and an increase in spinel phase. But the reduction degradation index decreased with increasing MgO content for the sinter when MgO was added through dolomite although the amount of hematite decreased and that of spinel phase increased with increasing MgO content. The only significant difference between the sinters to which fused magnesia and dolomite were added, is higher concentration of columnar and blocky SFCA in the sinter to which dolomite was added. This behaviour can presumably be explained by the fact that the sintering temperature was lower for this sinter compare to the sinter with added fused magnesia. Theoretically, the sintering temperature was low due to the heat consumed by the decomposition of dolomite and some other amount of heat was consumed by dehydration after hydration of burnt dolomite.

III.3.2.3 Tumble index (TI)

The influence of MgO content of the sinter on the strength of the sinter when dolomite and fused magnesia were added as MgO-bearing materials is given in Tables 33(a, b) and Figures 32 (a, b).

Table 33a Variation of the TI with MgO (mass%) content

MgO	*Tumble index (TI, %)*			
Mass %	***Fused magnesia***		***Dolomite***	
1.0	77.67	77.59	74.93	74.16
2.0	76.24	72.88	75.19	74.12
2.8	76.37	77.90	73.60	74.45

Table 33b Variation of the AI with MgO (mass%) content

MgO	*Abrasion index (AI, %)*			
Mass %	***Fused magnesia***		***Dolomite***	
1.0	4.16	4.22	4.53	4.18
2.0	2.66	4.21	4.10	4.87
2.8	3.78	4.28	4.78	4.79

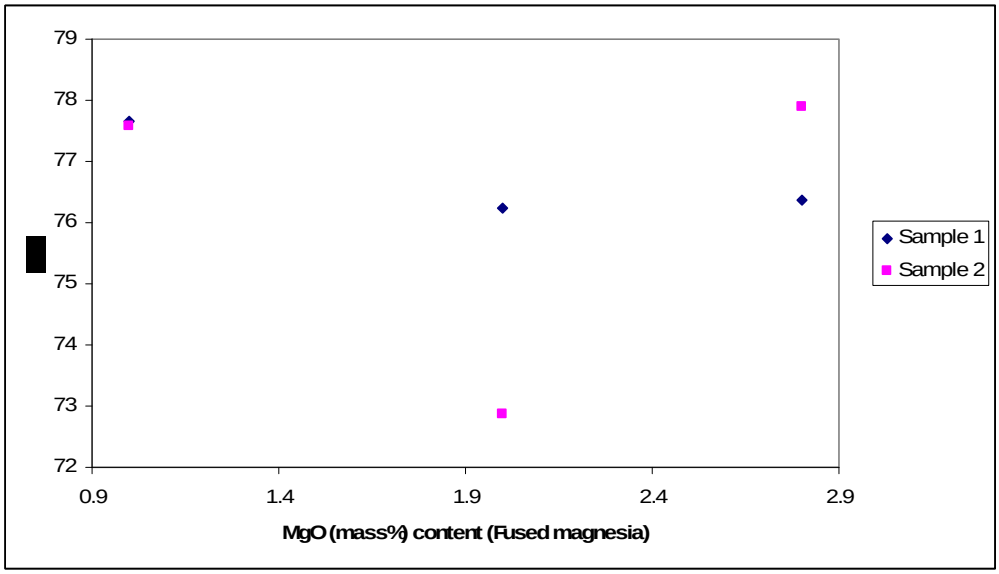

Figure32 (a) Influence of MgO content on TI

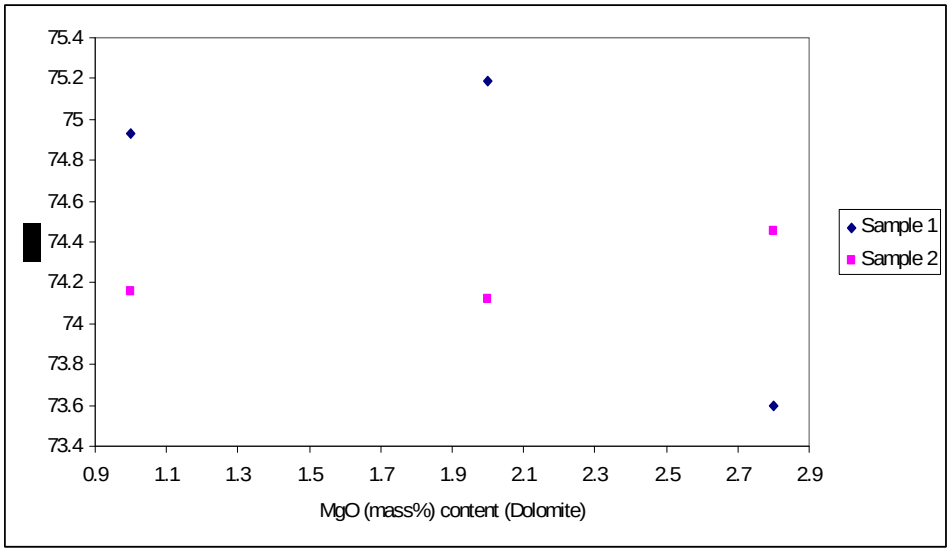

Figure32 (b) Influence of MgO content on TI

It can be seen that the tumble index decreased slightly with increasing MgO content when both fused magnesia and dolomite were used. This is explained by a slight increase in the glassy phase, which has high stress. The behavior shown here by the tumble index might be influenced by a further addition of silica added.

Also, comparing the values obtained with addition of fused magnesia to those obtained with the addition of dolomite, it can be seen that higher values are associated with fused magnesia addition.

III.3.2.4 Abrasion index

The influence of MgO on the abrasion index of the sinters to which dolomite and fused magnesia were added as MgO-bearing materials is given in Table 33b and shown in Figures 33 (a, b).

The trends of the abrasion index were not the same for the sinter produced where the MgO content was increased through dolomite addition compared to that where MgO was added through fused magnesia addition. The comparison shows that the abrasion index of the sinter to which dolomite was added increased with increasing MgO content of the sinter. This was similar to what was observed in the low silica-low alumina sinter.

But, the abrasion index of the sinter to which fused magnesia was added decreased with increasing MgO content. The variation in abrasion index can therefore not be explained by an increase in basicity index. This behaviour is not fully understood.

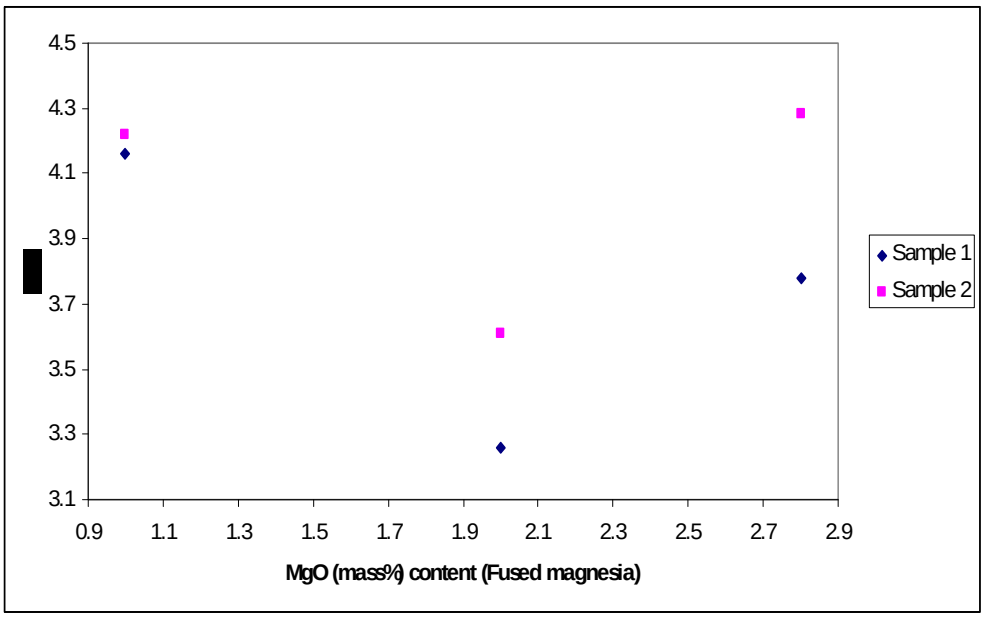

Figure 33(a) Influence of MgO content of the sinter on the AI

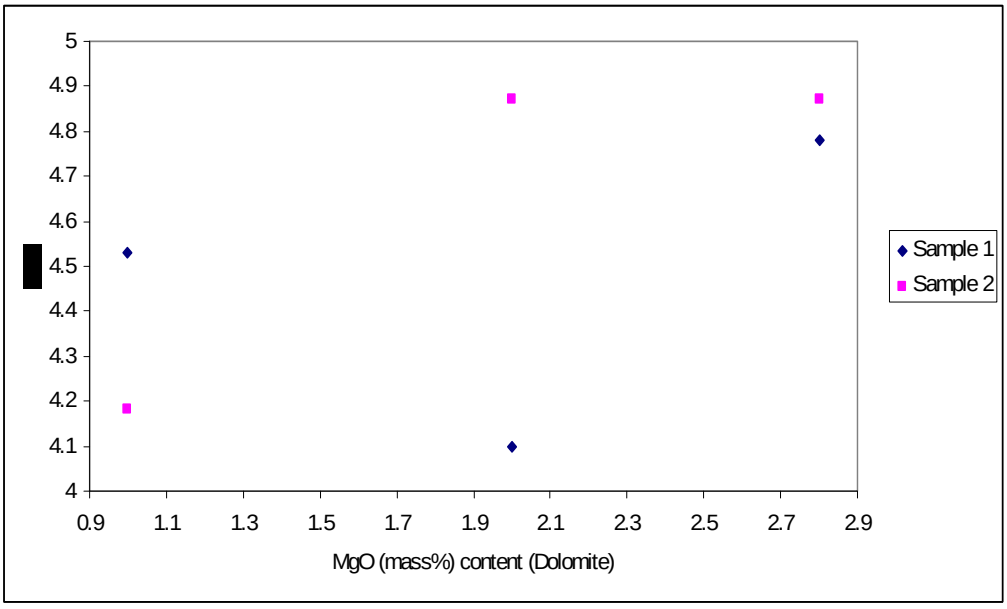

Figure 33(b) Influence of MgO content of the sinter on the AI

III.3.2.5 Influence of MgO on coke breeze rate

The influence of MgO addition on the coke rate is given Tables 34 and Figure 34.

Table 34 Variation of coke breeze rate [kg/t sinter] with MgO added

Mass % MgO	Fused magnesia	Dolomite
1	74.00	76.29
2	74.73	76.93
2.8	77.13	79.66

From the variation shown in Figure 34, it can be seen that the coke breeze rate increased with increasing MgO for both sinters where MgO has been added through dolomite and through fused magnesia addition. The coke breeze rate was higher for the sinter where MgO was added through dolomite. This could be due to more heat required for the decomposition of magnesium and calcium carbonates.

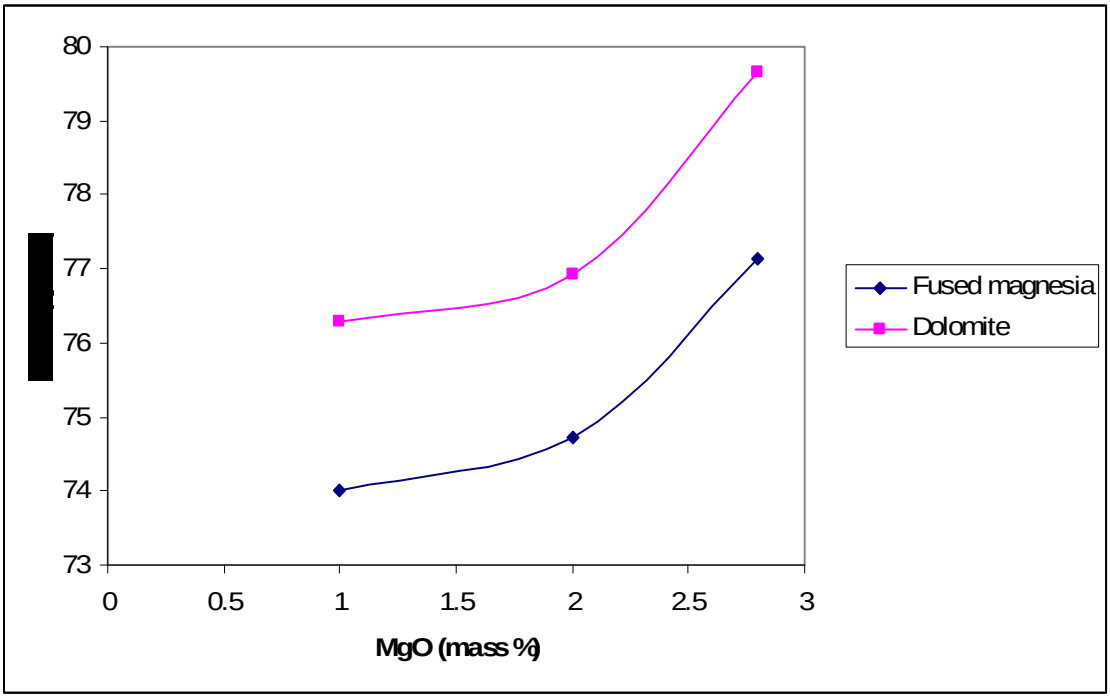

Figure34(a) Influence of MgO content on the coke breeze rate

III.3.3 Conclusions

The addition of MgO changes the mineralogy as well as the properties of the sinter product. MgO was added through dolomite and fused magnesia. From the results obtained, the following conclusions were established:

The volume percentage of the spinel phase increased with increasing MgO content while the total hematite decreased with increasing MgO. This was similar to what was found previously in the low alumina – low silica sinter. The amount of the spinel phase was slightly higher where fused magnesia was added than where dolomite was added. It can also be seen that the total hematite decreased with increasing MgO content of the sinter, similar to what was reported for the low alumina – low silica sinter (section III.2). However, the decrease in total hematite for the sinter to which fused magnesia was added was more pronounced than in the sinter to which dolomite was added.

The total amount of SFCA decreased in both types of sinters with increasing MgO content. However, more of the SFCA phase was produced with dolomite addition. The SFCA acicular/columnar ratio also decreased with increasing MgO. The same trends have been found in the low silica – low alumina sinter although the total SFCA, columnar and acicular as well as dendritic and eutectic SFCA contents of the high silica – low alumina sinter are higher than in the low silica –low alumina sinter.

The crystalline silicates increased as well as glass while the MO/(Fe,Mg)O phase increased only slightly for both sinters with increasing MgO content. But, more crystalline silicate was formed with dolomite addition. The high silica – low alumina sinters contain more crystalline silicates, but less glass, than that in the low silica – low alumina sinters.

The reducibility of sinters to which both fused magnesia and dolomite were added, increased with increasing MgO content. The reducibility obtained in this sinter were lower than those obtained with low SiO_2 –low alumina sinter. This could most probably be due to the fact that when SiO_2 and CaO content are low in the sinter, the formation of crystalline silicates containing ferrous oxides might have been restricted.

The values of the reducibility index obtained when MgO was added through dolomite addition were higher than those obtained with fused magnesia. This could be explained by the fact that higher amount of SFCA was formed in the sinter where dolomite was used. Also, dolomite being a carbonate, some of the heat provided by the combusted coke was used to decompose the carbonate. This might have avoided reaching higher temperatures, which, led to more SFCA being formed when MgO was added through dolomite. The oxygen partial pressure would also be relatively higher due to the evolution of CO_2.

However, the reducibility increased with increasing MgO content in the sinter. This is opposite to what was found in the low silica-low alumina sinter. The increase in silica content might have had a remarkable effect on the reducibility. More recently, the same trend was obtained by Matsumura *et al.*, 2005 in their research work [39].

For the sinter where MgO was added through fused magnesia, the reduction degradation index increased with increasing MgO content. This could be due to a decrease in hematite and an increase in spinel phase. But the reduction degradation index decreased with increasing MgO content for the sinter when MgO was added through dolomite although the amount of hematite decreased and that of spinel phase increased with increasing MgO content. This could have led to an increase in reduction degradation index as found with sinters where MgO addition was done through fused magnesia and in the low alumina – low silica sinter. This behaviour must be related to the temperature which was slightly lower, and the pO_2 slightly higher, compared to when fused magnesia was added, but it is not fully understood.

The tumble index decreased slightly with increasing MgO content when both fused magnesia and dolomite were used. This may be explained by a slight increase in the glassy phase. The behaviour shown here by the tumbler index is presumably influenced by the higher silica concentration. Also, comparing the values obtained with addition of fused magnesia to those obtained with addition of dolomite, it can be seen that higher TI values were obtained with fused magnesia addition. But, the tumbler index in the low silica-low alumina sinter did not show a clear trend when the MgO content increased from 2% MgO to 2.8 % MgO.

The trends of the abrasion index for the sinter produced where the MgO content was increased through dolomite addition compared to that when MgO was added through fused magnesia

addition were not the same. The comparison showed that the abrasion index of the sinter to which dolomite was added increased with increasing MgO content of the sinter. This is similar to what was observed in the low silica-low alumina sinter. But, the abrasion index of the sinter to which fused magnesia was added decreased with increasing MgO content. This behaviour is not fully understood.

The coke breeze rate increased with increasing MgO for both sinters where MgO has been added through dolomite and through fused magnesia addition. The coke breeze rate was higher for the sinter where MgO was added through dolomite. This is presumably due to more heat required for the decomposition of magnesium and calcium carbonates in the dolomite. As mentioned earlier, the decomposition of dolomite is accompanied by the hydration of burnt dolomite, which in turn requires heat for dehydration.

III.4 HIGH SILICA – HIGH ALUMINA SINTER

The silica content of this sinter was kept constant at 5.6% while the alumina content of the sinter was increased up to 3% through the addition of bauxite. The chemical composition of the bauxite used is given in Table 35. The MgO content was kept constant at 2.8 mass %. The sintering conditions are given in Table 36.

Table 35 Chemical composition of the bauxite

Compound	**Al_2O_3**	**SiO_2**	**Ti O_2**	**CaO +MgO**	**Na_2O + K_2O**	**P_2O_5**	**Fe_2O_3**
Mass %	80	11.9	2.5	0.7	0.4	<4.0	<1.5

Table 36 Sintering process conditions for the production of high alumina- high silica sinter

Sinter composition (mass %)		***Sinter pot test conditions***	
Basicity (CaO/SiO_2)	2	**Ignition**	
FeO	7.0-9.0	Temperature [^{0}C]	1051^0 C
Fe	53.0	Time [min]	1.5
CaO	10.7	Pressure drop [mmH_2O]	500
SiO_2	5.6	**Sintering**	
Al_2O_3	3.0	Pressure drop [mmH_2O]	1200
MgO	2.8	**Cooling**	
		Pressure drop [mmH_2O]	1500

Table 37 Chemical composition of the High alumina – High silica sinter

Fe (tot)	**FeO**	**Fe_2O_3**	**Fe (met)**	**CaO**	**MgO**	**SiO_2**	**Al_2O_3**	**K_2O**	**Na_2O**	**TiO 2**	**Mn O**	**P**	**S**	**C**	**Basici-ty**
54.9	**7.9**	**69.6**	**0.1**	**10.7**	**2.6**	**5.8**	**2.9**	**0.0**	**0.0**	**0.3**	**0.0**	**0.0**	**0.0**	**0.0**	**1.9**

III.4.1 Quantification of phases

The amount of different phases present in the high silica – high alumina sinter is given in Table 38.

The amounts of spinel phase is higher than that obtained in the Base Case sinter at the ignition temperature of 1053^{o}C, lower than that obtained at 2.8% MgO content in the Low alumina – low silica sinter, but is lower for high silica – low alumina sinter when MgO is added through dolomite and fused magnesia.

The amount of hematite relict is lower than that obtained at an ignition temperature of 1053^{o}C for the Base case sinter, and that obtained at 2.8% MgO content for the low alumina – low silica sinter as well as those obtained for the high silica – low alumina sinter at 2.8% MgO content when fused magnesia and dolomite are added.

The amount of hematite rhombic is slightly higher than that obtained at the ignition temperature of 1053^{o}C for the Base Case sinter and that obtained at 2.8% MgO content for the low silica –low alumina sinter, and is higher than those obtained at 2.8% MgO for the high silica – low alumina sinter when fused magnesia and dolomite are added.

The amount of hematite finely granular is higher than that obtained at the ignition temperature of 1053^{o}C for the Base Case sinter, higher than that obtained at 2.8% MgO content for the low silica – low alumina sinter and higher than those obtained at 2.8% MgO content when fused magnesia and dolomite are added.

The amount of hematite skeletal is lower than that obtained at 1053^{o}C as ignition temperature for the Base Case sinter, lower than that obtained at 2.8% MgO content as well as those obtained for the high silica – low alumina sinter at 2.8% MgO content when fused magnesia and dolomite are added.

The SFCA acicular/ columnar ratio is low compared to that obtained at the same ignition temperature of 1053^{o}C for the Base Case sinter, but is slightly higher than those obtained with 2.8% MgO content added through dolomite addition for the high silica – low alumina sinter.

Table 38 Quantification of phases of the high alumina-high silica sinter

Point-counting categories	Volume %
Spinel	35.5±0.01
Hematite relict	1.3±0.01
Hematite rhombic	4.4±0.01
Hematite finely granular	2.4±0.01
Hematite skeletal	3.8±0.02
Total hematite	11.9±0.01
SFCA acicular	11.3±0.01
SFCA columnar & blocky	25.4±0.01
SFCA dendritic & eutectic	4.1±0.02
Total SFCA	40.8±0.02
MO/(Mg,Fe)O	3.2±0.01
Periclase	0.3±0.01
Crystalline silicates	3.5±0.01
Glass	4.4±0.01
Comment: SFCA acic/col.	0.44

III.4.2 Sinter properties

The sinter property result is given in Table 39.

Table 39 Sinter properties of the high alumina-high silica sinter.

RI (%/min)	RDI (%)		TI (%)	AI (%)	Coke rate [Kg/t sinter]	Yield (%)	Pro. rate* Kg/m^2/day
	+6.3mm	*+3.15mm*					
0.7	74.6	89.9	66.4	4.35	87.32	85	30.85

*****_Pro. Rate= Production rate_

The reducibility index was 0.7. This is less than the minimum requirement ≥ of 1%/min for Kumba Iron Ore. This is the lowest compared to those associated with the other sinters studied in this research project.

The reduction degradation index is higher than 70%. This met the requirement of Kumba Iron Ore of ≥ 70 for the +6.3mm size fraction, but is the lowest value obtained compared to other sinters produced in this research project.

The tumbler index is of 66.4 %, which is less than the minimum requirement of Kumba Iron Ore of 70%.

The abrasion index is 4.35 % which is better than for other sinters investigated in this project.

The coke rate is the highest compared to other sinters produced in this project. The increase in alumina content increased further the coke breeze rate.

The yield is 85%, which also is higher than for the other sinters investigated in this work project.

III.4.3 Conclusions

The results show that the reducibility index, the reduction degradation index and the tumbler index were lower than the required values by Kumba Iron Ore while the abrasion index met the requirement while the coke consumption was the highest compared to all sinters investigated in this project.

Chapter IV SUMMARY AND CONCLUSIONS

IV.1 Influence of ignition temperature on the mineralogy and properties of iron sinter

The results showed that the optimum ignition temperature was 1053 ^{o}C. The amounts of the spinel phase showed a sharp increase at 1100^{o}C while the total amount of hematite decreased with increasing ignition temperature. The ratio of acicular SFCA to columnar SFCA remained almost constant and only decreased considerably at an ignition temperature of 1100^{o}C while the amount of crystalline silicates reached a maximum at 1053^{o} C ignition temperature and then decreased at 1100^{o} C. The amount of glassy phase reached its maximum at an ignition temperature of 1100^{o}C.

The RI remained almost constant at a value of approximately 1%/min with increasing ignition temperature while the RDI decreased slightly with increasing ignition temperature.

The sinter of lowest quality, according to the requirements of Kumba Iron Ore, was obtained at an ignition temperature of 897^{o}C (RDI of 65 %), while the highest quality sinter was obtained at an ignition temperature of 917 ^{o}C (RDI 81%).

The TI as well as the AI values increased slightly with increasing ignition temperature. The TI of the sinters produced at all ignition temperatures exceeded the minimum requirement of 70%. Only the sinter produced at an ignition temperature of 963^{o}C conformed to the requirement of Kumba Iron Ore of an AI of ≤5%. The crystalline silicate phase increased with increasing ignition temperature. But, no allotropic transformation from β- Ca_2SiO_4 to γ- Ca_2SiO_4 did take place because during the cooling stage reason why TI and AI increased.

The yield increased with increasing ignition temperature.

The production rate obtained at the ignition temperature of 963^{o}C was the highest. The lowest coke consumption was obtained at the ignition temperature of 1053^{o} C.

According to the requirements of Kumba Iron Ore the sinter of highest quality (considering the RI, RDI, TI, AI, Yield and production rate) and taking into account the economical aspects (coke consumption), the sinter that was ignited at 1053^{o}C met the requirements of Kumba Iron Ore.

IV.2 Low silica - Low alumina sinter

IV.2.1 Sinter mineralogy

The amount of the spinel phase increased with increasing MgO content of the sinter.

The ratio SFCA acicular/columnar as well as the total SFCA decreased with increasing MgO content while the amount of magnesio-wustite phase increased with increasing MgO and the amount of crystalline silicates decreased with increasing MgO.

IV.2.2 Sinter properties

The reducibility index decreased with increasing MgO content of the sinter while the RDI increased with increasing MgO.

The tumbler index for the Base Case sinter at an ignition temperature of 1053^{o} was almost the similar to the TI obtained for the low silica – low alumina sinter with 2.8% MgO content, and exceeded the minimum acceptable value of 70% for the TI.

The abrasion index increased with increasing MgO content while the coke breeze rate increased with increasing MgO.

IV.3 High Silica – Low Alumina

The influence of silica addition on the sinter quality as well as a comparative study of MgO addition through dolomite and fused magnesia was investigated.

IV.3.1 Sinter mineralogy

The amount of the spinel phase increased with increasing MgO content irrespective of the MgO-bearing mineral and was slightly higher when fused magnesia was added than dolomite while the total hematite decreased with increasing MgO and was similar to what was found in the low alumina – low silica sinter. The decrease in total hematite for the sinter to which fused magnesia was added was remarkably higher than in the sinter to which dolomite was added.

The total amount of SFCA and the SFCA acicular/columnar decreased in both types of sinters with increasing MgO content. However, more of the SFCA phase was produced with dolomite addition.

The crystalline silicates increased and glass while the MO/(Fe,Mg)O phase increased only slightly for both sinters with increasing MgO content and more crystalline silicate formed with dolomite addition.

The reducibility of sinters to which both fused magnesia and dolomite were added, increased with increasing MgO content. The reducibility indexes obtained when MgO was added through dolomite addition were higher than those obtained with fused magnesia.

For the sinter where MgO was added through fused magnesia, the reduction degradation index increased with increasing MgO content while it decreased with increasing MgO content for the sinter when MgO was added through dolomite and is not fully understood.

The tumbler index decreased slightly with increasing MgO content when both fused magnesia and dolomite were used. Higher TI values were obtained with fused magnesia addition.

The AI for the sinter produced where the MgO content increased through dolomite addition compared to that with fused magnesia addition were not the same. The comparison showed that the abrasion index of the sinter to which dolomite was added increased with increasing MgO content of the sinter, but decreased for the sinter to which fused magnesia was added decreased with increasing MgO content. This behaviour is not well understood.

The coke breeze rate increased with increasing MgO irrespective of MgO-bearing mineral used, but was higher for the sinter where MgO was added through dolomite.

IV.4 High Alumina – High Silica

IV.4.1 Sinter mineralogy

The amounts of spinel phase is higher than in the Base Case sinter at the ignition temperature of 1053^{o}C, lower than that obtained at 2.8% MgO content in the Low alumina –low silica sinter, but is lower for high silica – low alumina sinter when dolomite and fused magnesia were added. But, the amount of hematite relict was lower than that obtained at an ignition temperature of 1053^{o}C for the Base case sinter, and that obtained at 2.8% MgO content for the low alumina – low silica sinter as well as those obtained with high silica – low alumina sinter at 2.8% MgO content when fused magnesia and dolomite are added.

The amount of hematite rhombic was slightly higher than that obtained at the ignition temperature of 1053^{o}C for the Base Case sinter and that obtained at 2.8% MgO content for the

low silica –low alumina sinter, and higher than those obtained at 2.8% MgO for the high silica – low alumina sinter fused magnesia and dolomite addition.

The SFCA acicular/ columnar ratio was low compared to that obtained at the same ignition temperature of 1053^{o}C for the Base Case sinter, but was slightly higher than those obtained with 2.8% MgO content added through dolomite addition for the high silica – low alumina sinter.

The RI was 0.7%. This is the lowest compared to those associated with the other sinters studied in this research project while the RDI, although did meet the requirement of Kumba Iron Ore of ≥ 70 for the +6.3mm size fraction, it was the lowest compared to other sinters produced in this research project.

The tumbler index is of 66.4 %, which is less than the minimum requirement of Kumba Iron Ore of 70%.

The abrasion index is 4.35 % which is better than for other sinters investigated in this project.

The coke rate is the highest compared to other sinters produced in this project while the yield is 85%, which also is higher than for the other sinters investigated in this work project.

CONCLUSION

1. The optimum ignition temperature was of 1050^{o}C.
2. Allotropic transformation of the crystalline (dicalcium) silicates phase from β-type (monoclinic) to γ-type (orthorhombic) does not take place in a sinter containing oxides such as P_2O_5, Cr_2O_5 or B_2O_3. Therefore in industrial sinters, no allotropic transformation of the dicacium silicates can be expected.
3. Low silica – low alumina as well as High silica – low alumina sinters with dolomite addition had overall better quality (good mineralogy and good physical properties) compared to High silica – low alumina sinter with addition of fused magnesia as well as high silica – high alumina sinter.
4. Very high silica concentration in the raw material is detrimental to the sinter mineralogy, thus to the sinter properties.

5. Fused magnesia, used as fluxes, produces a sinter of low quality compared to dolomite; but uses lesser coke than dolomite due to extra coke needed to dehydrate $Mg(OH)_2$ as well as $Ca(OH)_2$ that forms after dolomite decomposition.
6. The presence of high silica and high alumina in the raw material are detrimental to the sinter quality although the basicity was kept constant.

Chapter V RECOMMENDATIONS

1) Further work involving temperature associated with pO_2 measurements at the Top, Middle and Bottom of the sinter bed for a better understanding of conditions of temperature and oxygen pressure under which different phases form with ease, thus determine the required working conditions to produce morphologies that lead to a better sinter quality.

2) A comparative study of the temperature and pO_2 when dolomite and fused magnesia are added in order to fully understand the effect of dolomite and fused magnesia on the oxygen pressure throughout the sinter, thus on the mineralogy and sinter properties.

Reference:

1. Egundebi, G.O.; and Whiteman, J.A.: "Evolution of Microstructure in Iron Ore Sinter", Ironmaking and steelmaking, 1989, vol.16, No.6, pp.379-385.

2. Pal, S.; Chandra, N.; Mishra, U.N, Singh, R.N.; & Mediratta, S.R.: "Effect of mineralogical composition of iron-bearing materials on softening-melting properties", ICSTI/Ironmaking conference proceedings 1998, pp.1615-1635.

3. Hsieh, L.H.: "Effect of Raw Material composition on the Sintering Properties", ISIJ International, Vol. 45 (2005), No.4, pp.551-559.

4. Choudary, M.K.; and Nandy, B.: "Effect of Flame Front Speed on Sinter structure of High Alumina iron ores", ISIJ International, Vol. 46 (2006), No.4, pp. 611-613.

5. Pimenta, H.P.; and Seshadri, V.: "Characterisation of structure of Iron Ore Sinter and its behaviour during reduction at low temperatures", Iron and Steelmaking, 2002, Vol.29, No.3, pp. 169-174.

6. Higuchi, K.; Naito, M.; Nakano, M.; and Takamoto, Y.: "Optimization of Chemical composition on microstructure of Iron Ore Sinter for low-temperature Drip of molten Iron with High Permeability", ISIJ International, Vol.44 (2004), No.12, pp. 2057-2066.

7. Pownceby, M.I.; and Clout, J.M.F.: "Importance of fine ore chemical composition and high temperature phase relations: applications to iron ore sintering and pelletising", Mineral Processing and Extractive Metallurgy: IMM Transactions Section C, Vol.12, No.1, April 2003, pp. 44-51 (8).

8. Ritz, V.J.; Kortman, H.A.; and Koch, K.: "Reduction, Softening and melting properties of pellets, sinters, lumpy ore and mixed blast furnace burden", 2nd International Congres on the Science and Technology of Ironmaking and 57th Ironmaking conference, Toronto, Canada; 22 – 25 March 1998, pp.1635-1654.

9. Ishikawa, Y.; Shimomura, Y.; Sasaki, M.; Hida, Y.; and Hideo, T.: "Improvement of Sinter quality based on the mineralogical properties of Ores", Ironmaking Proceedings, vol.42, pp.17-29, Atlanta, Ga., U.S.A, 17-20, April 1983.

10. Wang, S.; Gao, W.; and Kong, L.: "Formation Mechanism of Silicoferrite of Calcium and Aluminium in Sintering Process", Ironmaking and steelmaking, 1998, vol.25, No.4, pp.296-301.

11. Panigraphy, S.C.; Jallouli, M.; and Rigaud, M.: "Porosity of Sinters and Pellets and its Relationship With Some of Their Properties", Ironmaking Proceedings, Vol. 43, AIME, Chicago, Illinois, USA; 1-4 April 1984, pp. 233- 240. 1984.

12. HSIEH, L.H.; and Whiteman, J.A.: "Effect of Oxygen Potential on Mineral Formation in Lime-fluxed Iron Ore sinter", ISIJ International, Vol.29, No.8, 1989, pp.625- 634.

13. HSIEH, L.H.; and Whiteman, J.A.: "Sintering conditions for simulating the Formation of Mineral Phases in Industrial Iron Ore Sinter", ISIJ International, Vol. 29, No. 1, 1989, pp.24-32.

14. Chaigneau, R. and Heerema, R.H.: "Calcium Ferrites and the Diversity in their Reduction Behavior", Ironmaking conference Proceedings, 1992, pp.111-120.

15. Biswas, A.K.: "Principles of the Blast Furnace", Cootha Publishing House, Brisbane, Australia 1981.

16. Chaigneau, R.: "Complex Calcium Ferrites in the Blast Furnace Process", PhD. Thesis, Delft University, 1994, Netherlands.

17. David, H.W.: "The Making, Shaping and Treatment of Steel", 11th Edition Ironmaking Volume 1999, pp.625-629.

18. Loo, C.E: "Some Progress in understanding the Science of Iron Ore Sintering", 2nd International Congres on the Science and Technology of Ironmaking and 57th Ironmaking conference, Toronto; Canada; 22 – 25 March 1998, pp.1299-1316.

19. Riquier, Y. : "Elaboration de la fonte, cours de Siderurgie 1, 1985, pp. IIa 10 – IIa 24, Faculte polytechnique de Mons, Belgique.

20. Goldring, D.C.; Jukes, L.M.; and Fray, T.A.T.: " Characterisation of Iron Ore Sinter from its Mineralogy", Instituite of Chemical Engineers, 5th International Symposium on Agglomeration, Brighton, UK; 25-27 Sept.1989 , pp.425-429.

21. Levin, E.M.; Robbins, C.R. and Mc Murdie, H.F., "Phase Diagrams for ceramists, 2nd edition, The American Ceramic Society Inc., Columbus, 1969, pp. 228

22. Lister, D.H. and Glasser, F.P., "Phase Relations in the System CaO-Al_2O_3-Iron oxide", Trans. Brit. Ceram. Soc., 66, 1967, pp.293-305

23. Goldring, D.C.; and Fray, T.A.T.: "Characterization of Iron Ores for Production of High quality Sinter", Ironmaking and Steelmaking, 1989, Vol.16, No. 2, pp.83-89.

24. Scarlett, N.V.Y.; Pownceby, M.I.; Madsen, I.C.; and Christensen, A.N.: "In-situ X-ray Diffraction Analysis of Iron Ore Sinter Phases", (2004) Journal of Applied Crystallography, 37 (3), pp.362-368.

25. Maeda, T.; Nishioka, K.; Nakashima, K.; and Shimizu, M.: "Formation Rate of Calcium Ferrite Melt Focusing on SiO_2 and Al_2O_3 component", ISIJ International, Vol. 44 (2004), No. 12, pp. 2046-2051.

26. Bristow, N.J. and Waters, A.G.: "Role of SFCA in promoting High-Temperature Reduction Properties of Iron Ore Sinters", The Institute of Mining and Metallurgy, 100, pp. C1-C10, January-April 1991.

27. Hida, Y.; Ito, K.; Okazaki, J.; and Sasaki. M.: "Mechanism of Formation of Acicular Calcium Ferrite (In-situ Observation and its Analysis of Sintering Process of Iron Ores- -II)", Transactions ISIJ, Vol.25, 1985, pp. B-234.

28. Yadav, U.S.; Pandey, B.D.; Das, B.K.; and Jena, D.N.: "Influence of Magnesia on sintering characteristics of Iron Ore", Ironmaking and Steelmaking, 2002, Vol. 29, No 2, pp. 91-95.

29. Kasai, E.; Otomo, T.; Maximiano, V.R. and Yoshio, W.: "Essential Factors Governing the Strength between Particles in the Iron Ore Sintering Process", ICSTI/Ironmaking Conference Proceedings, ISS and AIME, (1998), pp. 115-122.

30. Kasai, E.; Rankin, W.J.; Lovel, R.R.; and Omori, Y.: "An Analysis of the Structure of Iron Ore Sinter Cake", ISIJ International, Vol. 29, 1989, No. 8, pp. 635- 641.

31. Panigraphy, S.C; and Dilewijns, J.: "Influence of MgO content on Magnetic susceptibility of Iron Ore Sinter" Ironmaking Steelmaking, 1984, 11, pp.83-87.

32. Kumba Iron Ore Ltd, "Iron ores – Determination of Tumble Strength", 2005.

33. Husslage, W.M.; Bakker, T.; Kock, M.E.; and Heerema, R.H.: "Influence of Reduction Conditions on the Expansion and Microstructure of Sintered Hematite compacts during the transition to Magnetite", Minerals & Metallurgical Processings, Vol.16, No.3, August 1999, pp.23-33.

34. Nagano, S.; Yanaka, H.; and Yamaoka, Y.: "Degradation of Sinter in the Upper Part of Blast Furnace", Transactions ISIJ, Vol. 24, 1984, pp. B-201.

35. Jordaan, W.J.; M-Eng thesis: "The variation of sinter strength in the sinter bed due to the mineral phase distribution", 2002, University of Pretoria.

36. HSIEH, L.H.: "Effect of Raw Material Compositions on the Sintering properties", ISIJ International, Vol. 45 (2005), No.4, pp. 551-559.

37. Kumba Iron Ore Ltd: "Statistic test for low temperature RDI", 2002.

38. Maeda, T.; Lim, B.I.; and Ono, Y.: "Effect of Basicity and Porosity on the Reducibility of Iron Ore Sinter", Transactions ISIJ, Vol. 24, 1984, p. B-332.

39. Matsumura, M.; Hoshi, M.; and Kawaguchi, T.: "Improvement of Sinter Softening Property and Reducibility by controlling chemical compositions", ISIJ International, Vol.45 (2005), No.4, pp. 594-602.

40. Bakker, T.; and Heerema, R.H.: "Determination of the fundamental softening and melting characteristics of blast Furnace burden materials", Ironmaking Conference Proceedings, 1997, pp. 365- 373.

41. Muan, A.; Osborn, E.F.: "Phase equilibria among oxides in Steelmaking", 1965, pp. 20-21 & 201.

42. Cappel, F.; and Kilian, A.: "The ignition of sinter mixtures", Stahl und Eisen 94Nr. 11, 1974, pp. 453-461.

43. Personal communication with Dippenaar, B.A; Chief Engineer Kumba Iron Ore, sinter pilot plant, Pretoria.

44. Panigraphy, S.C.; Verstraeten, P.; and Dilewijns, J.: "Influence of MgO addition on mineralogy of Iron Ore Sinter", Metallurgical Transactions B, Vol. 15B, March 1984, pp. 23-32.

45. Panigraphy, S.C.; Verstraeten, P.; and Dilewijns, J.: "Effect of MgO addition on strength characteristics of iron ore sinter", Ironmaking and Steelmaking, 1984, Vol. 11, N0. 1, pp. 17 – 22.

Reference:

1. Egundebi, G.O.; and Whiteman, J.A.: "Evolution of Microstructure in Iron Ore Sinter", Ironmaking and steelmaking, 1989, vol.16, No.6, pp.379-385.

2. Pal, S.; Chandra, N.; Mishra, U.N, Singh, R.N.; & Mediratta, S.R.: "Effect of mineralogical composition of iron-bearing materials on softening-melting properties", ICSTI/Ironmaking conference proceedings 1998, pp.1615-1635.

3. Hsieh, L.H.: "Effect of Raw Material composition on the Sintering Properties", ISIJ International, Vol. 45 (2005), No.4, pp.551-559.

4. Choudary, M.K.; and Nandy, B.: "Effect of Flame Front Speed on Sinter structure of High Alumina iron ores", ISIJ International, Vol. 46 (2006), No.4, pp. 611-613.

5. Pimenta, H.P.; and Seshadri, V.: "Characterisation of structure of Iron Ore Sinter and its behaviour during reduction at low temperatures", Iron and Steelmaking, 2002, Vol.29, No.3, pp. 169-174.

6. Higuchi, K.; Naito, M.; Nakano, M.; and Takamoto, Y.: "Optimization of Chemical composition on microstructure of Iron Ore Sinter for low-temperature Drip of molten Iron with High Permeability", ISIJ International, Vol.44 (2004), No.12, pp. 2057-2066.

7. Pownceby, M.I.; and Clout, J.M.F.: "Importance of fine ore chemical composition and high temperature phase relations: applications to iron ore sintering and pelletising", Mineral Processing and Extractive Metallurgy: IMM Transactions Section C, Vol.12, No.1, April 2003, pp. 44-51 (8).

8. Ritz, V.J.; Kortman, H.A.; and Koch, K.: "Reduction, Softening and melting properties of pellets, sinters, lumpy ore and mixed blast furnace burden", 2nd International Congres on the Science and Technology of Ironmaking and 57th Ironmaking conference, Toronto, Canada; 22 – 25 March 1998, pp.1635-1654.

9. Ishikawa, Y.; Shimomura, Y.; Sasaki, M.; Hida, Y.; and Hideo, T.: "Improvement of Sinter quality based on the mineralogical properties of Ores", Ironmaking Proceedings, vol.42, pp.17-29, Atlanta, Ga., U.S.A, 17-20, April 1983.

10. Wang, S.; Gao, W.; and Kong, L.: "Formation Mechanism of Silicoferrite of Calcium and Aluminium in Sintering Process", Ironmaking and steelmaking, 1998, vol.25, No.4, pp.296-301.

11. Panigraphy, S.C.; Jallouli, M.; and Rigaud, M.: "Porosity of Sinters and Pellets and its Relationship With Some of Their Properties", Ironmaking Proceedings, Vol. 43, AIME, Chicago, Illinois, USA; 1-4 April 1984, pp. 233- 240. 1984.

12. HSIEH, L.H.; and Whiteman, J.A.: "Effect of Oxygen Potential on Mineral Formation in Lime-fluxed Iron Ore sinter", ISIJ International, Vol.29, No.8, 1989, pp.625- 634.

13. HSIEH, L.H.; and Whiteman, J.A.: "Sintering conditions for simulating the Formation of Mineral Phases in Industrial Iron Ore Sinter", ISIJ International, Vol. 29, No. 1, 1989, pp.24-32.

14. Chaigneau, R. and Heerema, R.H.: "Calcium Ferrites and the Diversity in their Reduction Behavior", Ironmaking conference Proceedings, 1992, pp.111-120.

15. Biswas, A.K.: "Principles of the Blast Furnace", Cootha Publishing House, Brisbane, Australia 1981.

16. Chaigneau, R.: "Complex Calcium Ferrites in the Blast Furnace Process", PhD. Thesis, Delft University, 1994, Netherlands.

17. David, H.W.: "The Making, Shaping and Treatment of Steel", 11th Edition Ironmaking Volume 1999, pp.625-629.

18. Loo, C.E: "Some Progress in understanding the Science of Iron Ore Sintering", 2nd International Congres on the Science and Technology of Ironmaking and 57th Ironmaking conference, Toronto; Canada; 22 – 25 March 1998, pp.1299-1316.

19. Riquier, Y. : "Elaboration de la fonte, cours de Siderurgie 1, 1985, pp. IIa 10 – IIa 24, Faculte polytechnique de Mons, Belgique.

20. Goldring, D.C.; Jukes, L.M.; and Fray, T.A.T.: " Characterisation of Iron Ore Sinter from its Mineralogy", Instituite of Chemical Engineers, 5th International Symposium on Agglomeration, Brighton, UK; 25-27 Sept.1989 , pp.425-429.

21. Levin, E.M.; Robbins, C.R. and Mc Murdie, H.F., "Phase Diagrams for ceramists, 2nd edition, The American Ceramic Society Inc., Columbus, 1969, pp. 228

22. Lister, D.H. and Glasser, F.P., "Phase Relations in the System CaO-Al_2O_3-Iron oxide", Trans. Brit. Ceram. Soc., 66, 1967, pp.293-305

23. Goldring, D.C.; and Fray, T.A.T.: "Characterization of Iron Ores for Production of High quality Sinter", Ironmaking and Steelmaking, 1989, Vol.16, No. 2, pp.83-89.

24. Scarlett, N.V.Y.; Pownceby, M.I.; Madsen, I.C.; and Christensen, A.N.: "In-situ X-ray Diffraction Analysis of Iron Ore Sinter Phases", (2004) Journal of Applied Crystallography, 37 (3), pp.362-368.

25. Maeda, T.; Nishioka, K.; Nakashima, K.; and Shimizu, M.: "Formation Rate of Calcium Ferrite Melt Focusing on SiO_2 and Al_2O_3 component", ISIJ International, Vol. 44 (2004), No. 12, pp. 2046-2051.

26. Bristow, N.J. and Waters, A.G.: "Role of SFCA in promoting High-Temperature Reduction Properties of Iron Ore Sinters", The Institute of Mining and Metallurgy, 100, pp. C1-C10, January-April 1991.

27. Hida, Y.; Ito, K.; Okazaki, J.; and Sasaki. M.: "Mechanism of Formation of Acicular Calcium Ferrite (In-situ Observation and its Analysis of Sintering Process of Iron Ores- -II)", Transactions ISIJ, Vol.25, 1985, pp. B-234.

28. Yadav, U.S.; Pandey, B.D.; Das, B.K.; and Jena, D.N.: "Influence of Magnesia on sintering characteristics of Iron Ore", Ironmaking and Steelmaking, 2002, Vol. 29, No 2, pp. 91-95.

29. Kasai, E.; Otomo, T.; Maximiano, V.R. and Yoshio, W.: "Essential Factors Governing the Strength between Particles in the Iron Ore Sintering Process", ICSTI/Ironmaking Conference Proceedings, ISS and AIME, (1998), pp. 115-122.

30. Kasai, E.; Rankin, W.J.; Lovel, R.R.; and Omori, Y.: "An Analysis of the Structure of Iron Ore Sinter Cake", ISIJ International, Vol. 29, 1989, No. 8, pp. 635- 641.

31. Panigraphy, S.C; and Dilewijns, J.: "Influence of MgO content on Magnetic susceptibility of Iron Ore Sinter" Ironmaking Steelmaking, 1984, 11, pp.83-87.

32. Kumba Iron Ore Ltd, "Iron ores – Determination of Tumble Strength", 2005.

33. Husslage, W.M.; Bakker, T.; Kock, M.E.; and Heerema, R.H.: "Influence of Reduction Conditions on the Expansion and Microstructure of Sintered Hematite compacts during the transition to Magnetite", Minerals & Metallurgical Processings, Vol.16, No.3, August 1999, pp.23-33.

34. Nagano, S.; Yanaka, H.; and Yamaoka, Y.: "Degradation of Sinter in the Upper Part of Blast Furnace", Transactions ISIJ, Vol. 24, 1984, pp. B-201.

35. Jordaan, W.J.; M-Eng thesis: "The variation of sinter strength in the sinter bed due to the mineral phase distribution", 2002, University of Pretoria.

36. HSIEH, L.H.: "Effect of Raw Material Compositions on the Sintering properties", ISIJ International, Vol. 45 (2005), No.4, pp. 551-559.

37. Kumba Iron Ore Ltd: "Statistic test for low temperature RDI", 2002.

38. Maeda, T.; Lim, B.I.; and Ono, Y.: "Effect of Basicity and Porosity on the Reducibility of Iron Ore Sinter", Transactions ISIJ, Vol. 24, 1984, p. B-332.

39. Matsumura, M.; Hoshi, M.; and Kawaguchi, T.: "Improvement of Sinter Softening Property and Reducibility by controlling chemical compositions", ISIJ International, Vol.45 (2005), No.4, pp. 594-602.

40. Bakker, T.; and Heerema, R.H.: "Determination of the fundamental softening and melting characteristics of blast Furnace burden materials", Ironmaking Conference Proceedings, 1997, pp. 365- 373.

41. Muan, A.; Osborn, E.F.: "Phase equilibria among oxides in Steelmaking", 1965, pp. 20-21 & 201.

42. Cappel, F.; and Kilian, A.: "The ignition of sinter mixtures", Stahl und Eisen 94Nr. 11, 1974, pp. 453-461.

43. Personal communication with Dippenaar, B.A; Chief Engineer Kumba Iron Ore, sinter pilot plant, Pretoria.

44. Panigraphy, S.C.; Verstraeten, P.; and Dilewijns, J.: "Influence of MgO addition on mineralogy of Iron Ore Sinter", Metallurgical Transactions B, Vol. 15B, March 1984, pp. 23-32.

45. Panigraphy, S.C.; Verstraeten, P.; and Dilewijns, J.: "Effect of MgO addition on strength characteristics of iron ore sinter", Ironmaking and Steelmaking, 1984, Vol. 11, N0. 1, pp. 17 – 22.

Reference:

1. Egundebi, G.O.; and Whiteman, J.A.: "Evolution of Microstructure in Iron Ore Sinter", Ironmaking and steelmaking, 1989, vol.16, No.6, pp.379-385.

2. Pal, S.; Chandra, N.; Mishra, U.N, Singh, R.N.; & Mediratta, S.R.: "Effect of mineralogical composition of iron-bearing materials on softening-melting properties", ICSTI/Ironmaking conference proceedings 1998, pp.1615-1635.

3. Hsieh, L.H.: "Effect of Raw Material composition on the Sintering Properties", ISIJ International, Vol. 45 (2005), No.4, pp.551-559.

4. Choudary, M.K.; and Nandy, B.: "Effect of Flame Front Speed on Sinter structure of High Alumina iron ores", ISIJ International, Vol. 46 (2006), No.4, pp. 611-613.

5. Pimenta, H.P.; and Seshadri, V.: "Characterisation of structure of Iron Ore Sinter and its behaviour during reduction at low temperatures", Iron and Steelmaking, 2002, Vol.29, No.3, pp. 169-174.

6. Higuchi, K.; Naito, M.; Nakano, M.; and Takamoto, Y.: "Optimization of Chemical composition on microstructure of Iron Ore Sinter for low-temperature Drip of molten Iron with High Permeability", ISIJ International, Vol.44 (2004), No.12, pp. 2057-2066.

7. Pownceby, M.I.; and Clout, J.M.F.: "Importance of fine ore chemical composition and high temperature phase relations: applications to iron ore sintering and pelletising", Mineral Processing and Extractive Metallurgy: IMM Transactions Section C, Vol.12, No.1, April 2003, pp. 44-51 (8).

8. Ritz, V.J.; Kortman, H.A.; and Koch, K.: "Reduction, Softening and melting properties of pellets, sinters, lumpy ore and mixed blast furnace burden", 2nd International Congres on the Science and Technology of Ironmaking and 57th Ironmaking conference, Toronto, Canada; 22 – 25 March 1998, pp.1635-1654.

9. Ishikawa, Y.; Shimomura, Y.; Sasaki, M.; Hida, Y.; and Hideo, T.: "Improvement of Sinter quality based on the mineralogical properties of Ores", Ironmaking Proceedings, vol.42, pp.17-29, Atlanta, Ga., U.S.A, 17-20, April 1983.

10. Wang, S.; Gao, W.; and Kong, L.: "Formation Mechanism of Silicoferrite of Calcium and Aluminium in Sintering Process", Ironmaking and steelmaking, 1998, vol.25, No.4, pp.296-301.

11. Panigraphy, S.C.; Jallouli, M.; and Rigaud, M.: "Porosity of Sinters and Pellets and its Relationship With Some of Their Properties", Ironmaking Proceedings, Vol. 43, AIME, Chicago, Illinois, USA; 1-4 April 1984, pp. 233- 240. 1984.

12. HSIEH, L.H.; and Whiteman, J.A.: "Effect of Oxygen Potential on Mineral Formation in Lime-fluxed Iron Ore sinter", ISIJ International, Vol.29, No.8, 1989, pp.625- 634.

13. HSIEH, L.H.; and Whiteman, J.A.: "Sintering conditions for simulating the Formation of Mineral Phases in Industrial Iron Ore Sinter", ISIJ International, Vol. 29, No. 1, 1989, pp.24-32.

14. Chaigneau, R. and Heerema, R.H.: "Calcium Ferrites and the Diversity in their Reduction Behavior", Ironmaking conference Proceedings, 1992, pp.111-120.

15. Biswas, A.K.: "Principles of the Blast Furnace", Cootha Publishing House, Brisbane, Australia 1981.

16. Chaigneau, R.: "Complex Calcium Ferrites in the Blast Furnace Process", PhD. Thesis, Delft University, 1994, Netherlands.

17. David, H.W.: "The Making, Shaping and Treatment of Steel", 11th Edition Ironmaking Volume 1999, pp.625-629.

18. Loo, C.E: "Some Progress in understanding the Science of Iron Ore Sintering", 2nd International Congres on the Science and Technology of Ironmaking and 57th Ironmaking conference, Toronto; Canada; 22 – 25 March 1998, pp.1299-1316.

19. Riquier, Y. : "Elaboration de la fonte, cours de Siderurgie 1, 1985, pp. IIa 10 – IIa 24, Faculte polytechnique de Mons, Belgique.

20. Goldring, D.C.; Jukes, L.M.; and Fray, T.A.T.: " Characterisation of Iron Ore Sinter from its Mineralogy", Instituite of Chemical Engineers, 5th International Symposium on Agglomeration, Brighton, UK; 25-27 Sept.1989 , pp.425-429.

21. Levin, E.M.; Robbins, C.R. and Mc Murdie, H.F., "Phase Diagrams for ceramists, 2nd edition, The American Ceramic Society Inc., Columbus, 1969, pp. 228

22. Lister, D.H. and Glasser, F.P., "Phase Relations in the System CaO-Al_2O_3-Iron oxide", Trans. Brit. Ceram. Soc., 66, 1967, pp.293-305

23. Goldring, D.C.; and Fray, T.A.T.: "Characterization of Iron Ores for Production of High quality Sinter", Ironmaking and Steelmaking, 1989, Vol.16, No. 2, pp.83-89.

24. Scarlett, N.V.Y.; Pownceby, M.I.; Madsen, I.C.; and Christensen, A.N.: "In-situ X-ray Diffraction Analysis of Iron Ore Sinter Phases", (2004) Journal of Applied Crystallography, 37 (3), pp.362-368.

25. Maeda, T.; Nishioka, K.; Nakashima, K.; and Shimizu, M.: "Formation Rate of Calcium Ferrite Melt Focusing on SiO_2 and Al_2O_3 component", ISIJ International, Vol. 44 (2004), No. 12, pp. 2046-2051.

26. Bristow, N.J. and Waters, A.G.: "Role of SFCA in promoting High-Temperature Reduction Properties of Iron Ore Sinters", The Institute of Mining and Metallurgy, 100, pp. C1-C10, January-April 1991.

27. Hida, Y.; Ito, K.; Okazaki, J.; and Sasaki. M.: "Mechanism of Formation of Acicular Calcium Ferrite (In-situ Observation and its Analysis of Sintering Process of Iron Ores- -II)", Transactions ISIJ, Vol.25, 1985, pp. B-234.

28. Yadav, U.S.; Pandey, B.D.; Das, B.K.; and Jena, D.N.: "Influence of Magnesia on sintering characteristics of Iron Ore", Ironmaking and Steelmaking, 2002, Vol. 29, No 2, pp. 91-95.

29. Kasai, E.; Otomo, T.; Maximiano, V.R. and Yoshio, W.: "Essential Factors Governing the Strength between Particles in the Iron Ore Sintering Process", ICSTI/Ironmaking Conference Proceedings, ISS and AIME, (1998), pp. 115-122.

30. Kasai, E.; Rankin, W.J.; Lovel, R.R.; and Omori, Y.: "An Analysis of the Structure of Iron Ore Sinter Cake", ISIJ International, Vol. 29, 1989, No. 8, pp. 635- 641.

31. Panigraphy, S.C; and Dilewijns, J.: "Influence of MgO content on Magnetic susceptibility of Iron Ore Sinter" Ironmaking Steelmaking, 1984, 11, pp.83-87.

32. Kumba Iron Ore Ltd, "Iron ores – Determination of Tumble Strength", 2005.

33. Husslage, W.M.; Bakker, T.; Kock, M.E.; and Heerema, R.H.: "Influence of Reduction Conditions on the Expansion and Microstructure of Sintered Hematite compacts during the transition to Magnetite", Minerals & Metallurgical Processings, Vol.16, No.3, August 1999, pp.23-33.

34. Nagano, S.; Yanaka, H.; and Yamaoka, Y.: "Degradation of Sinter in the Upper Part of Blast Furnace", Transactions ISIJ, Vol. 24, 1984, pp. B-201.

35. Jordaan, W.J.; M-Eng thesis: "The variation of sinter strength in the sinter bed due to the mineral phase distribution", 2002, University of Pretoria.

36. HSIEH, L.H.: "Effect of Raw Material Compositions on the Sintering properties", ISIJ International, Vol. 45 (2005), No.4, pp. 551-559.

37. Kumba Iron Ore Ltd: "Statistic test for low temperature RDI", 2002.

38. Maeda, T.; Lim, B.I.; and Ono, Y.: "Effect of Basicity and Porosity on the Reducibility of Iron Ore Sinter", Transactions ISIJ, Vol. 24, 1984, p. B-332.

39. Matsumura, M.; Hoshi, M.; and Kawaguchi, T.: "Improvement of Sinter Softening Property and Reducibility by controlling chemical compositions", ISIJ International, Vol.45 (2005), No.4, pp. 594-602.

40. Bakker, T.; and Heerema, R.H.: "Determination of the fundamental softening and melting characteristics of blast Furnace burden materials", Ironmaking Conference Proceedings, 1997, pp. 365- 373.

41. Muan, A.; Osborn, E.F.: "Phase equilibria among oxides in Steelmaking", 1965, pp. 20-21 & 201.

42. Cappel, F.; and Kilian, A.: "The ignition of sinter mixtures", Stahl und Eisen 94Nr. 11, 1974, pp. 453-461.

43. Personal communication with Dippenaar, B.A; Chief Engineer Kumba Iron Ore, sinter pilot plant, Pretoria.

44. Panigraphy, S.C.; Verstraeten, P.; and Dilewijns, J.: "Influence of MgO addition on mineralogy of Iron Ore Sinter", Metallurgical Transactions B, Vol. 15B, March 1984, pp. 23-32.

45. Panigraphy, S.C.; Verstraeten, P.; and Dilewijns, J.: "Effect of MgO addition on strength characteristics of iron ore sinter", Ironmaking and Steelmaking, 1984, Vol. 11, N0. 1, pp. 17 – 22.

APPENDIX

NOMENCLATURE

BC 897: Base case sinter at an ignition temperature of 897^{o}C

BC 963: Base case sinter at an ignition temperature of 963^{o}C

BC 983: Base case sinter at an ignition temperature of 983^{o}C

BC 1100: Base case sinter at an ignition temperature of 1100^{o}C

BC 1053: Low silica – Low alumina sinter with 2.8 mass % MgO content at an ignition temperature of 1053^{o}C

RMT 2148: High silica – Low alumina sinter with 2.8 mass % MgO added through dolomite

RMT 2206: High silica – Low alumina sinter with 2.8 mass % MgO added through fused magnesia

RMT 2219: High silica – High alumina sinter

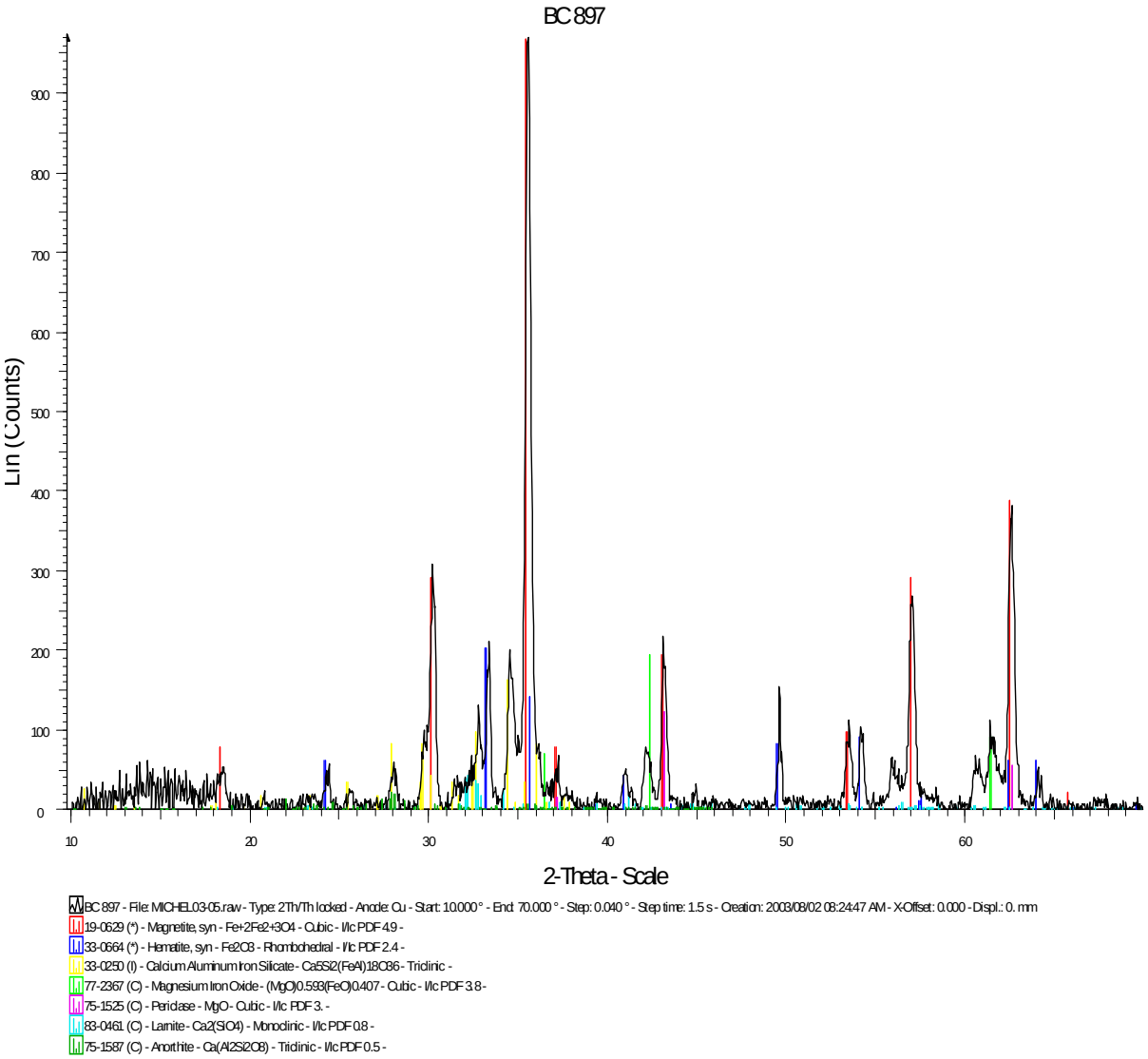
BC 897
Lin (Counts)
0
100
200
300
400
500
600
700
800
900
10
20
30
40
50
60
2-Theta - Scale
BC 897 - File: MICHEL03-05.raw - Type: 2Th/Th locked - Anode: Cu - Start: 10.000 ° - End: 70.000 ° - Step: 0.040 ° - Step time: 1.5 s - Creation: 2003/08/02 08:24:47 AM - X-Offset: 0.000 - Displ.: 0. mm
19-0629 (*) - Magnetite, syn - Fe+2Fe2+3O4 - Cubic - I/Ic PDF 4.9 -
33-0664 (*) - Hematite, syn - Fe2O3 - Rhombohedral - I/Ic PDF 2.4 -
33-0250 (I) - Calcium Aluminum Iron Silicate - Ca5Si2(Fe4l)18O36 - Triclinic -
77-2367 (C) - Magnesium Iron Oxide - (MgO)0.593(FeO)0.407 - Cubic - I/Ic PDF 3.8 -
75-1525 (C) - Peridase - MgO - Cubic - I/Ic PDF 3. -
83-0461 (C) - Larnite - Ca2(SiO4) - Monoclinic - I/Ic PDF 0.8 -
75-1587 (C) - Anorthite - Ca(Al2Si2O8) - Triclinic - I/Ic PDF 0.5 -

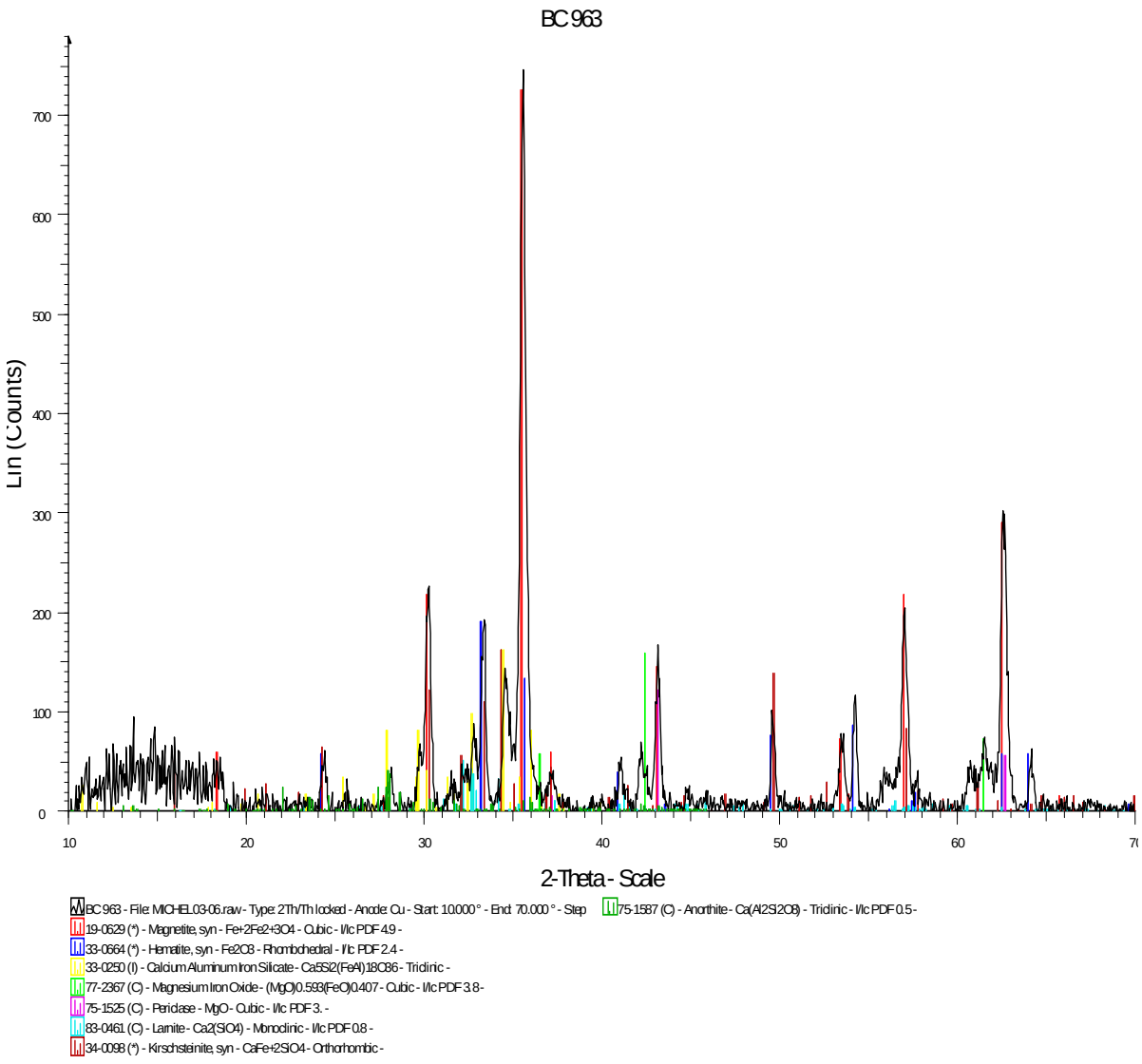
BC 963
Lin (Counts)
0
100
200
300
400
500
600
700
10
20
30
40
50
60
2-Theta - Scale
BC 963 - File: MICHEL03-06.raw - Type: 2Th/Th locked - Anode: Cu - Start: 10.000 ° - End: 70.000 ° - Step
75-1587 (C) - Anorthite - Ca(Al2Si2O8) - Triclinic - I/Ic PDF 0.5 -
19-0629 (*) - Magnetite, syn - Fe+2Fe2+3O4 - Cubic - I/Ic PDF 4.9 -
33-0664 (*) - Hematite, syn - Fe2O3 - Rhombohedral - I/Ic PDF 2.4 -
33-0250 (I) - Calcium Aluminum Iron Silicate - Ca5Si2(Fe4I).18O86 - Triclinic -
77-2367 (C) - Magnesium Iron Oxide - (MgO)0.593(FeO)0.407 - Cubic - I/Ic PDF 3.8 -
75-1525 (C) - Periclase - MgO - Cubic - I/Ic PDF 3. -
83-0461 (C) - Larnite - Ca2(SiO4) - Monoclinic - I/Ic PDF 0.8 -
34-0098 (*) - Kirschsteinite, syn - CaFe+2SiO4 - Orthorhombic -

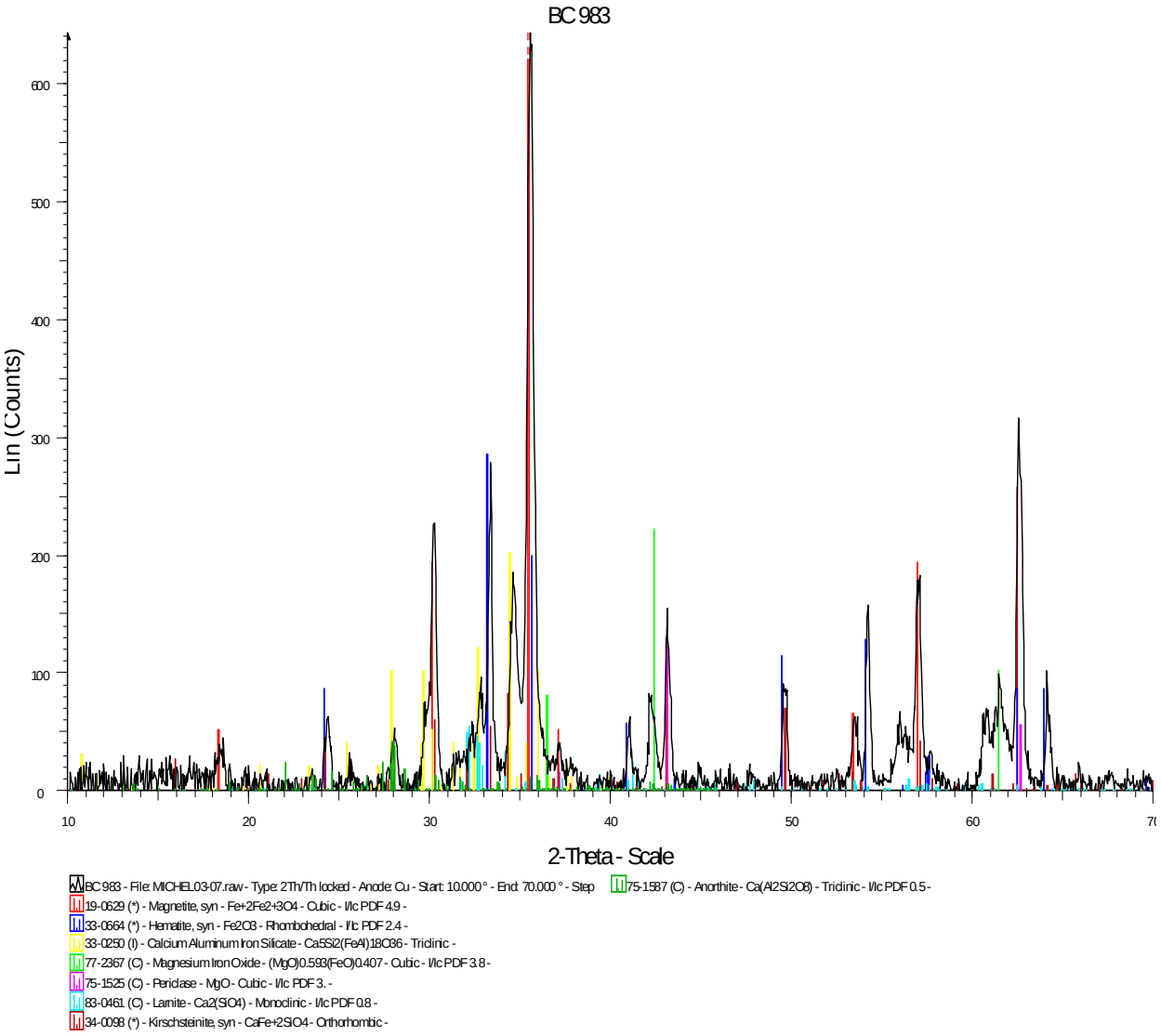
BC 983
Lin (Counts)
0
100
200
300
400
500
600
10
20
30
40
50
60
2-Theta - Scale
BC 983 - File: MICHEL03-07.raw - Type: 2Th/Th locked - Anode: Cu - Start: 10.000 ° - End: 70.000 ° - Step
75-1587 (C) - Anorthite - Ca(Al2Si2O8) - Triclinic - I/Ic PDF 0.5 -
19-0629 (*) - Magnetite, syn - Fe+2Fe2+3O4 - Cubic - I/Ic PDF 4.9 -
33-0664 (*) - Hematite, syn - Fe2O3 - Rhombohedral - I/Ic PDF 2.4 -
33-0250 (I) - Calcium Aluminum Iron Silicate - Ca5Si2(FeAl)18O36 - Triclinic -
77-2367 (C) - Magnesium Iron Oxide - (MgO)0.593(FeO)0.407 - Cubic - I/Ic PDF 3.8 -
75-1525 (C) - Periclase - MgO - Cubic - I/Ic PDF 3. -
83-0461 (C) - Larnite - Ca2(SiO4) - Monoclinic - I/Ic PDF 0.8 -
34-0098 (*) - Kirschsteinite, syn - CaFe+2SiO4 - Orthorhombic -

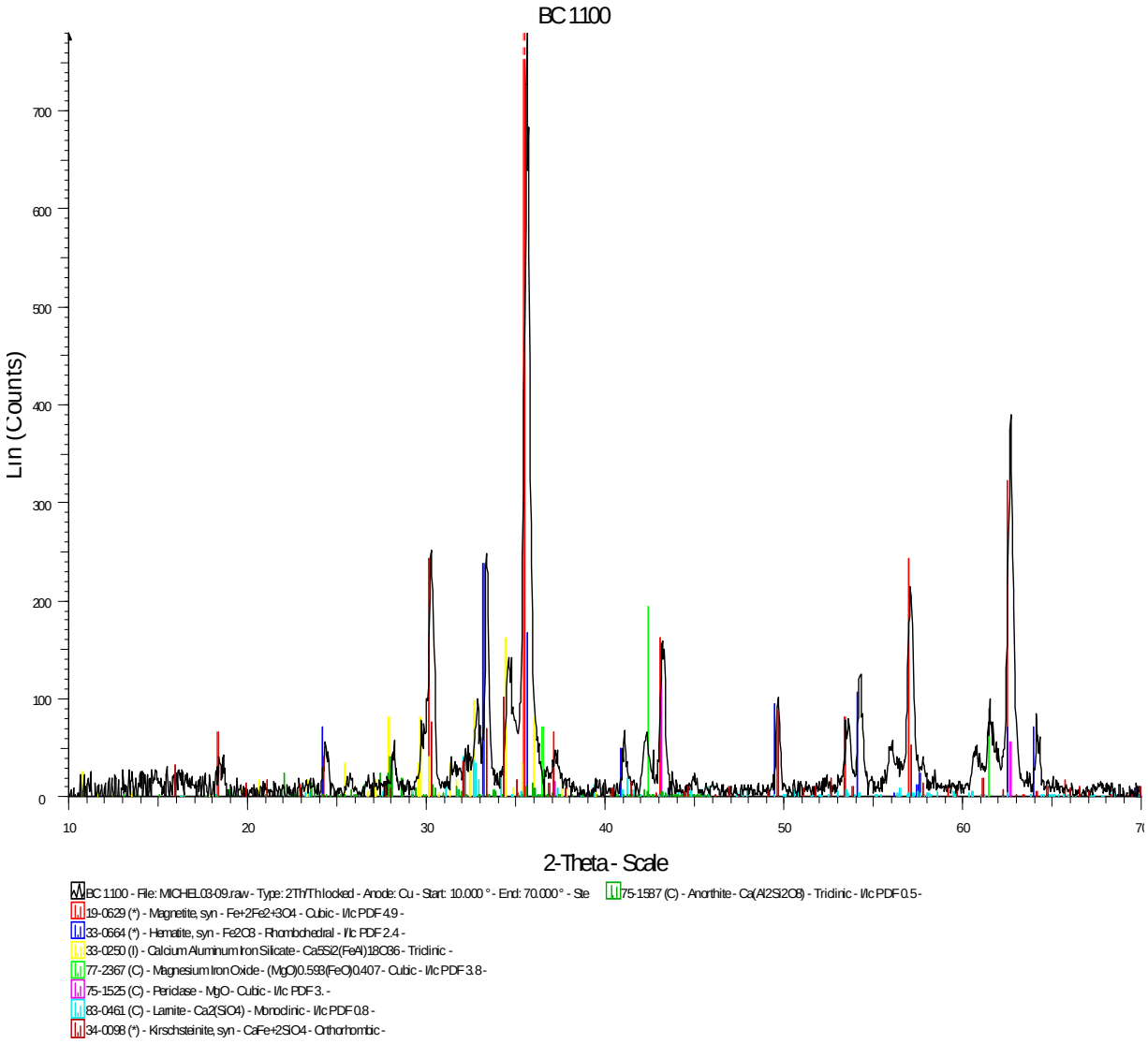
BC 1100
Lin (Counts)
0
100
200
300
400
500
600
700
10
20
30
40
50
60
2-Theta - Scale
BC 1100 - File: MICHEL03-09.raw - Type: 2Th/Th locked - Anode: Cu - Start: 10.000 ° - End: 70.000 ° - Ste
19-0629 (*) - Magnetite, syn - Fe+2Fe2+3O4 - Cubic - I/Ic PDF 4.9 -
33-0664 (*) - Hematite, syn - Fe2O3 - Rhombohedral - I/Ic PDF 2.4 -
33-0250 (I) - Calcium Aluminum Iron Silicate - Ca5Si2(Fe4Al)18O36 - Tridinic -
77-2367 (C) - Magnesium Iron Oxide - (MgO)0.593(FeO)0.407 - Cubic - I/Ic PDF 3.8 -
75-1525 (C) - Periclase - MgO - Cubic - I/Ic PDF 3. -
83-0461 (C) - Larnite - Ca2(SiO4) - Monoclinic - I/Ic PDF 0.8 -
34-0098 (*) - Kirschsteinite, syn - CaFe+2SiO4 - Orthorhombic -
75-1587 (C) - Anorthite - Ca(Al2Si2O8) - Tridinic - I/Ic PDF 0.5 -

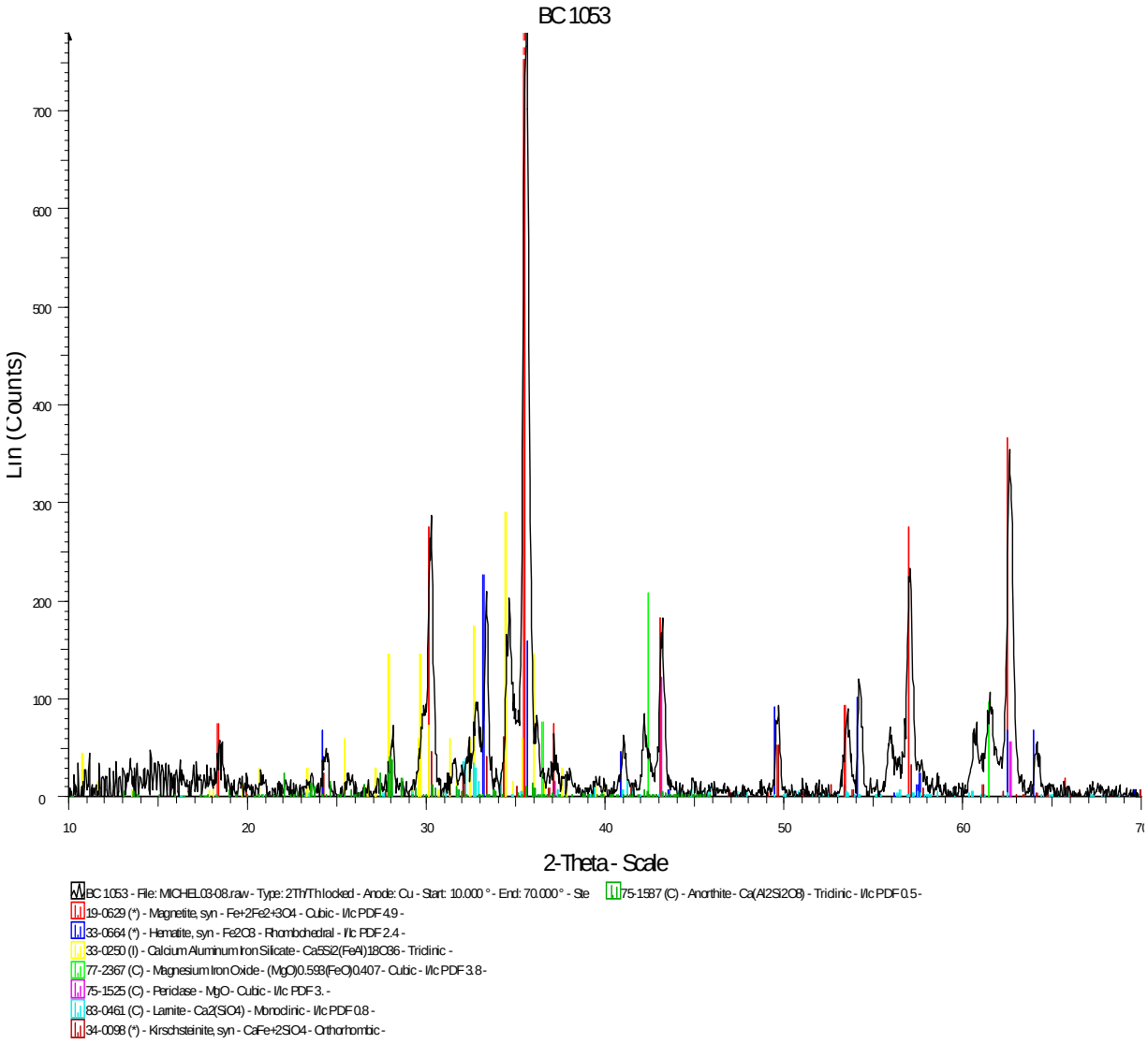
BC 1053
Lin (Counts)
0
100
200
300
400
500
600
700
10
20
30
40
50
60
2-Theta - Scale
BC 1053 - File: MICHEL03-08.raw - Type: 2Th/Th locked - Anode: Cu - Start: 10.000 ° - End: 70.000 ° - Ste
19-0629 (*) - Magnetite, syn - Fe+2Fe2+3O4 - Cubic - I/Ic PDF 4.9 -
33-0664 (*) - Hematite, syn - Fe2O3 - Rhombohedral - I/Ic PDF 2.4 -
33-0250 (I) - Calcium Aluminum Iron Silicate - Ca5Si2(FeAl)18O36 - Tridinic -
77-2367 (C) - Magnesium Iron Oxide - (MgO)0.593(FeO)0.407 - Cubic - I/Ic PDF 3.8 -
75-1525 (C) - Periclase - MgO - Cubic - I/Ic PDF 3. -
83-0461 (C) - Larnite - Ca2(SiO4) - Monoclinic - I/Ic PDF 0.8 -
34-0098 (*) - Kirschsteinite, syn - CaFe+2SiO4 - Orthorhombic -
75-1587 (C) - Anorthite - Ca(Al2Si2O8) - Tridinic - I/Ic PDF 0.5 -

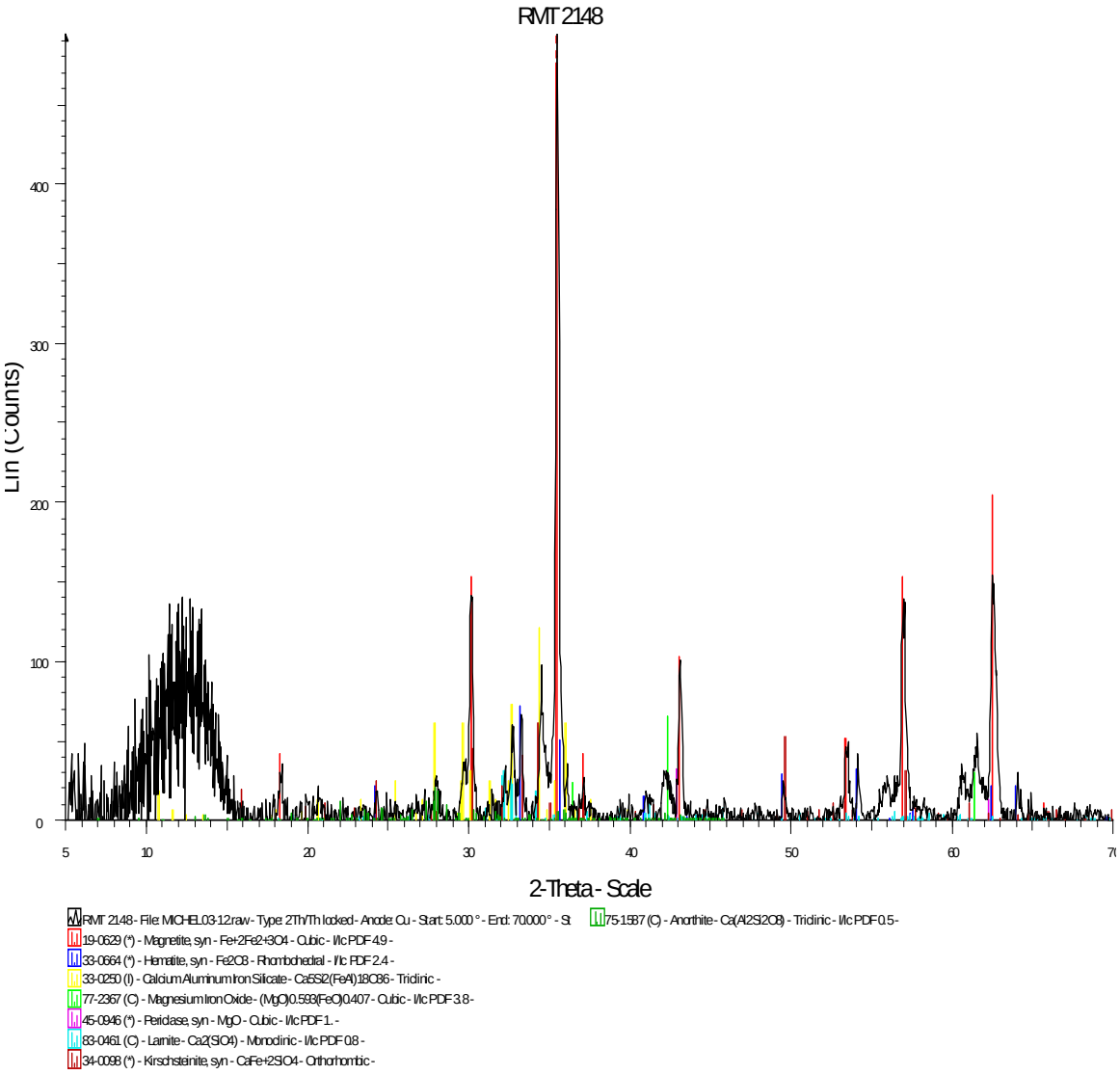
RMT 2148
Lin (Counts)
0
100
200
300
400
5
10
20
30
40
50
60
2-Theta - Scale
RMT 2148 - File: MICHEL03-12.raw - Type: 2Th/Th locked - Anode: Cu - Start: 5.000 ° - End: 70.000 ° - St
75-1587 (C) - Anorthite - Ca(Al2Si2O8) - Triclinic - I/Ic PDF 0.5 -
19-0629 (*) - Magnetite, syn - Fe+2Fe2+3O4 - Cubic - I/Ic PDF 4.9 -
33-0664 (*) - Hematite, syn - Fe2O3 - Rhombohedral - I/Ic PDF 2.4 -
33-0250 (I) - Calcium Aluminum Iron Silicate - Ca5Si2(Fe4)18O36 - Triclinic -
77-2367 (C) - Magnesium Iron Oxide - (MgO)0.593(FeO)0.407 - Cubic - I/Ic PDF 3.8 -
45-0946 (*) - Periclase, syn - MgO - Cubic - I/Ic PDF 1. -
83-0461 (C) - Larnite - Ca2(SiO4) - Monoclinic - I/Ic PDF 0.8 -
34-0098 (*) - Kirschsteinite, syn - CaFe+2SiO4 - Orthorhombic -

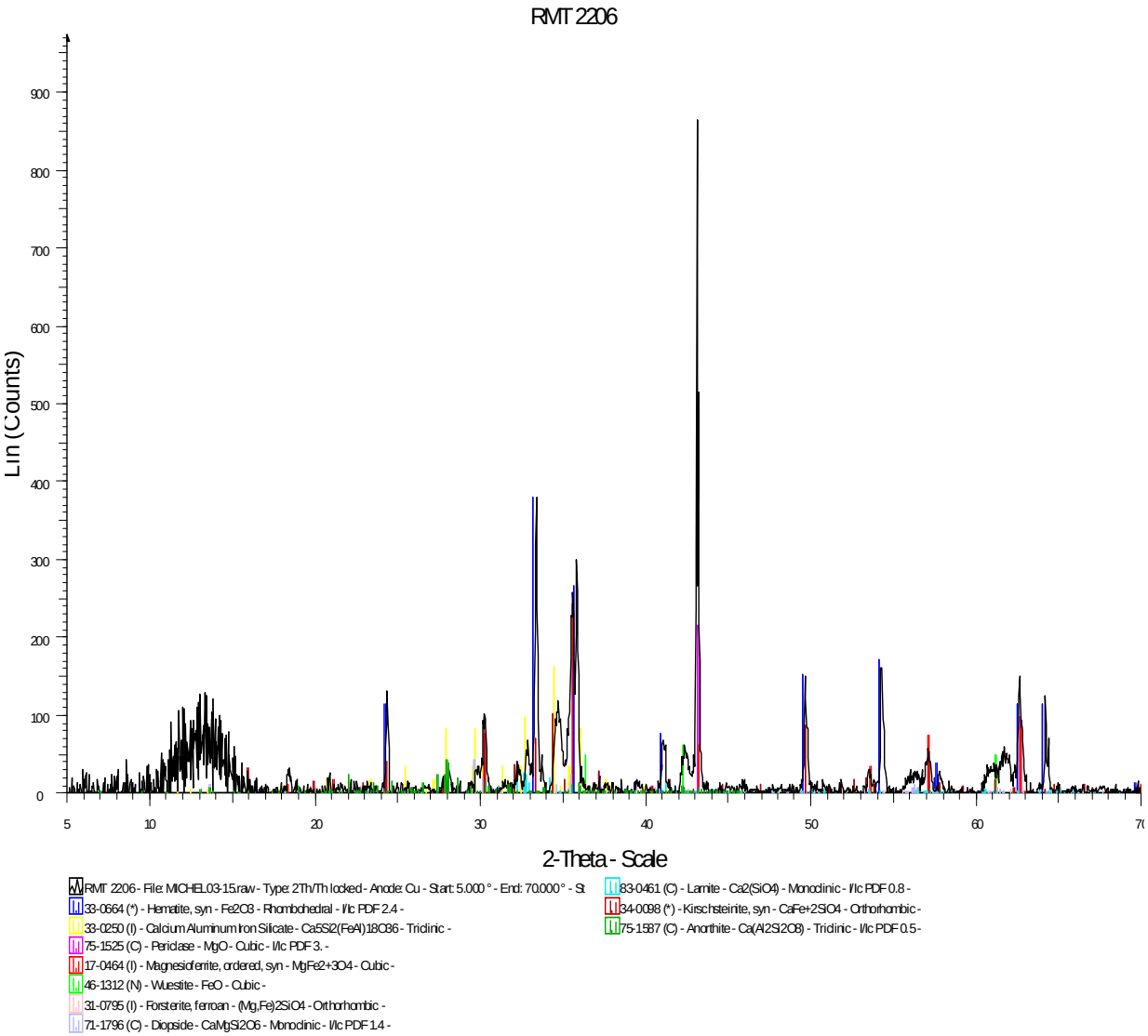
RMT 2206
Lin (Counts)
0
100
200
300
400
500
600
700
800
900
5
10
20
30
40
50
60
2-Theta - Scale
RMT 2206 - File: MICHEL03-15.raw - Type: 2Th/Th locked - Anode: Cu - Start: 5.000 ° - End: 70.000 ° - St
33-0664 (*) - Hematite, syn - Fe2O3 - Rhombohedral - I/Ic PDF 2.4 -
33-0250 (I) - Calcium Aluminum Iron Silicate - Ca5Si2(Fe4l)18O36 - Triclinic -
75-1525 (C) - Periclase - MgO - Cubic - I/Ic PDF 3. -
17-0464 (I) - Magnesioferrite, ordered, syn - MgFe2+3O4 - Cubic -
46-1312 (N) - Wuestite - FeO - Cubic -
31-0795 (I) - Forsterite, ferroan - (Mg,Fe)2SiO4 - Orthorhombic -
71-1796 (C) - Diopside - CaMgSi2O6 - Monoclinic - I/Ic PDF 1.4 -
83-0461 (C) - Larnite - Ca2(SiO4) - Monoclinic - I/Ic PDF 0.8 -
34-0098 (*) - Kirschsteinite, syn - CaFe+2SiO4 - Orthorhombic -
75-1587 (C) - Anorthite - Ca(Al2Si2O8) - Triclinic - I/Ic PDF 0.5 -

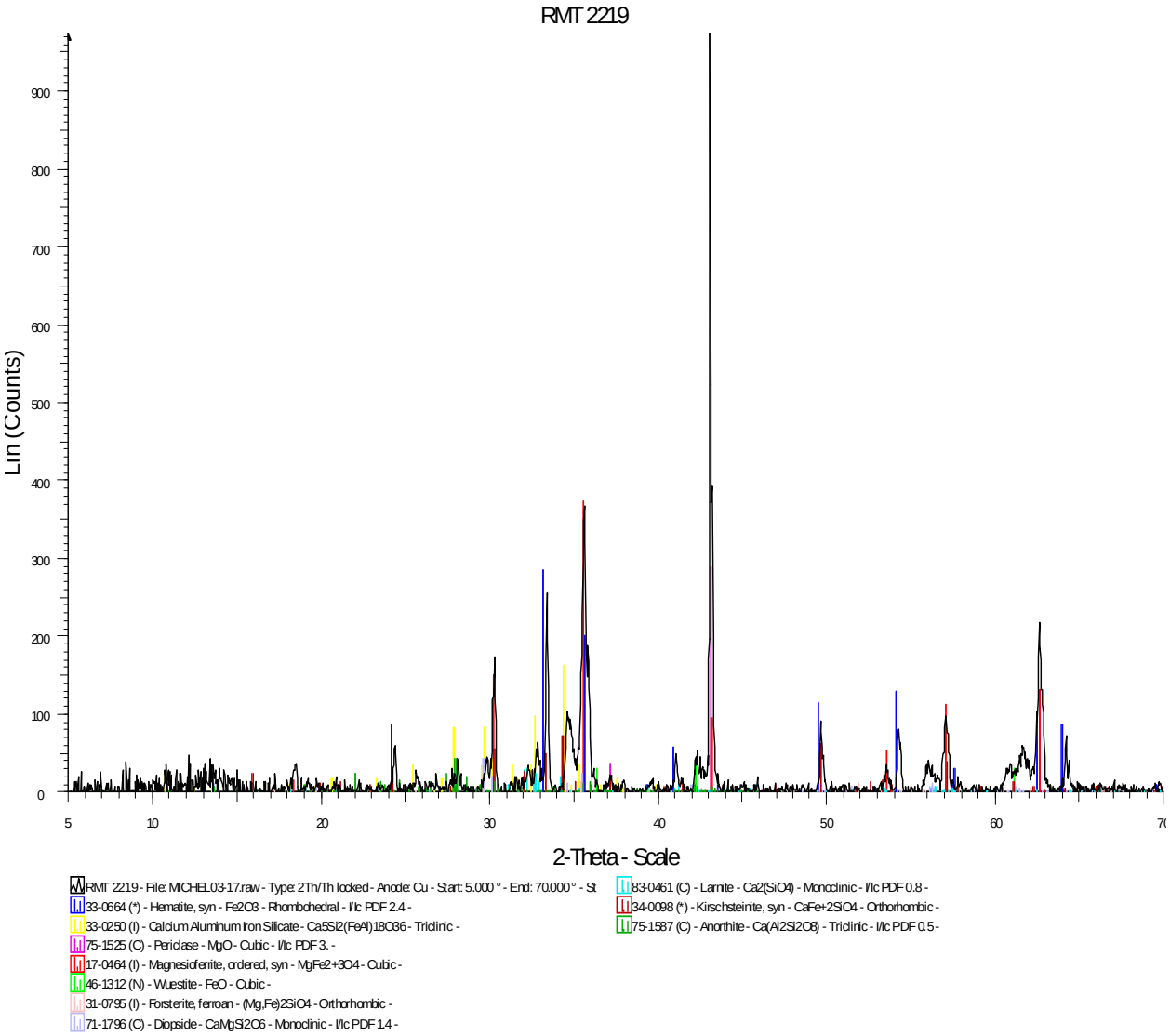
RMT 2219
Lin (Counts)
0
100
200
300
400
500
600
700
800
900
5
10
20
30
40
50
60
2-Theta - Scale
RMT 2219 - File: MICHEL03-17.raw - Type: 2Th/Th locked - Anode: Cu - Start: 5.000 ° - End: 70.000 ° - St
33-0664 (*) - Hematite, syn - Fe2O3 - Rhombohedral - I/Ic PDF 2.4 -
33-0250 (I) - Calcium Aluminum Iron Silicate - Ca5Si2(FeAl)18O36 - Triclinic -
75-1525 (C) - Periclase - MgO - Cubic - I/Ic PDF 3. -
17-0464 (I) - Magnesioferrite, ordered, syn - MgFe2+3O4 - Cubic -
46-1312 (N) - Wuestite - FeO - Cubic -
31-0795 (I) - Forsterite, ferroan - (Mg,Fe)2SiO4 - Orthorhombic -
71-1796 (C) - Diopside - CaMgSi2O6 - Monoclinic - I/Ic PDF 1.4 -
83-0461 (C) - Larnite - Ca2(SiO4) - Monoclinic - I/Ic PDF 0.8 -
34-0098 (*) - Kirschsteinite, syn - CaFe+2SiO4 - Orthorhombic -
75-1587 (C) - Anorthite - Ca(Al2Si2O8) - Triclinic - I/Ic PDF 0.5 -